THE UNIVERSITY OF QUEENSLAND

SCHOOL OF CIVIL ENGINEERING

REPORT CH101/15

UNSTEADY TURBULENT VELOCITY PROFILING IN OPEN CHANNEL FLOWS AND TIDAL BORES USING A VECTRINO PROFILER

AUTHORS: Xinqian LENG and Hubert CHANSON

HYDRAULIC MODEL REPORTS

This report is published by the School of Civil Engineering at the University of Queensland. Lists of recently-published titles of this series and of other publications are provided at the end of this report. Requests for copies of any of these documents should be addressed to the Civil Engineering Secretary.

School of Civil Engineering
The University of Queensland
Brisbane QLD 4072
AUSTRALIA

Telephone: (61 7) 3365 4163
Fax: (61 7) 3365 4599

URL: http://www.civil.uq.edu.au/

First published in 2016 by
School of Civil Engineering
The University of Queensland, Brisbane QLD 4072, Australia

ISBN No. 978-1-74272-145-3

The University of Queensland, St Lucia QLD, Australia

Unsteady Turbulent Velocity Profiling in Open Channel Flows and Tidal Bores using a Vectrino Profiler

by
Xinqian LENG
Ph.D. Research student, The University of Queensland, School of Civil Engineering, Brisbane QLD 4072, Australia
and
Hubert CHANSON
Professor, The University of Queensland, School of Civil Engineering, Brisbane QLD 4072, Australia, Email: h.chanson@uq.edu.au

HYDRAULIC MODEL REPORT No. CH101/15
ISBN 978-1-74272-145-3
The University of Queensland, School of Civil Engineering,
February 2016

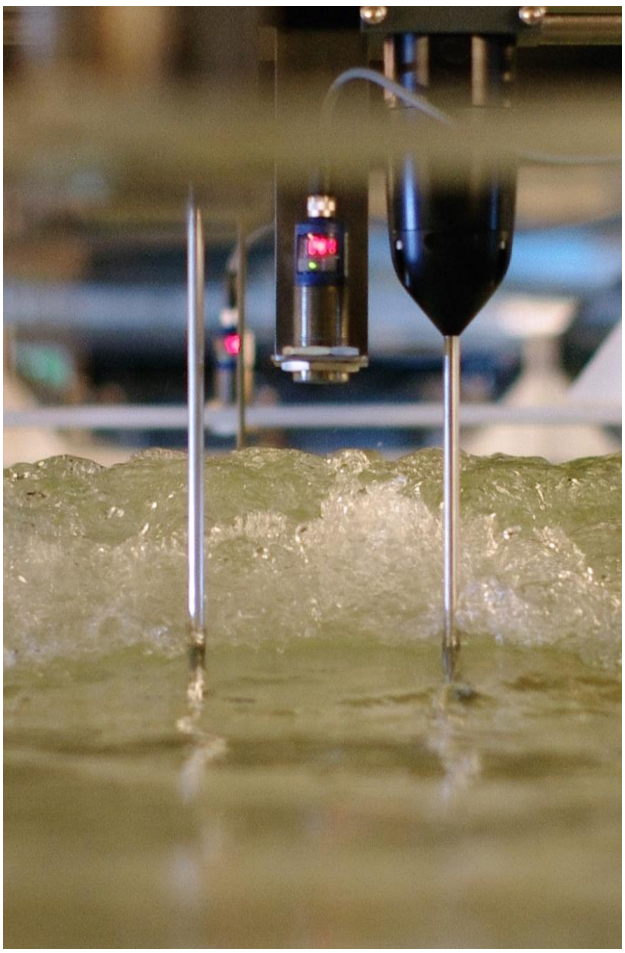

Incoming breaking bore with ADV Vectrino+ and ADV Vectrino II Profiler in the foreground, with an acoustic displacement meter unit in between

ABSTRACT

New experiments were conducted using an acoustic Doppler velocimeter (ADV) Vectrino II Profiler under controlled flow conditions in a relatively large-size laboratory facility. The aim of the experiments was to study the unsteady turbulent properties of tidal bores propagating in open channel flows, with a fine spatial and temporal resolution. The ADV Profiler was equipped with a fixed stem and down-looking head, able to sample simultaneously the instantaneous velocities at 35 points in a 35 mm vertical profile. The sampling frequency was 100 Hz, and the Profiler was synchronised with a series of acoustic displacement meters (ADMs) sampling at the same frequency for the measurements of instantaneous water depth. The physical study encompassed a wide range of steady and rapidly-varied unsteady flow conditions, the latter being tidal bores with Froude numbers ranging from 1.2 to 2.1. The unsteady velocity measurements were performed using an ensemble-averaged technique, in which all experiments were repeated 25 times and the median flow properties and their fluctuations were obtained.

Key experimental findings of the present study included the followings. First the unsteady velocity and Reynolds stress data measured using an ADV Vectrino II Profiler agreed closely with previous unsteady velocity and stress data measured by a (traditional) ADV Vectrino+. Second the Profiler data highlighted that not only in the initially steady flow, but also during the rapidly varied and unsteady flow phases, the longitudinal velocity component within the inner wall region followed the log law for smooth turbulent flows. Third the turbulent time and length scales of the flow before, during and after the passage of tidal bores were analysed from the Profiler data; the results suggested the anisotropic nature of the flow with much larger turbulent time and length scales in the longitudinal and vertical directions compared to the transverse direction. The orders of magnitude of turbulent time and length scales compared well with previous experimental findings. Fourth the present study found errors in estimating the time-averaged velocity and velocity fluctuations (RMS) outside of the developing turbulent boundary layers for all flow conditions. The results also indicated errors in velocity fluctuations (RMS) within the turbulent boundary layer, except for the "sweet spot" of the measuring profile (usually located at the mid-point). The errors were believed to be instrumental, and the present study chose to avoid conducting experiments at the locations where obvious errors were detected.

Overall, the study demonstrated that the propagation of tidal bores is a highly unsteady turbulent process, and the performance of Vectrino II Profiler in such a rapidly-varied unsteady turbulent flow was satisfactory, provided that careful validation was undertaken for all Profiler outputs.

Keywords: Tidal bores, Unsteady turbulence, Instantaneous velocity, Turbulent Reynolds shear stresses, Ensemble-averages, Physical modelling, Turbulent time and length scales, ADV Vectrino II Profiler, acoustic Doppler velocimetry.

TABLE OF CONTENTS

LIST OF SYMBOLS

The following symbols are used in this report:

A channel cross-section area (m^2);

A_1 initial channel cross-section area (m^2) immediately prior to the tidal bore passage;

B free-surface width (m);

B_1 initial free-surface width (m) immediately prior to the tidal bore passage;

D_H hydraulic diameter (m);

d water depth (m);

d_1 initial water depth (m) immediately prior to the tidal bore passage;

d_b brink depth (m);

d_2 conjugate water depth (m) immediately behind the tidal bore;

Fr Froude number;

Fr_o Froude number of initial subcritical flow:

$$Fr_o = \frac{V_1}{\sqrt{g \times d_1}}$$

Fr_1 tidal bore Froude number defined as:

$$Fr_1 = \frac{V_1 + U}{\sqrt{g \times \frac{A_1}{B_1}}}$$

For a bore in a rectangular channel:

$$Fr_1 = \frac{V_1 + U}{\sqrt{g \times d_1}}$$

f Darcy-Weisbach friction factor;

g gravity acceleration (m/s^2): $g = 9.80$ m/s^2 in Brisbane, Australia;

H total head (m);

h Tainter gate opening (m) after gate closure;

$L_{z,i}$ turbulent integral length scale (m) which representing a characteristic vertical size of a large vortical structure found in the velocity direction i;

N exponent;

Q water discharge (m^3/s);

q water discharge per unit width (m^2/s);

R_{ii} normalised auto-correlation function of the i-velocity fluctuations;

$R_{z1z2,i}$ cross-correlation of instantaneous velocity i-component signals measured simultaneously between two points z_1 and z_2 separated by a vertical distance Δz in a vertical profile;

S_f friction slope;

S_o bed slope: $S_o = \sin\theta$;

T_E Eulerian integral time scale (s), also called auto-correlation time scale;

$T_{z,i}$	turbulent integral time scale (s) characterising the time scale (or lifespan) of a large vortical structure found in the velocity direction i;
t	time (s); herein t = 0 at Tainter gate closure;
U	celerity (m/s) of the bore roller toe positive upstream;
V	instantaneous velocity (m/s);
$\overline{V}$	ensemble-averaged velocity (m/s);
$\vec{V}$	velocity vector;
V_{recirc}	maximum recirculation velocity (m/s) at end of deceleration phase;
V_{max}	free-stream velocity (m/s);
V_x	instantaneous longitudinal velocity component (m/s);
V_y	instantaneous horizontal transverse velocity component (m/s);
$V_{y,min}$	minimum transverse velocity (m/s) after the arrival of the bore in the upper water column;
V_z	instantaneous vertical velocity component (m/s);
$V_{z,max}$	maximum vertical velocity in the upper water column (m/s) at bore arrival;
V_z'	initial vertical acceleration (m/s^2) at bore arrival;
V_1	initial cross-sectional averaged flow velocity (m/s) immediately prior to the tidal bore passage;
V_{25}	instantaneous first quartile of velocity ensemble (m/s);
V_{75}	instantaneous third quartile of velocity ensemble (m/s);
V_*	shear velocity (m/s);
v	velocity fluctuation (m/s): $v = V - \overline{V}$
v_x	instantaneous longitudinal velocity fluctuation (m/s);
v_y	instantaneous horizontal transverse velocity fluctuation (m/s);
v_z	vertical velocity fluctuation (m/s);
v_x'	root mean square of longitudinal velocity fluctuation (m/s);
v_y'	root mean square of horizontal transverse velocity fluctuation (m/s);
v_z'	root mean square of vertical velocity fluctuation (m/s);
W	rectangular channel width (m);
x	longitudinal distance (m) positive downstream;
x_{gate}	longitudinal position (m) of Tainter gate;
y	transverse distance (m) positive towards the right sidewall;
z	vertical distance (m) positive upwards;
z_{max}	vertical elevation (m) of highest point of velocity profile;
α	void fraction;
Δt_V	time lag (s) between bore passage and maximum velocity fluctuations;
ΔT	time lag (s) between bore passage and maximum shear stress fluctuations;
Δy	transverse separation (m);
Δz	vertical separation (m): $\Delta z = z_1 - z_2$;

Δz_{max}	maximum vertical separation (m);
δ	boundary layer thickness (m) defined in terms of 99% of the free-stream velocity;
κ	von Karman constant: $\kappa = 0.4$;
μ	water dynamic viscosity (Pa.s);
ν	water kinematic viscosity (m^2/s);
θ	angle between channel bed slope and horizontal;
ρ	water density (kg/m^3);
τ	time lag (s);
τ_{ij}	Reynolds shear stress component (Pa);
τ_o	boundary shear stress (s);
$\|\|\tau\|\|$	Reynolds stress tensor;

Subscript

max	maximum value;
med	cross-sectional median value;
median	cross-sectional median value;
i	coordinate: i = x, y or z;
j	coordinate: j = x, y or z;
x	longitudinal component;
y	horizontal transverse component;
z	vertical component;
1	initial flow property immediately prior to the tidal bore passage;
25	first quartile;
75	third quartile;

Abbreviations

ADM	acoustic displacement meter;
ADV	acoustic Doppler velocimetry;
AEB	advanced engineering building;
ms	millisecond;
PDF	probability distribution function;
RMS	root mean square;
SNR	signal to noise ratio;
STD	standard deviation;
s	second;
UQ	The University of Queensland.

1. INTRODUCTION

In an open channel, steady flow conditions may be achieved when the discharge and boundary conditions remain constant for a reasonable period of time. The operation of any regulation device such as a gate is associated an unsteady flow motion. Unsteady open channel flows may be analysed using the Saint-Venant equations and the method of characteristics in channels of relatively simple geometry. The Saint-Venant equations decribe the variations with time of the water depth d and flow velocity V:

$$B \times \frac{\partial d}{\partial t} + A \times \frac{\partial V}{\partial x} + B \times V \times \frac{\partial d}{\partial x} + V \times \left(\frac{\partial A}{\partial x} \right)_{d=constant} = 0 \quad (1\text{-}1)$$

$$\frac{\partial V}{\partial t} + V \times \frac{\partial V}{\partial x} = -g \times \frac{\partial d}{\partial x} + g \times (S_o - S_f) \quad (1\text{-}2)$$

where x is the longitudinal co-ordinate positive downstream, A is the flow cross-section area, B is the free-surface width, g is the gravity acceleration, S_o is the bed slope and S_f is the friction slope (LIGGETT 1994, CHANSON 2004). A typical geophysical application is a tidal bore (Fig. 1-1). A tidal bore may form during the spring tides when the tidal range exceeds 5-6 m and the flood tide is confined to a narrow funnelled estuary with low freshwater levels (CHANSON 2011). Its propagation is known to be a highly turbulent process, with intensive mixing and large scale of sediment motions occurring underneath. The sediment motions involve the stirring and mixing of the bed materials, advection and diffusion of organic matters, and transportation of fish eggs (CHEN et al. 1990, TESSIER and TERWINDT 1994, CHANSON and TAN 2010, KHEZRI and CHANSON 2012a,b). The existence of a tidal bore is vital to the balance of ecosystem in rivers and estuaries, maintain of bio habitats and geological structures, and the proper functioning of ecological processes. Other real-world examples of tidal bore-like motion include the incoming front of a tsunami entering a river channel and the propagation of flood tides (TANAKA et al. 2012, CHANSON and LUBIN 2013). Such a event can be hazardous, causing serious damages to natural banks, man-made structures and human lives.

Some famous tidal bores include the bore in Qiangtang River (China), Garonne and Dordogne Rivers (France), Styx and Daly Rivers (Australia) (CHANSON 2011). Figure 1-1 illustrates real bore events in the Qiangtang River and Carentan channel, featuring respectively a breaking bore and an undular bore. These have become major tourism attractions to surfers and cultural heritage of the local community. The formation of a tidal bore is a delicate process which can be easily disturbed by change of boundary conditions due to mankind activities. The bore in Seine River in France, which was known to be one of the largest bore event worldwide, no longer exists nowadays, as a result of extensive training works and dredging (CHANSON 2011). Once formed, the tidal bore is analogical to a translating hydraulic jump (RAYLEIGH 1908, LIGHTHILL 1978). In a

rectangular prismatic channel, the shape of the bore front may be characterised by its Froude number Fr_1 defined as:

$$Fr_1 = \frac{V_1 + U}{\sqrt{g \times d_1}} \quad (1\text{-}3)$$

where V_1 is the initial flow velocity positive downstream, U is the bore celerity positive upstream, g is the gravitational acceleration, d_1 is the initial water depth. Figure 1-2 illustrates the propagation of a tidal bore in a rectangular channel, with a photograph taken in the laboratory and a definition sketch. For $Fr_1 < 1$, the tidal wave cannot become a tidal bore. For Fr_1 between unity and 1.3-1.4, the bore is undular, with bore front followed by a train of secondary waves that are well-formed, quasi-periodic undulations (TRESKE 1994, KOCH and CHANSON 2008, SIMON and CHANSON 2013). For $Fr_1 > 1.4$ to 1.5, the leading edge of the bore is characterised by a breaking roller (HORNUNG et al. 1995, LENG and CHANSON 2015a,b). The bore roller is associated with a sudden increase in water depth, a highly turbulent flow with large-scale vortical structures, some kinetic energy dissipation, a two-phase air-water flow region and strong turbulence interactions with the free surface associated with splashes and droplet ejections (KOCH and CHANSON 2009, CHANSON 2010).

Herein, new unsteady velocity measurements were performed systematically under controlled flow conditions in a relatively large laboratory facility. Steady and unsteady velocity characteristics were recorded usinga Nortek^{TM} acoustic Doppler velocimeter Vectrino II Profiler equipped with a fixed-probe down-looking head. The ADV Profiler was a high-resolution profiling velocimeter, able to sample the longitudinal, transverse and vertical velocities for a complete vertical profile of up to 35 mm in length. An ensemble-averaged technique was applied in the present study to investigate tidal bores. In unsteady flows, all experiments were repeated 25 times for each controlled flow condition and the results were ensemble-averaged. The number of repeats, 25 in the present study, was determined based upon a sensitivity study. The velocity characteristics, Reynolds stress properties and turbulent scales were deduced from the ensemble-averaged velocity measurements. The quality and accuracy of the present data set obtained using the Profiler were validated against data collected with an Nortek^{TM} acoustic Doppler velocimeter Vectrino+. The report is supported by appendices, including a sensitivity analysis of Vectrino II Profiler ensemble-averaged measurements and spectral analyses of steady flow velocity measured by the Vectrino II Profiler.

(A) Breaking bore in Qiantang River, Yanguan, China (12/10/2014) - Bore propagation from left to right

(B) Undular bore in Carentan channel, Carentan, France (21/05/2015) - Bore propagation from right to left

Fig. 1-1 - Photographs of tidal bore events in China and France.

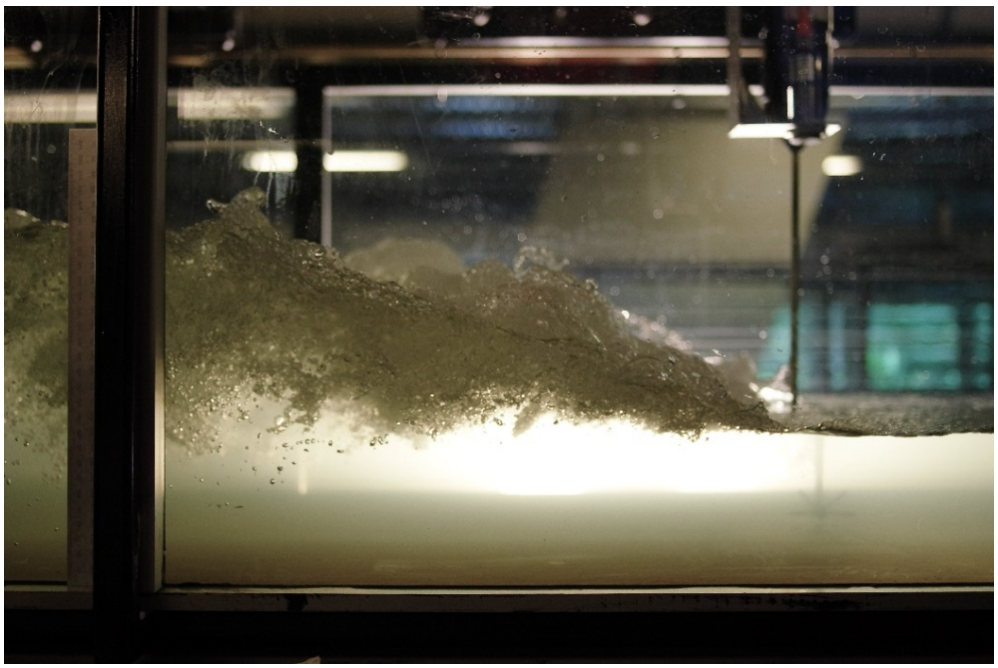

(A) Photograph of a breaking bore in the AEB hydraulic laboratory of the University of Queensland ($Q = 0.102\ m^3/s$, $Fr_1 = 2.3$) - Bore propagation from left to right

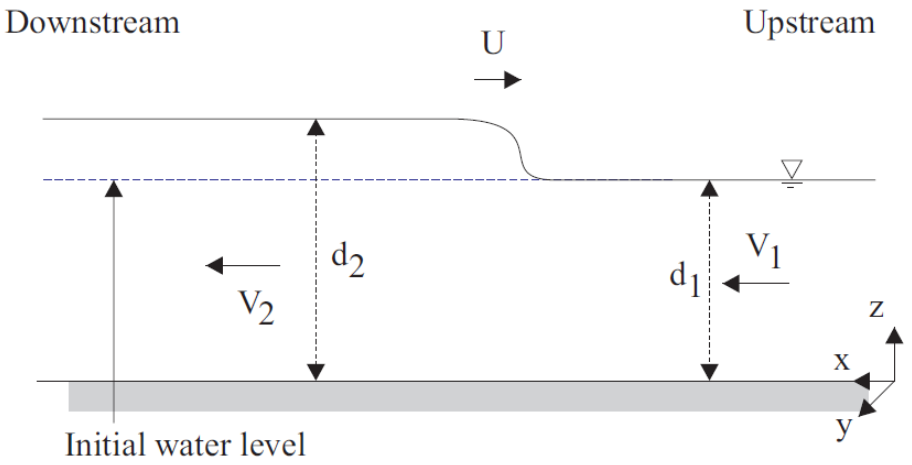

(B) Definition sketch of a tidal bore in a rectangular prismatic channel

Fig. 1-2 - Tidal bore propagation in rectangular prismatic channel.

2. EXPERIMENTAL FACILITY AND INSTRUMENTATION

The experimental channel was 19 m long and 0.7 m wide, made of glass side walls and smooth PVC horizontal bed with adjustable channel slope. The same channel was previously used by LENG and CHANSON (2015a,b,c). The initially steady flow was supplied by the upstream water tank equipped with flow calming devices and flow straighteners, leading to the glass-sidewalled test section through a smooth convergent intake. The discharge was measured by a magneto flow meter with an accuracy of 10^{-5} m^3/s, and was checked against the brink depth d_b at the downstream end of the flume ([1]). A fast-closing Tainter gate was located next to the downstream end of the channel at x = 18.1 m, where x is measured from the upstream end of the channel. The tidal bore was generated by rapidly closing the Tainter gate and the bore propagated upstream (Fig. 2-1). A radial gate was located at x = 18.88 m to control the initial water depth. The Tainter and radial gates were identical to those previously used by and described in LENG and CHANSON (2015c). Figure 2-1 presents an overview of the experimental channel and facility setup.

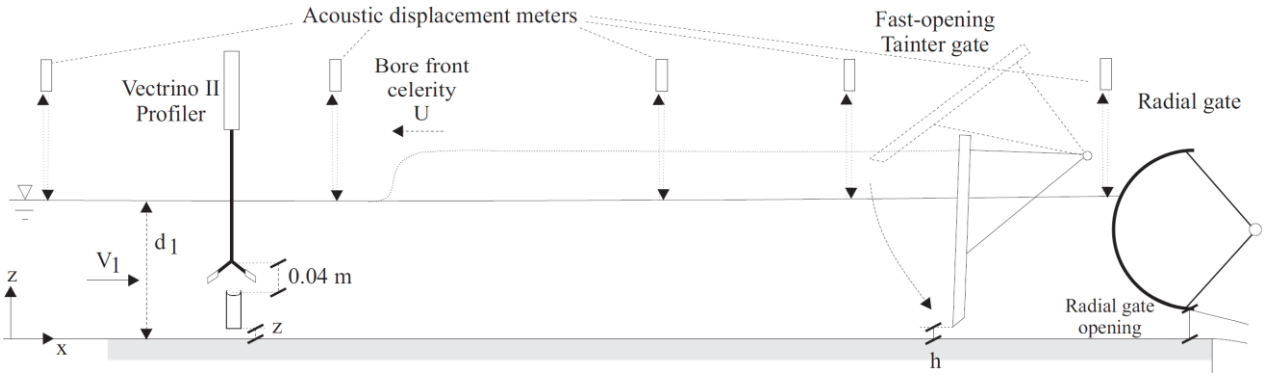

Fig. 2-1 - Definition sketch of the experimental facility.

2.1 ACOUSTIC DISPLACEMENT METER (ADM)

In steady flows, the water depths were measured using point gauges with an accuracy of 0.001 m. The unsteady water depths were recorded with a series of acoustic displacement meters (ADMs). A Microsonic™ Mic+35/IU/TC unit was located at x = 18.17 m immediately downstream of the Tainter gate. Further nine acoustic displacement meters Microsonic™ Mic+25/IU/TC were spaced along the channel at x = 17.81 m, 17.41 m, 14.96 m, 12.46 m, 9.96 m, 8.5 m, 6.96 m, 3.96 m and 1.75 m. A photograph of ADM sensor mounting is shown in Figure 2-2. All acoustic displacement meters (ADMs) were calibrated against point gauge measurements in steady flows and the sensors were sampled at 100 Hz. Table 2-1 reports some information on the characteristics of the sensors.

[1] with the Tainter and radial gates fully-opened.

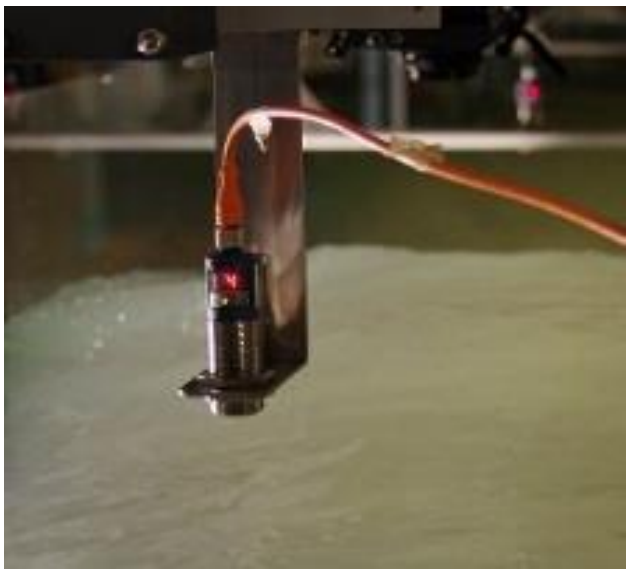

Fig. 2-2 - Mounting of the acoustic displacement meter (ADM) above the channel centreline.

Table 2-1 - Characteristics of the ultrasonic acoustic displacement meters

Characteristic parameter	Microsonic™ Mic+25	Microsonic™ Mic+35
Accuracy (mm)	0.18	0.18
Response time (ms)	50	70
Ultrasonic frequency (kHz)	320	400
Wave length (at 20ºC) (mm)	1.1	0.9
Detection zone radius at operating range (mm)	22	37.5
Blind zone (mm)	30	60
Operating range (mm)	250	350
Maximum range (mm)	350	600

Reference: Microsonic™ webpage {http://www.microsonic.de/}

2.2 VELOCITY MEASUREMENTS

Two velocimeters were deployed in the present study. The measurements were performed with a Nortek™ acoustic Doppler velocimeter (ADV) Vectrino II Profiler (Serial number P27338, Hardware ID VNO 1366) and a Nortek™ acoustic Doppler velocimeter Vectrino+ (Serial number P21419, Hardware ID VNO 0436). The latter, referred to as ADV in the following text, was used to validate the Profiler data.

The Vectrino II Profiler is a high-resolution acoustic Doppler velocimeter used to measure turbulence and three-dimensional water velocity in a wide variety of applications from the laboratory to the ocean (Nortek 2012). The basic measurement technology is coherent Doppler processing, which is characterised by accurate data and no appreciable zero offset (ZEDEL and HAY 2011, Nortek 2012). Herein the Vectrino II Profiler was equipped with a fixed downward-

looking head, equipped with one central emitter and four receivers. The Vectrino II Profiler was capable of recording velocity components simultaneously in a vertical profile of up to 35 mm in height (Fig. 2-3A). The minimum distance from the emitter was 40 mm to the first point of the profile ([2]). The height of each cell was 1 mm and a total of 35 cells were sampled in a 35 mm profiling range. The velocity range was ±1.0 m/s and the sampling frequency was 100 Hz ([3]). The Profiler was located at x = 7.87 m or 8.5 m, sampling simultaneously with the ADMs. The synchronisation between instruments was within ± 1 ms.

The ADV Vectrino+ was equipped with a three-dimensional side-looking head, capable of measuring three velocity components (longitudinal, transverse and vertical) at a single point within the water column (Fig. 2-3B). The velocity range was ±1.0 m/s and the sampling rate was 100 Hz. The data accuracy was 1% of the velocity range. The ADV was set up with a transmit length of 0.3 mm, a sampling volume of 1.5 mm height and power setting High.

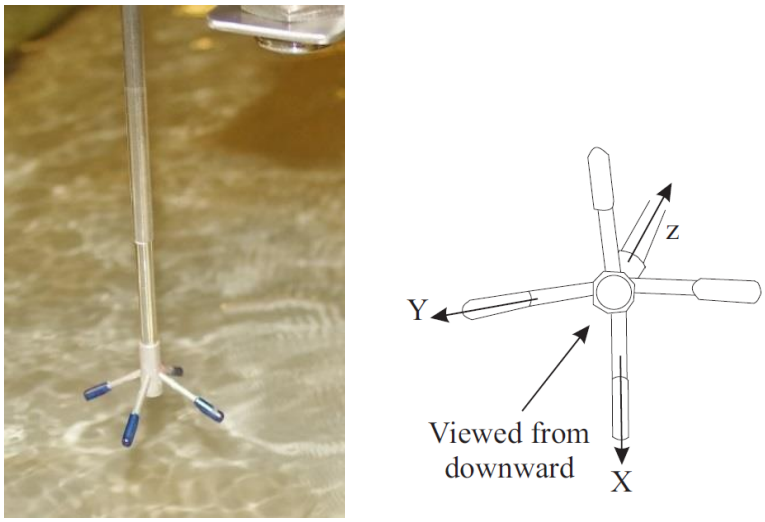

(A) ADV Vectrino II Profiler: photograph (left) and a coordinated sketch (right)

[2] For a number of preliminary experiments, a minimum distance of 45 mm and a profile of 30 mm height were used. For all instantaneous and ensemble-averaged experiments, a minimum distance of 40 mm and a profile of 35 mm height were utilised.

[3] When the ADV Vectrino II Profiler and ADV Vectrino+ units were sampled simultaneously, both units were synchronised and sampled at 100 Hz. When used alone, the ADV Vectrino II Profiler unit was sampled at 100 Hz. For preliminary experiments on interactions between instruments, the ADV Vectrino II Profiler was sampled at 100Hz while the ADV Vectrino+ was sampled at 200 Hz (Appendix A). Previous experiments with the ADV Vectrino+ unit only were recorded at 200 Hz (LENG and CHANSON 2015c).

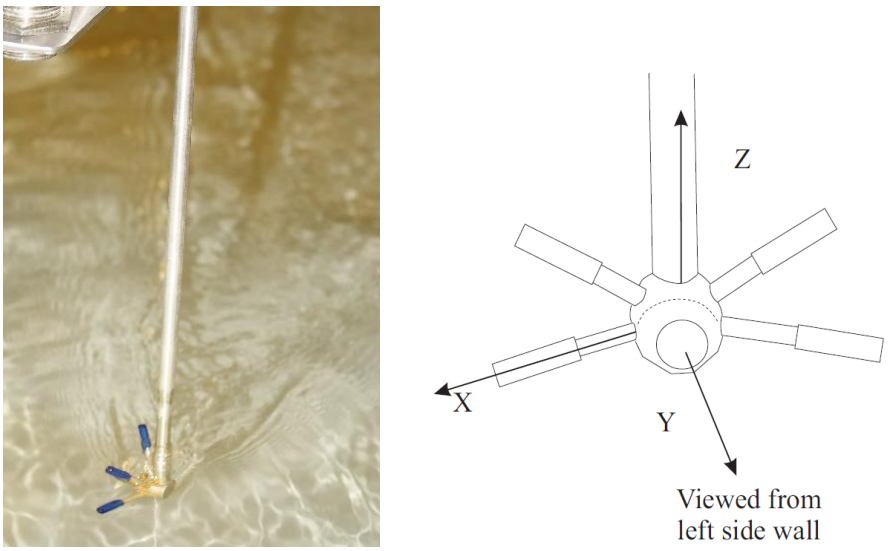

(B) ADV Vectrino+: photograph (left) and a coordinated sketch (right)

Fig. 2-3 - Photographs and sketches of ADV Vectrino II Profiler and ADV Vectrino+.

The output data of the Profiler were saved as MATLAB files. Steady flow data were post-processed by the MATLAB program VTMT version 1.1, designed and written by Jan BECKER from Federal Waterways Engineering and Research Institute (BAW), Karlsruhe (BECKER 2014). In steady flows, the post-processing of ADV Vectrino II Profiler data included the removal of data with average correlation values less than 90% and average signal to noise ratio less than 5 dB ([4]). In addition, the phase-space thresholding technique developed by GORING and NIKORA (2002) was applied to removal spurious points in the data set. In the unsteady flows, the above post-processing technique was not applicable (NIKORA 2004, *Person. Comm.*, CHANSON 2008,2010, KOCH and CHANSON 2009) and raw data was used directly for analysis.

2.3 EXPERIMENTAL FLOW CONDITIONS

During unsteady flow experiments, the tidal bore was generated by rapidly closing the downstream Tainter gate and the bore propagated upstream. The gate closure time was less than 0.2 s, short enough to have no effect on the bore propagation. For each experiment, all instruments were started 60 s prior to the gate closure, and the sampling ended when the bore reached the upstream intake.

In the present study, an ensemble-averaged technique was applied. Specifically 25 experimental runs were repeated for each set of flow conditions. The number of repeats was determined based upon a sensitivity analysis (Appendix B). The results were ensemble-averaged to obtain the median

[4] For comparison, the post-processing of ADV Vectrino+ data was conducted with the software WinADV 2.028 and included the removal of data with average correlation values less than 60% and average signal to noise ratio less than 5 dB, the application of the phase-space thresholding despiking technique and the removal of communication errors.

properties and the associated fluctuations.

The ensemble-averaged measurements were performed systematically at x = 8.5 m under controlled flow conditions. The channel slope S_o, Tainter gate opening h after the rapid closure, and opening of the downstream radial gate were adjusted to achieve a wide range of Froude numbers. A series of overlapping velocity profile measurements were conducted at different vertical elevations within the initial flow depth, each profile covering a vertical range of 35 mm. Both breaking and undular bores were experimented. The detailed experimental flow conditions were summarised in Table 2-2.

Table 2-2 - Experimental flow conditions for ensemble-averaged Profiler measurements

S_o	Q (m^3/s)	d_1 (m)	Radial gate opening (m)	h (m)	z_{max}/d_1	Bore type	Instrumentation	U (m/s)	Fr_1
0	0.099	0.169	N/A	0	0.2	Breaking	Profiler & ADMs	1.2	1.6
0	0.103	0.173	N/A	0	0.3	Breaking	Profiler & ADMs	1.3	1.6
0	0.099	0.17	N/A	0	0.7	Breaking	Profiler & ADMs	1.1	1.6
0	0.099	0.196	0.125	0.071	0.2	Undular	Profiler & ADMs	1.0	1.2
0	0.099	0.197	0.125	0.071	0.3	Undular	Profiler & ADMs	1.0	1.2
0	0.099	0.199	0.125	0.071	0.6	Undular	Profiler & ADMs	1.0	1.2
0.0075	0.099	0.097	N/A	0	0.4	Breaking	Profiler & ADMs	0.6	2.1

Note: z_{max}: vertical elevation of highest point in velocity profile, measured from the channel bed ([5]).

2.4 INITIALLY STEADY FLOW CONDITIONS

Some issues with the ADV Vectrino II Profiler were documented in steady turbulent flows: e.g. poor signal quality outside the measurements sweet spot, inaccurate velocity variance and error estimation of mean velocity at the ends of the measurement profile (ZEDEL and HAY 2011, MACVICAR et al. 2014, THOMAS and McLELLAND 2015, Present study). However mean velocity profiles and Reynolds stress measurements using a ADV Vectrino II Profiler were found to be in good agreement with validated instrumentations, including ADV Vectrino and PIV (CRAIG et al. 2011, ZEDEL and HAY 2011, MACVICAR et al. 2014). Compared to the ADV Vectrino+ equipped with a side-looking head, an advantage of the ADV Vectrino II Profiler was its ability to record velocity data at points as close as 1 mm from the channel bed, although the effects of the bed proxirnity on the ADV Profiler output should be carefully assessed ([6]). The boundary layer characteristics within the inner flow region may hence be quantified.

At x = 8.5 m, the experimental data indicated that the initially-steady flow was partially developed

[5] With the ADV Vectrino II Profiler, the first point was the highest point in the velocity profile.

[6] The proximity of a solid boundary was found to affect adversely traditional ADVs' outputs (FINELLI et al. 1999, MARTIN et al. 2002, CHANSON et al. 2007).

and the dimensionless boundary layer thickness δ/d_1 was between 0.3 and 0.5 (LENG and CHANSON 2015c). In a steady developing boundary layer flow, the inner flow region may be sub-divided into a wall region, a buffer zone and a viscous sublayer (SCHLICHTING 1979, POPE 2000, CHANSON 2009). In the wall region, the vertical distribution of the time-averaged streamwise velocity V_x follows a logarithmic velocity law, also called the log law or law of wall. For a smooth turbulent boundary layer, the log law gives:

$$\frac{V_x}{V_*} = \frac{1}{\kappa} \times Ln\left(\rho \times \frac{V_* \times z}{\mu}\right) + D_1 \qquad 30 \text{ to } 70 < \rho \times \frac{V_* \times z}{\mu} \text{ and } \frac{z}{\delta} < 0.1 \text{ to } 0.2 \quad (2\text{-}1)$$

where V_x is the longitudinal velocity, V_* is the shear velocity: $V_* = (\tau_o/\rho)^{1/2}$, κ is the von Karman constant ($\kappa = 0.4$), τ_o is the boundary shear stress, z is the vertical elevation from the surface of the channel bed, ρ and μ are the fluid density and dynamic viscosity respectively, D_1 is an integration constant equal to 5 (SCHLICHTING 1979, CHANSON 2014).

Present longitudinal velocity data within the inner region of the boundary layer ($z/\delta < 0.1$ to 0.2) were compared to the theoretical log law profile (Eq. (2-1)). In each case, the shear velocity was estimated using the best fit of the log law. Figure 2-5 presents whole profiles of time-averaged longitudinal velocity for a range of flow conditions; the ADV Profiler data are compared to previous ADV measurements (LENG and CHANSON 2015c) and the log law within the inner region. Overall, the majority of the inner region data followed the theoretical log law curve, except for the first four to five data points, corresponding to locations less than 6 mm from the bed. The Profiler measurements compared well with previous ADV measurements, except in the close vicinity of the bed ($z/\delta < 0.1$), where no ADV data was available due to physical limitation (i.e. side-looking head design).

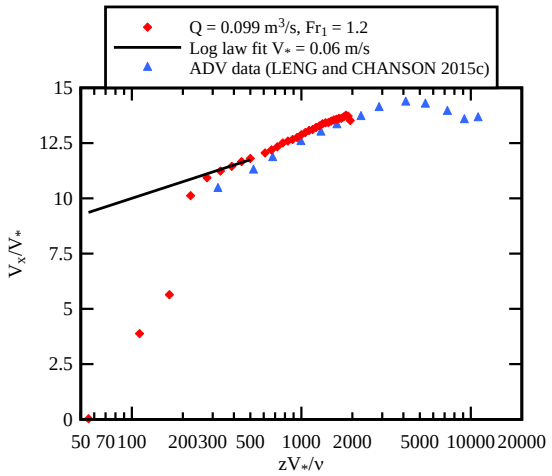

(A) Q = 0.099 m^3/s, d_1 = 0.197 m

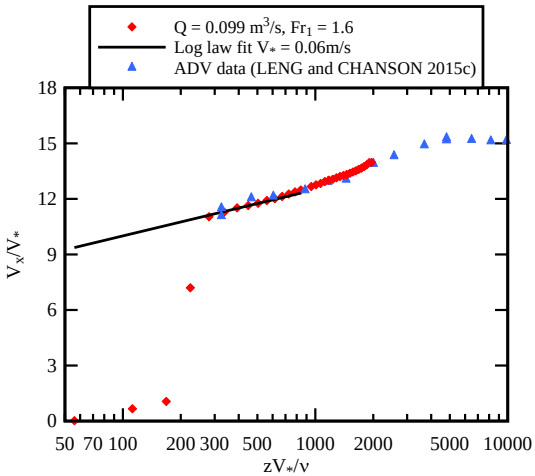

(B) Q = 0.099 m^3/s, d_1 = 0.171 m

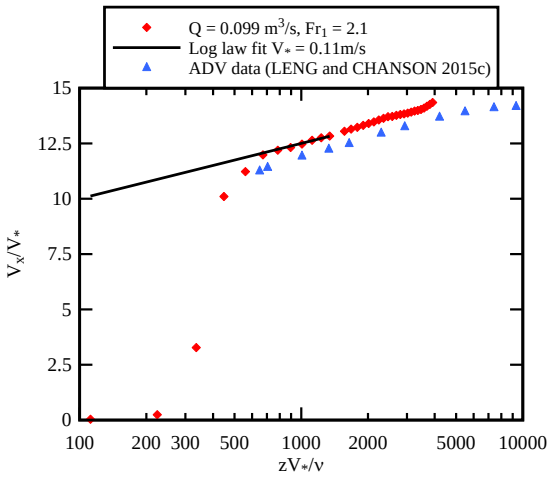

(C) Q = 0.099 m^3/s, d_1 = 0.097 m

Fig. 2-5 - Logarithmic velocity profiles in the initially-steady flow at x = 8.5 m - Present Profiler data in red symbols, ADV data (LENG and CHANSON 2015c) in blue symbols and theoretical log law with a black line.

In steady flows, the boundary friction τ_o may be estimated using several methods. Herein, τ_o deduced from the best fit of the log law best and of longitudinal free-surface profile, and compared to the tangential Reynolds stress $\rho \times v_x \times v_z$ in the vicinity of the bed, The results are summarised in Table 2-3 in terms of the dimensionless boundary shear stress (i.e. Darcy-Weisbach friction factor). In Table 2-3, f_1 is calculated based upon the shear velocity of the log law best fit: $f_1 = 8 \times V_*^2/V_1^2$, f_2 is estimated by fitting a backwater profile to the steady flow free-surface data ([7]), and f_3 is approximated based upon the tangential Reynolds stress $\rho \times v_x \times v_z$ in steady flows very near the bed. Indeed, for vertical elevations immediately above the channel bed, the tangential Reynolds stress $\rho \times v_x \times v_z$ may be used to approximate the boundary shear stress (NEZU and NAKAGAWA 1993). All methods yielded boundary friction factors of the same order of magnitude, ranging from 0.02 to 0.06, but for one data. The results suggested however slight quantitative differences in terms of dimensionless boundary shear stress. The best fit of the log law yielded the highest boundary friction factors compared to the other two methods. The backwater calculations and the Reynolds stress estimate gave very similar results. The boundary friction approximated using the tangential Reynolds stress data $\rho v_x v_z$ was considered to be the least accurate, possibly due to some effect of bubbles entrained in the wake of the intruding Profiler stem.

[7] In gradually-varied steady open channel flow, the differential form of the energy equation becomes: $\partial H/\partial x = - S_f$, where H is the depth-averaged total head and S_f is the friction slope: $S_f = (f/D_H) \times V^2/(2 \times g)$, with D_H being the hydraulic diameter (HENDERSON 1966, CHANSON 2004). Herein f_2 is the value of the friction factor for which the differential form of the energy equation gave the best data fit in terms of the longitudinal free-surface profile.

Table 2-3 - Free-stream velocity, shear velocity and dimensionless boundary shear stress (Darcy-Weisbach friction factor) in the initially steady flow

Q	d_1	V_1	Fr_1	Fr_o	V_{max}	Log law		Backwater	$\rho \times v_x \times v_z$
						V_*	f_1	f_2	f_3
(m^3/s)	(m)	(m/s)			(m/s)	(m/s)			
0.099	0.197	0.72	1.2	0.52	0.77	0.06	0.06	0.04	0.04
0.099	0.171	0.83	1.6	0.64	0.88	0.06	0.04	0.02	0.03
0.099	0.097	1.46	2.1	1.50	1.58	0.11	0.05	0.02	***0.60***

Notes: Fr_1: bore Froude number; Fr_o: steady flow Froude number; V_{max}: free-stream velocity in steady flow; V_*: shear velocity deduced from best fit of log law; f_1: dimensionless boundary shear stress deduced from best fit of log law ($f_1 = 8 \times V_*^2/V_1^2$); f_2: dimensionless boundary shear stress deduced from best fit of backwater profile to the steady flow free-surface data; f_3: dimensionless boundary shear stress deduced from the tangential Reynolds stress $\rho \times v_x \times v_z$ in steady flows near bed; ***Bold italic***: anomalous/suspicious data point.

The vertical distributions of longitudinal velocity component compared well to previous velocity data recorded using an acoustic Doppler velocimeter (ADV) throughout the entire developing boundary layer (LENG and CHANSON 2015c). The data followed closely a 1/N power law, as seen in Figure 2-6. N ranged from 8 to 11. Overall the vertical distribution of longitudinal velocity component measured by the Profiler were close to that measured by the ADV for all experimental flow conditions, with a closer agreement within the boundary layer (Fig. 2-5 and 2-6). The free-stream velocity data V_{max} are reported in Table 2-3. The data were checked against the equation of conservation of mass. For a power law velocity profile in the boundary layer, this yields:

$$q = \left(\left(\frac{N}{N+1} - 1 \right) \times \frac{\delta}{d_1} + 1 \right) \times V_{max} \times d_1 \quad (2\text{-}2)$$

where q is the discharge per unit width: q = Q/B, B is the channel width, N is derived from the best fit of power law, δ is the boundary layer thickness and d_1 is the initial flow water depth. Equation (2-2) compared well to the measured specific discharge within 10% for all flow conditions. The results indicated that the free-stream velocity of the experimental data satisfied the continuity principle. Outside of the boundary layer, the theoretical velocity distribution was a straight line: $V_x = V_{max}$. The ADV data showed a close match to the theoretical estimate, whereas the ADV Profiler data deviated slightly from the ADV and theoretical results, mostly at the top and bottom cells of each profile as suggested by MACVICAR et al. (2014).

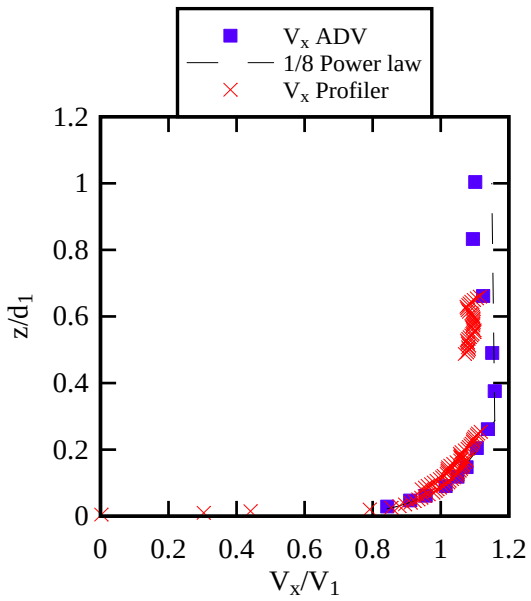

(A) Q = 0.099 m^3/s, d_1 = 0.197 m

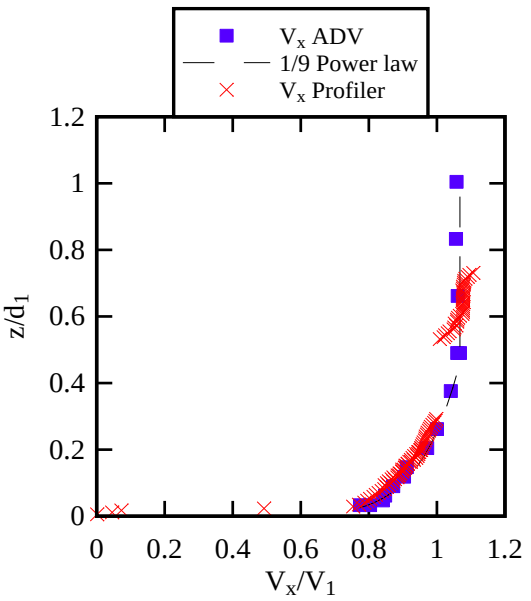

(B) Q = 0.099 m^3/s, d_1 = 0.171 m

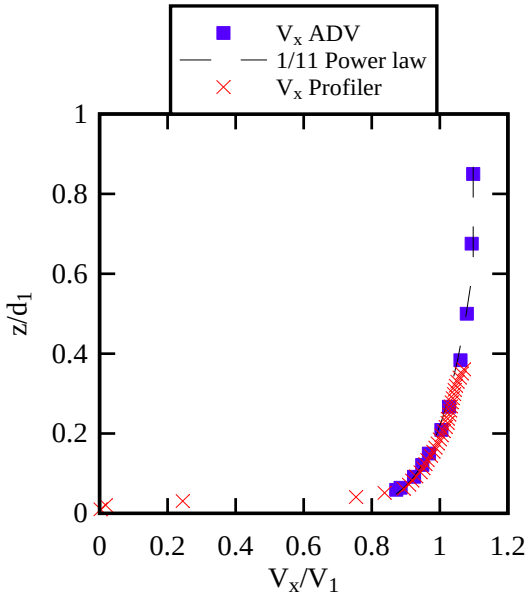

(C) Q = 0.099 m^3/s, d_1 = 0.097 m

Fig. 2-6 - Dimensionless longitudinal velocity distributions in the initially-steady flow at x = 8.5 m - Comparison with ADV data and power law.

3. UNSTEADY VELOCITY MEASUREMENTS USING THE PROFILER

3.1 INSTANTANEOUS VELOCITY MEASUREMENTS

Typical instantaneous velocity data are presented in Figures 3-1 and 3-2. The data showed respectively a breaking and undular bore for Froude numbers of 1.6 and 1.2. The instantaneous time-variation of the water depth, measured at the same location (x = 8.5 m) is indicated with black symbols (Fig. 3-1 & 3-2). The time origin t = 0 corresponded to the time of the rapid Tainter gate closure. Out of the total 35 vertical elevations of a single profile, velocity data for 8 elevations are presented in Figures 3-1 and 3-2 with 0.004 m intervals between two selected elevations. Overall the Profiler data showed comparable instantaneous velocity time-variations to those previously observed using an ADV, documented by LENG and CHANSON (2015c).

The longitudinal velocity data showed a rapid deceleration as the water depth increased during the bore passage, for all elevations and Froude numbers. With undular bores, the longitudinal velocity oscillated out of phase with the oscillations of the free-surface following the bore passage. At low vertical elevations, some recirculation velocity was observed, associated with negative longitudinal velocity components at the end of the deceleration phase with both undular and breaking bores. For undular bores, the range of elevations associated with recirculation velocity was $0 < z/d_1 < 0.2$, while some recirculation was observed for $0 < z/d_1 < 0.3$ to 0.5 with breaking bores. The findings were consistent with the ADV measurements for similar Froude numbers, which highlighted some recirculation next to the bed in breaking and undular bores (LENG and CHANSON 2015c) ([1]). For comparison, field measurements only documented recirculation in prototype breaking bores (CHANSON and TOI 2015), although previous laboratory and numerical studies suggested that recirculation take place in both undular and breaking bores. The differences could be caused by potential scale effects and different bore generation mechanisms in physical, numerical models and prototypes, as well as an absence of prototype measurements in undular bore close to the bed (WOLANSKI et al. 2004).

The transverse and vertical velocity components showed large fluctuations associated with the propagation of tidal bores at all elevations for the range of Froude numbers. The vertical velocity components first increased with the free-surface rise, then decreased before the free-surface reached its maximum value before fluctuating around a zero mean value, the phenomenon being more clearly observed at higher vertical elevations. In undular bores, the vertical velocity oscillated in

[1] In undular bores, some recirculation velocity was observed for $Q = 0.055$ m^3/s, $Fr_1 = 1.2$ and $z/d_1 = 0.1$ with the ADV. For $Q = 0.101$ m^3/s, $Fr_1 = 1.2$ and $z/d_1 = 0.1$, no recirculation was recorded with ADV, although measurements could not be performed for z/d_1 with the ADV Vectrino+. The Profiler data showed recirculation up to $z/d_1 = 0.2$, although the recirculation velocity was close to 0 (i.e. negligible) between $0.1 < z/d_1 < 0.2$.

phase with the oscillation of the free-surface, with periods more distinctive than those measured by the ADV.

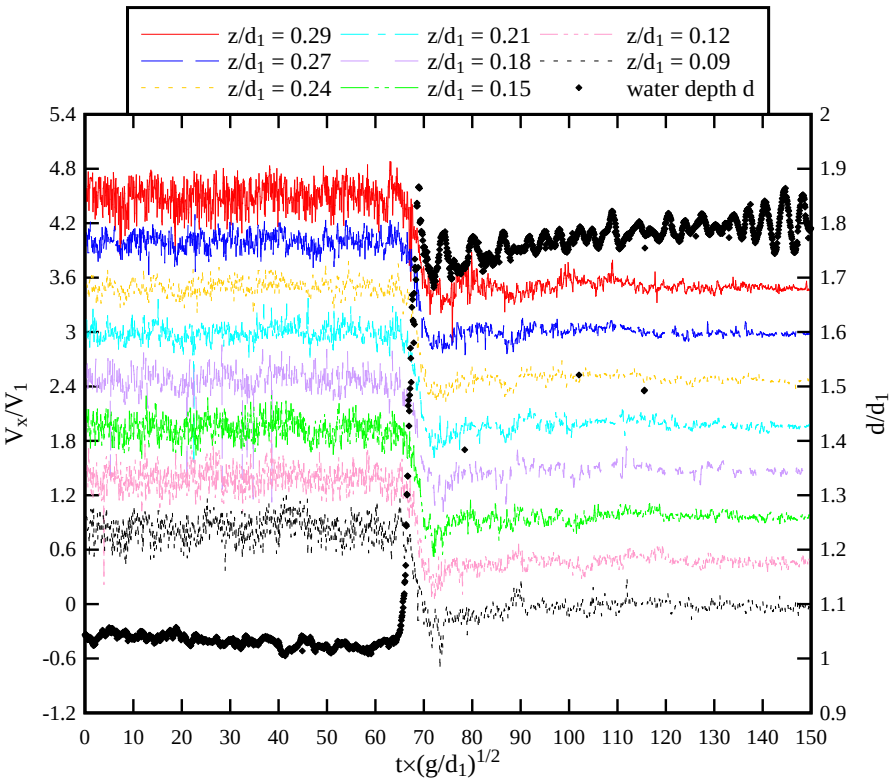

(A) Longitudinal velocity V_x

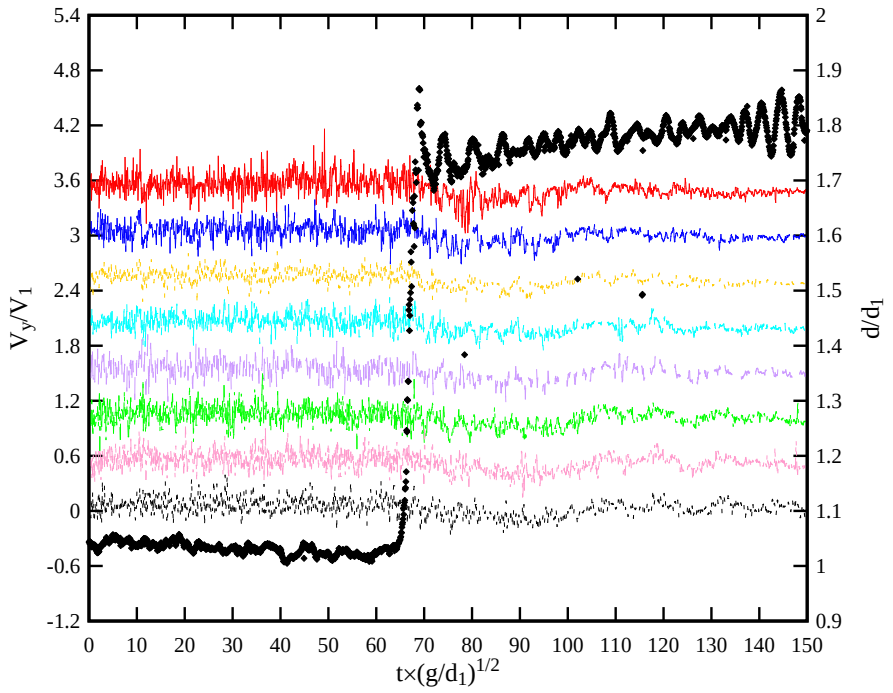

(B) Transverse velocity V_y

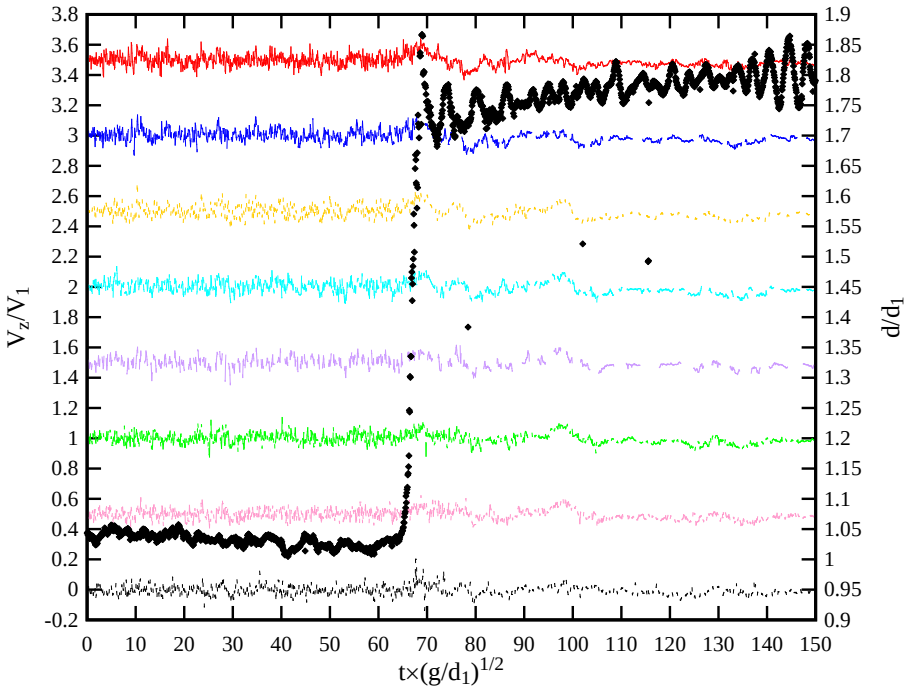

(C) Vertical velocity V_z

Fig. 3-1 - Instantaneous time variations of velocity components for a velocity profile from z = 0.016 m to 0.05 m with instantaneous water depth measured at the velocity sampling location - Flow conditions: Q = 0.099 m^3/s, Fr_1 = 1.6 - Velocity offset by +0.5 for each higher elevation.

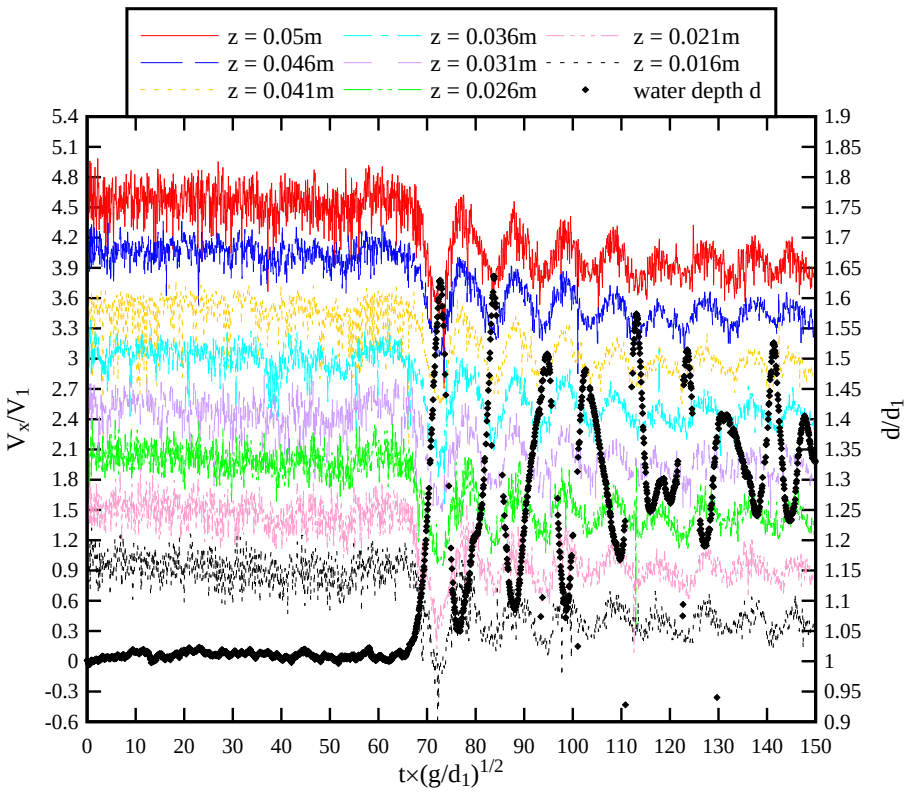

(A) Longitudinal velocity V_x

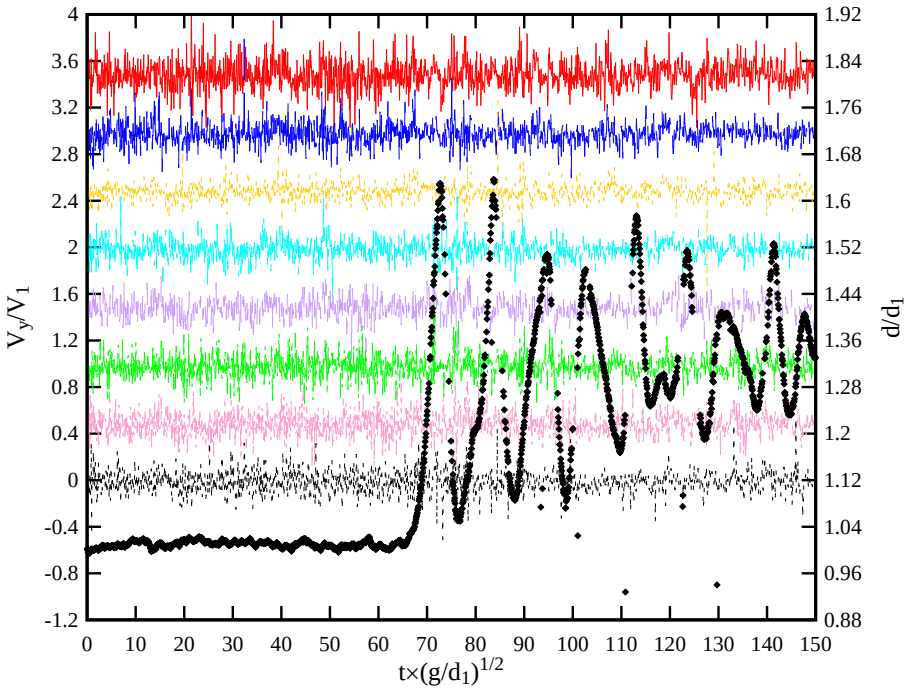

(B) Transverse velocity V_y

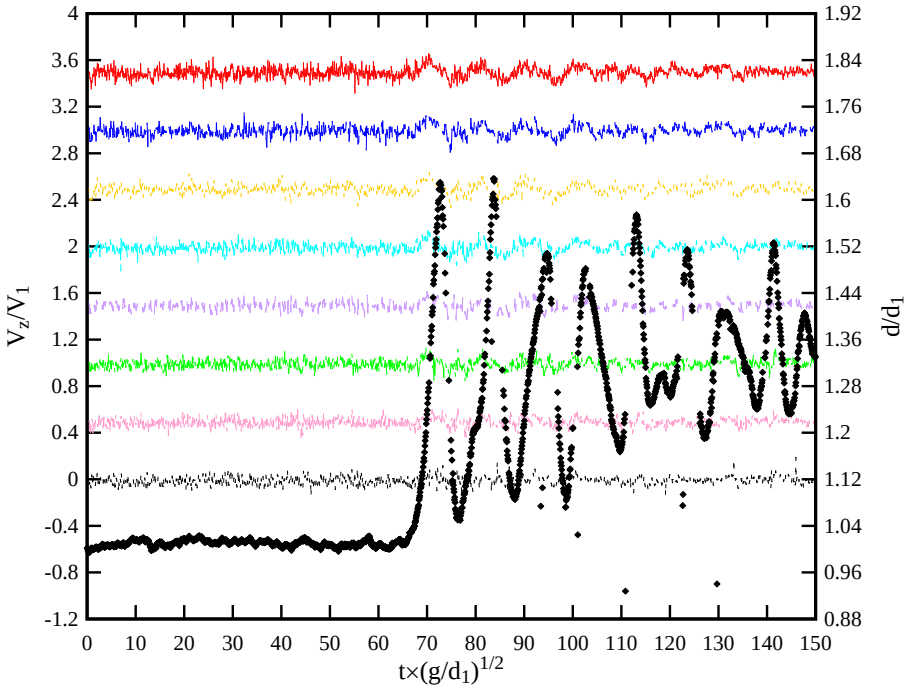

(C) Vertical velocity V_z

Fig. 3-2 - Instantaneous time variations of velocity components for a velocity profile from z = 0.016 m to 0.05 m with instantaneous water depth measured at the velocity sampling location - Flow conditions: Q = 0.099 m^3/s, Fr_1 = 1.2 - Velocity offset by +0.5 for each higher elevation.

3.2 ENSEMBLE-AVERAGED VELOCITY MEASUREMENTS

Since the propagation of tidal bores is a highly unsteady turbulent process, a time average is meaningless in the characterisation of turbulent properties. Herein ensemble-averaged free-surface and velocity measurement were conducted systematically using the flow conditions documented in Table 2-2. The free-surface elevations were measured non-intrusively using a series of ADMs and the velocity measurements were performed using the ADV Vectrino II Profiler. The Profiler and ADMs were synchronised within ± 1 ms and sampled simultaneously on the channel centreline. For each set of flow conditions, the experiments were repeated 25 times, and the results were ensemble-averaged to obtain the median free-surface and velocity properties and associated instantaneous fluctuations for the total ensemble. The number of repeats was determined from a sensitivity analysis, with details reported in Appendix B.

Altogether, the ensemble-averaged velocity and velocity fluctuations measured by the Profiler agreed qualitatively and quantitatively with the ADV data (LENG and CHANSON 2015c). Figures 3-3 and 3-4 present typical time-variations of ensemble-averaged velocity and velocity fluctuations at different vertical elevations for breaking and undular bores respectively. The data highlighted a rapid longitudinal deceleration and large fluctuations in all velocity components at all elevations for both breaking and undular bores, except for the vertical elevations that were very close to the bed ($z/d_1 < 0.03$). Next to the bed, negative longitudinal velocities were observed at the end of the deceleration phase, indicating a transient flow reversal, under both breaking and undular bores. Such a finding was similar to the results with the ADV data. For undular bores, the longitudinal velocity after the bore front passage varied with time in a quasi-periodic manner, with periods of oscillation equal to the free-surface oscillation but out of phase by π.

The transverse velocity component in breaking bores, originally zero in the initially steady flow, showed large fluctuations associated with the bore passage at all vertical elevations. At higher vertical elevations next to the free-surface, the transverse velocity decreased to negative values as the free-surface elevation increased with the bore arrival, indicating a transverse recirculation motion towards the left sidewall, and then shifted to negative values, before fluctuating about zero. In undular bores, the transverse velocity components fluctuated with the free-surface oscillation in a quasi-periodic manner, with periods out of phase by π. Some transverse recirculation was also observed in undular bores.

At vertical elevations close to the free-surface, the vertical velocity in breaking bores showed an initial increase to positive values with the rise in free-surface, then some decrease before the free-surface reached its maximum. Beneath the whelps, the vertical velocity oscillated in a quasi-periodic manner linked to the oscillation of free-surface. The periods of the vertical velocity oscillations seemed to be equal to and out of phase by $\pi/2$ compared to the free-surface oscillations.

Herein the instantaneous velocity fluctuations were quantified in terms of the difference between the third and first quartiles ($V_{75} - V_{25}$). For a Gaussian distribution of an ensemble around its mean, the difference between the third and first quartiles would be equal to 1.3 times its standard deviation (SPIEGEL 1972). In the present study, the instantaneous velocity fluctuations in the longitudinal, transverse and vertical directions showed some abrupt increase associated with the passage of tidal bores at all vertical elevations for all Froude numbers. The magnitudes of the velocity fluctuations were larger at vertical elevations close to the bed, compared to those recorded in the upper water column. The longitudinal velocity data were typically associated with the largest magnitudes in instantaneous velocity fluctuations, compared to the transverse and vertical components. The results differed from the ADV Vectrino+ observations, for which the vertical direction was associated with the largest velocity fluctuations typically ([2]).

Maximum velocity fluctuations were observed at some time lag Δt_V after the onset of the free-surface rise, as previously observed in the ADV data (Fig. 3-5). When the bore reached the sampling point, the onset of free-surface rise would correspond to the first instance at which the derivative of the free-surface curve as a function of time deviated from zero and became positive. The maximum velocity fluctuations $(V_{75}\text{-}V_{25})_{max}$ were defined as the first marked peak in terms of $(V_{75}\text{-}V_{25})$ after the bore arrival. The time lag Δt_V was defined as the time difference between the occurrence of maximum velocity fluctuations and tidal bore arrival. Herein both the maximum velocity fluctuations $(V_{75}\text{-}V_{25})_{max}$ and associated time lag Δt_V were quantified for the Profiler data, and the results are compared to ADV data of LENG and CHANSON (2015c) in Table 3-1.

Overall, both the maximum velocity fluctuations and the associated time lag measured by the Profiler and ADV units gave values of the same orders of magnitudes for similar flow conditions. The maximum velocity fluctuations measured by the Profiler in the longitudinal direction were in general larger than those measured by the ADV, albeit with shorter time lags. The transverse velocity recorded by the Profiler showed much larger fluctuations for all flow conditions at all time and no obvious peak was observed. The vertical velocity fluctuations of the ADV measurements, however, were larger compared to the Profiler data.

[2] A number of studies showed that, with the ADV Vectrino+, the vertical velocity component V_z data might be affected adversely by the bed proximity for $z < 0.030$ m (CHANSON and DOCHERTY 2012). This was associated with unusually large vertical velocity fluctuations throughout most of the water column (CHANSON 2010, CHANSON and DOCHERTY 2012, LENG and CHANSON 2015c).

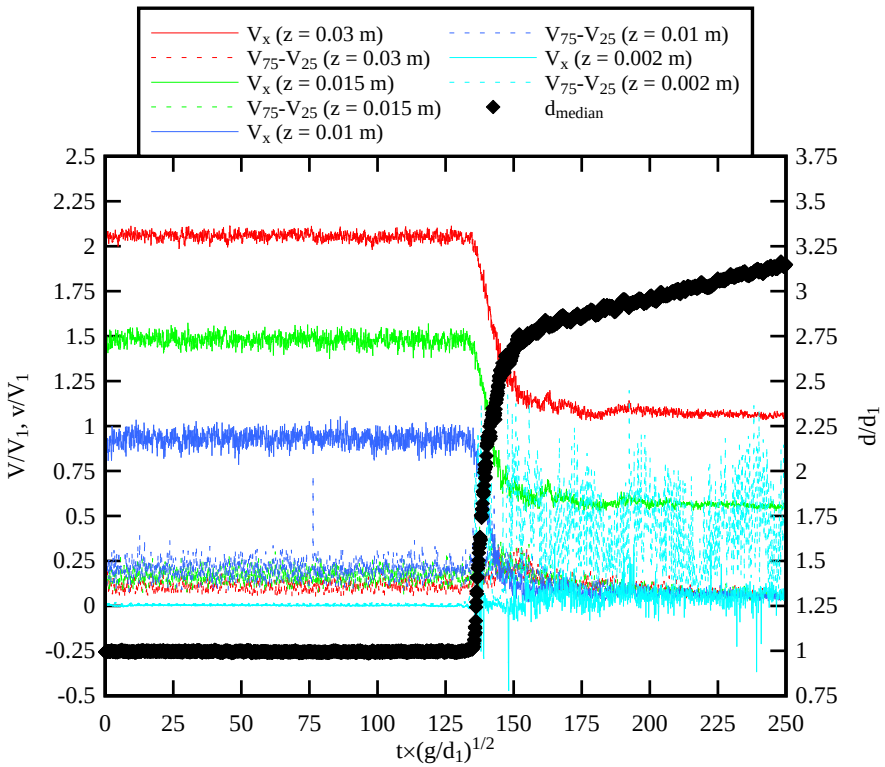

(A) Longitudinal velocity V_x

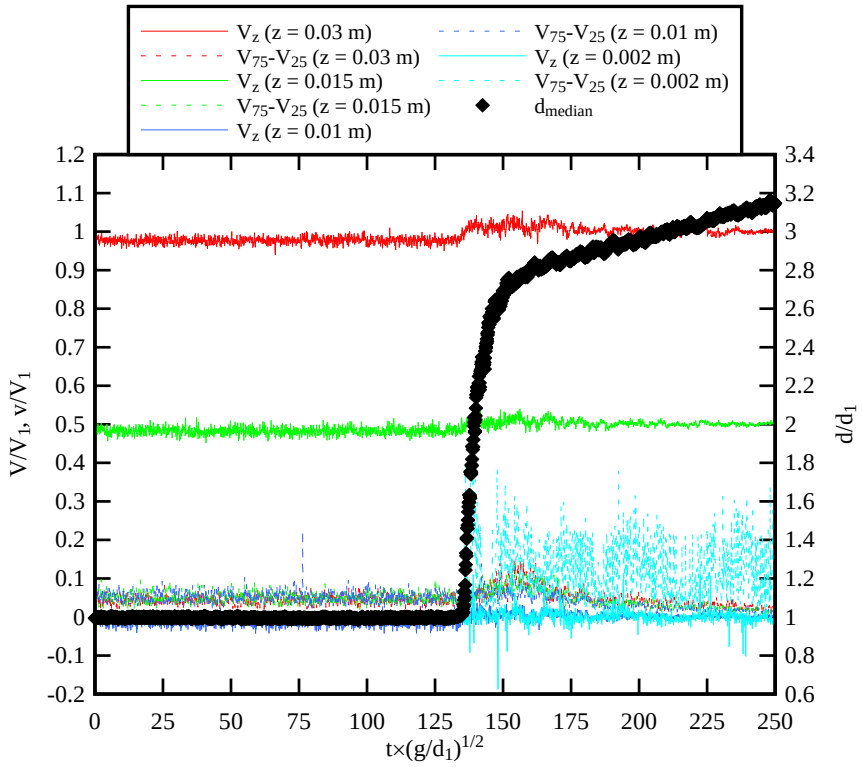

(B) Vertical velocity V_z

Fig. 3-3 - Ensemble-averaged time variations of velocity and velocity fluctuations in the longitudinal (A) and vertical (B) directions for a velocity profile from z = 0.001 m to 0.035 m with ensemble-averaged water depth measured at the velocity sampling location - Flow conditions: Q = 0.099 m^3/s, Fr_1 = 2.1 - Velocity offset by +0.5 for two higher elevations.

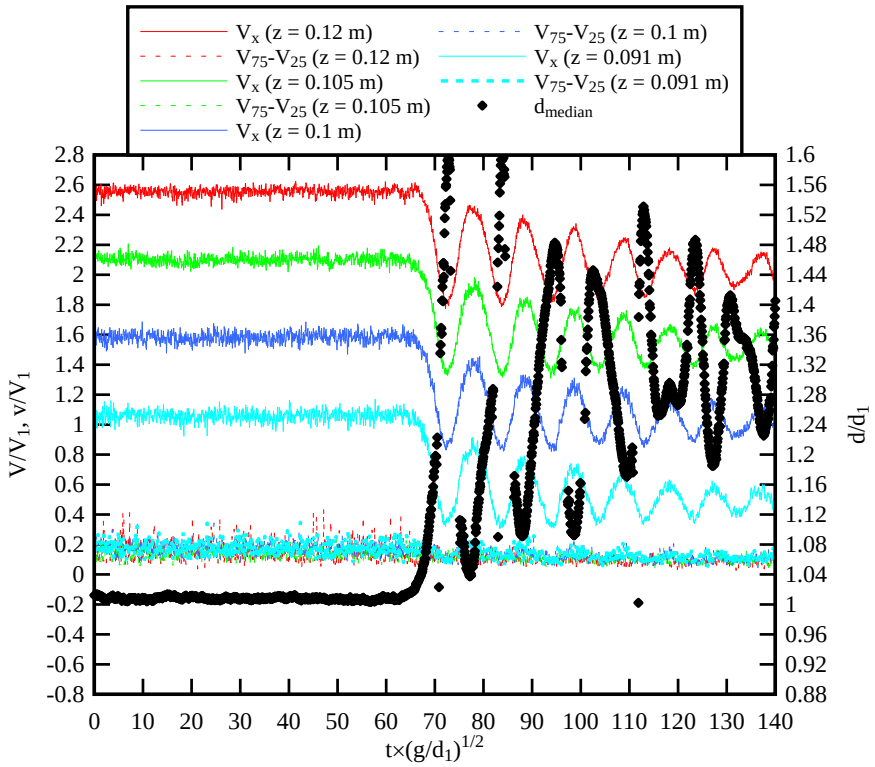

(A) Longitudinal velocity V_x

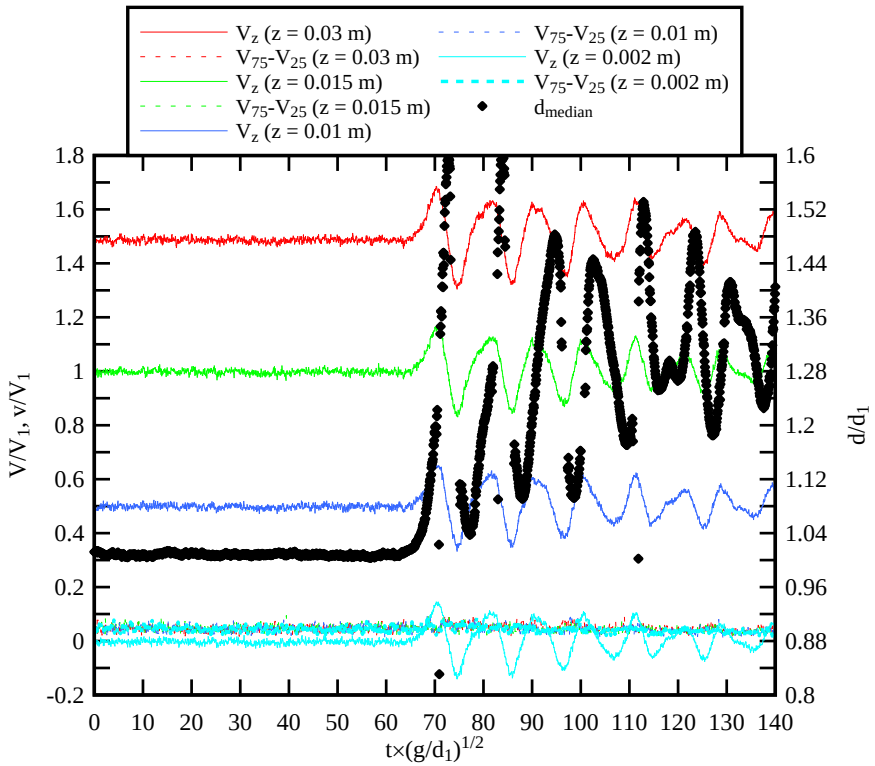

(B) Vertical velocity V_z

Fig. 3-4 - Ensemble-averaged time variations of velocity and velocity fluctuations in the longitudinal (A) and vertical (B) directions for a velocity profile from z = 0.091 m to 0.125 m with ensemble-averaged water depth measured at the velocity sampling location - Flow conditions: Q = 0.099 m^3/s, Fr_1 = 1.2 - Velocity offset by +0.5 for three higher elevations.

Selected turbulent velocity characteristics were analysed for both Profiler and ADV data (LENG and CHANSON 2015c) to validate the accuracy of the Profiler measurements in the characterisation of the rapidly fluctuating properties. Specifically, these included the recirculation velocity V_{recirc} at the lower water column and the associated time lag, the minimum transverse velocity after the arrival of the bore $V_{y,min}$ at the upper water column and the associated time lag, the maximum vertical velocity $V_{z,max}$ at the upper water column and the associated vertical acceleration V_z' were investigated for velocity measurements at similar dimensionless elevations using two instruments. The minimum transverse velocity $V_{y,min}$ after the bore arrival was taken as the first negative reached by the transverse velocity component following the bore passage. The vertical acceleration V_z' was calculated as the temporal mean acceleration between the initially steady flow vertical velocity (approximately zero) and the maximum vertical velocity following the bore passage. All time lags were quantified as the time delay in relation to the bore arrival time. Figure 3-5 presents the time variation of the ensemble averaged median longitudinal velocity and instantaneous velocity fluctuations for both Profiler and ADV data, highlighting some key velocity characteristics, and detailed results were tabulated in Table 3-1.

Altogether, the analysis for all flow conditions showed that the recirculation velocity and the associated time lag agreed closely between Profiler and ADV data. The minimum transverse velocity measured by the Profiler and ADV were of the same order of magnitude, although the ADV data showed shorter time lag Δt_V than the Profiler data. The maximum vertical velocity measured by the two instruments agreed qualitatively. The ADV data was generally associated with larger maximum vertical velocity compared to Profiler data at a similar elevation. This was likely caused by the interferences induced by the bed on the signals of top ADV receivers, with a side-looking head configuration. In turn, the vertical acceleration was higher in the ADV data, compared to the Profiler data.

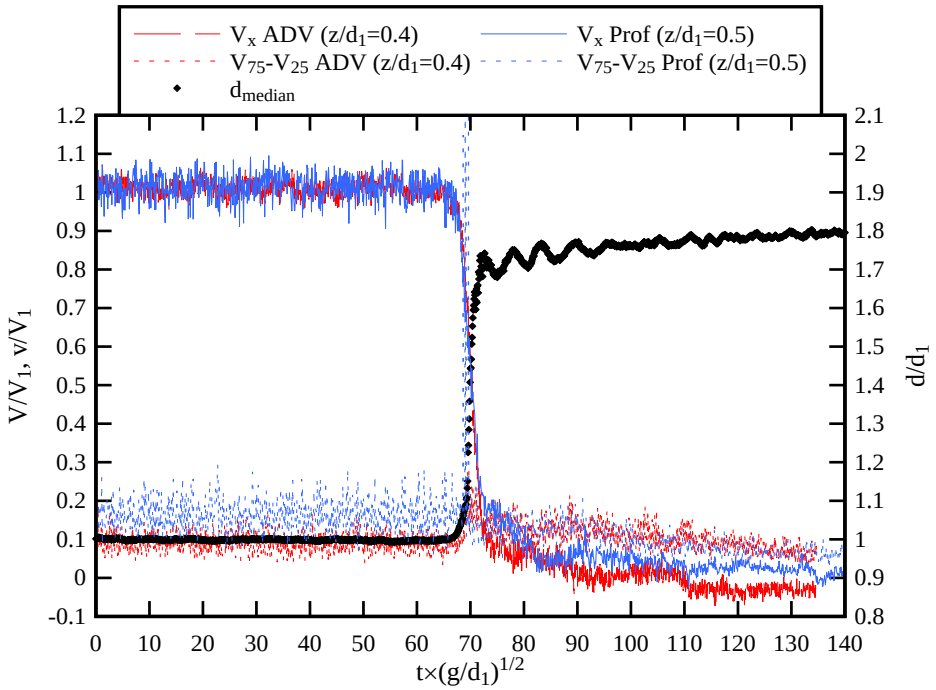

(A) Longitudinal velocity

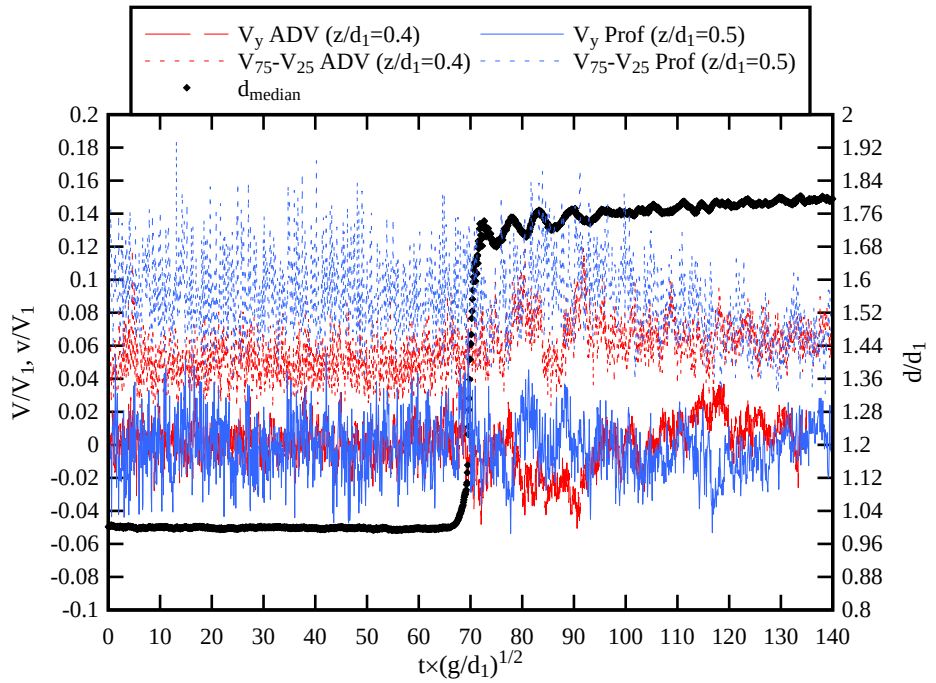

(B) Transverse velocity

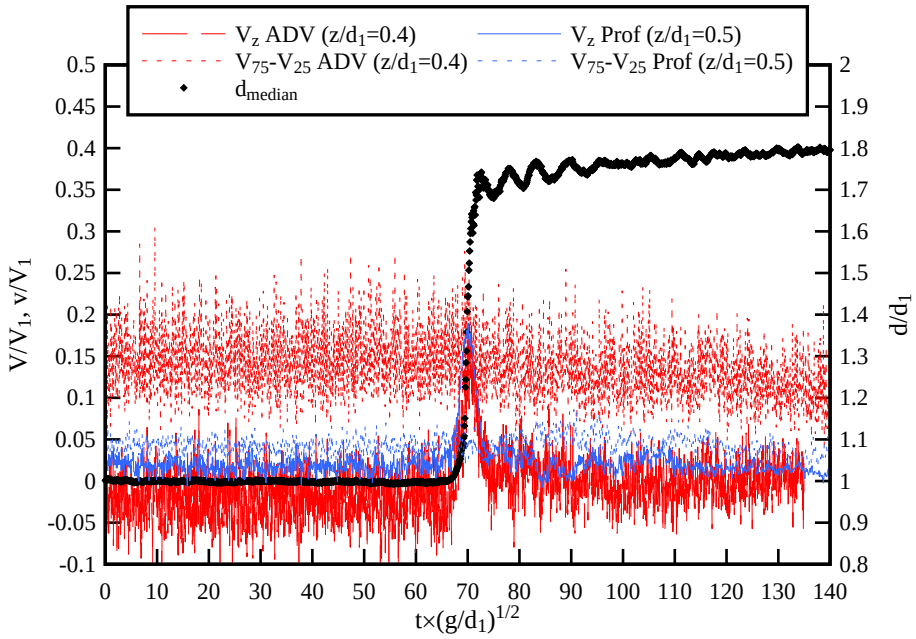

(C) Vertical velocity

Fig. 3-5 - Ensemble-averaged time variations of longitudinal, transverse and vertical velocity and velocity fluctuations at z/d_1 = 0.5 - Comparison between Profiler (blue curves) and ADV (red curves) (LENG and CHANSON 2015c) - Flow conditions: Q = 0.099 m^3/s, Fr_1 = 1.6.

The vertical profile of the median longitudinal velocity within the wall region (i.e. $z/\delta < 0.2$, $\rho \times V_* \times z/\mu > 70$) were tested during the rapid deceleration phase and the early flood tide phase ([3]). Typical data are plotted in Figure 3-6 where the data are compared to the log law. Figure 3-6A presents breaking bore data (Fr_1 = 2.1) while Figure 3-6B shows undular bore data (Fr_1 = 1.2). Altogether the data demonstrated that, during the rapid deceleration phase, the majority of the data within the wall region compared well to the log law, although a larger scatter was observed during the breaking bores. During the early flood tide phase, the longitudinal velocity profile for a breaking bore with Fr_1 = 2.1 did not as agree as well with the log law as during the rapid decceleration phase. The shear velocity V_* obtained from the best fit of log law differed between the two phases: that is, $V_* \approx 0.060$ m/s for the rapid deceleration and $V_* \approx 0.009$ m/s during the early flood tide. Both values were different from the steady flow shear velocity: $V_* = 0.110$ m/s ([4]).

For undular bores, the data during both the rapid deceleration and early flood tide phases were close qualitatively and quantitatively. The best fit of the log law yielded: $V_* = 0.050$ m/s, a result close to the steady flow shear velocity ($V_* = 0.060$ m/s).

[3] Herein the early flood tide phase is defined as the phase starting immediately after the end of the rapid deceleration phase.

[4] For breaking bore with Fr_1 = 1.6, the longitudinal velocity component was mostly negative in the wall region during and after the bore passage, and the data were not compared with log law.

Table 3-1 - Maximum velocity fluctuations and the time lag in relation to the time of initiation of free-surface rise: comparison between Profiler data (normal font) and previous ADV data (LENG and CHANSON 2015c)

Ref	Q (m^3/s)	S_o	d_1 (m)	z/d_1	Surge type	Fr_1	$(V_{x,75}-V_{x,25})_{max}$ (m/s)	$\Delta t_{V,x}$ (s)	$(V_{y,75}-V_{y,25})_{max}$ (m/s)	$\Delta t_{V,y}$ (s)	$(V_{z,75}-V_{z.25})_{max}$ (m/s)	$\Delta t_{V,z}$ (s)	*$(V_{x,75}-V_{x.,25})_{max}$ (m/s)*	*$\Delta t_{V,x}$ (s)*	*$(V_{y,75}-V_{y,25})_{max}$ (m/s)*	*$\Delta t_{V,y}$ (s)*	*$(V_{z,75}-V_{z,25})_{max}$ (m/s)*	*$\Delta t_{V,z}$ (s)*
1a	0.099	0	0.169	0.1	Breaking	1.6	0.28	0.41	N/A	N/A	N/A	N/A	*0.21*	*0.63*	*0.09*	*1.03*	*N/A*	*N/A*
1b	0.099	0	0.17	0.5	Breaking	1.6	N/A	0.31	N/A	N/A	N/A	N/A	*0.23*	*0.41*	*0.08*	*1.19*	*N/A*	*N/A*
2a	0.099	0	0.196	0.1	Undular	1.2	0.23	0.81	N/A	N/A	N/A	N/A	*0.18*	*0.96*	*N/A*	*N/A*	*N/A*	*N/A*
2b	0.099	0	0.199	0.5	Undular	1.2	N/A	N/A	N/A	N/A	0.07	1.71	*N/A*	*N/A*	*N/A*	*N/A*	*N/A*	*N/A*
3a	0.099	0.0075	0.097	0.1	Breaking	2.1	0.89	1.08	N/A	N/A	0.20	0.68	*0.66*	*1.13*	*N/A*	*N/A*	*0.59*	*0.77*
3b	0.099	0.0075	0.097	0.4	Breaking	2.1	0.85	0.80	N/A	N/A	0.25	1.99	*0.54*	*1.65*	*N/A*	*N/A*	*0.49*	*1.30*

Notes: (*italic underlined*): previous ADV data for similar flow conditions; N/A: no obvious peak observed.

Table 3-2 - Turbulent velocity characteristics: comparison between Profiler data (normal font) and previous ADV data (LENG and CHANSON 2015c)

Ref	V_{recirc} (m/s)	Δt_{recirc} (s)	$V_{y,min}$ (m/s)	$\Delta t_{y,min}$ (s)	$V_{z,max}$ (m/s)	V_z' (m/s^2)	*V_{recirc} (m/s)*	*Δt_{recirc} (s)*	*$V_{y,min}$ (m/s)*	*$\Delta t_{y,min}$ (s)*	*$V_{z,max}$ (m/s)*	*V_z' (m/s^2)*
1a	-0.24	0.98	N/A	N/A	0.04	0.06	*-0.24*	*1.30*	*-0.06*	*0.86*	*0.10*	*0.21*
1b	N/A	N/A	-0.04	1.33	0.16	0.30	*N/A*	*N/A*	*-0.04*	*0.73*	*0.16*	*0.35*
2a	N/A	N/A	N/A	N/A	0.03	0.00	*N/A*	*N/A*	*-0.04*	*1.02*	*0.07*	*0.10*
2b	N/A	N/A	-0.04	1.3	0.10	0.11	*N/A*	*N/A*	*-0.04*	*1.08*	*0.15*	*0.16*
3a	0.03	2.32	N/A	N/A	0.05	0.14	*0.02*	*1.57*	*N/A*	*N/A*	*0.15*	*0.32*
3b	N/A	N/A	N/A	N/A	0.07	0.16	*N/A*	*N/A*	*N/A*	*N/A*	*0.13*	*0.69*

Notes: (*italic underlined*): previous ADV data for similar flow conditions; N/A: no obvious peak observed.

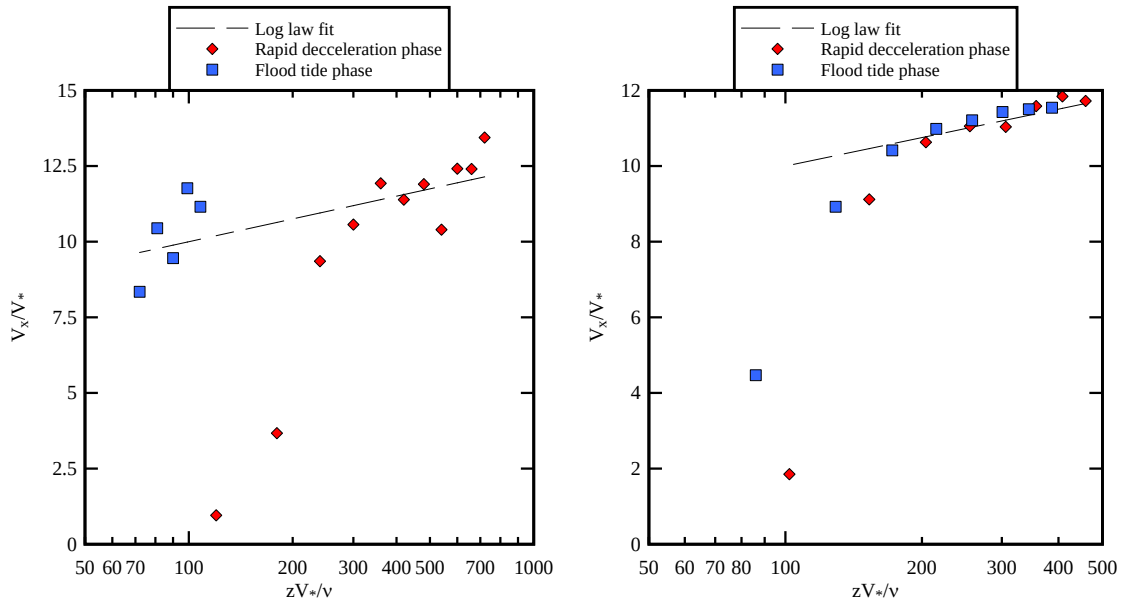

(A, Left) Q = 0.099 m^3/s, d_1 = 0.097 m, Fr_1 = 2.1, Breaking bore

(B, Right) Q = 0.099 m^3/s, d_1 = 0.197 m, Fr_1 = 1.2, Undular bore

Fig. 3-6 - Logarithmic profile of the ensemble-averaged median longitudinal velocity during the rapidly-varied and unsteady flow regions of propagating breaking and undular bores.

A feature of the Profiler was its ability to provide data at vertical elevations very close to the channel bed ($z/d_1 < 0.03$), where ADV data were not available. In the very close vicinity of the bed ($z/d_1 < 0.01$ to 0.02), the longitudinal velocity data showed first some acceleration with the initial free-surface rise prior to the arrival of the roller, a phenomena associated with breaking bores of $Fr_1 < 2$ (Fig. 3-7). For bores with $Fr_1 > 2$, a slight initial longitudinal acceleration was also observed close to bed, however not as significant as bores with lower Froude numbers. This very-short period of initial longitudinal acceleration lasted only for a dimensionless time of less than 3 to 5, corresponding in real time to less than 0.6 s, before the rapid deceleration phase, during rapid free-surface rise when the bore front passed. This initial longitudinal acceleration was more clearly marked at the second lowest vertical elevation in the velocity profile (z = 0.002 m) compared to at the lowest vertical elevation (z = 0.001 m). Simultaneously, the vertical velocity decreased to negative valued, to maintain conservation of mass and momentum at the locations where an initial longitudinal acceleration was observed. The transverse velocity showed some large fluctuation, although no obvious pattern in time-variations was observed. At vertical elevation increased above z = 0.003 m ($z/d_1 > 0.01$ to 0.02), the initial longitudinal acceleration phase disappeared, and the longitudinal velocity data showed an immediate deceleration shortly after the onset of free-surface rise. This was accompanied by marked positive vertical velocity components, consistent with previous ADV data.

The initial longitudinal acceleration in the bed vicinity was observed in breaking bores as well as in

undular bores. Previous numerical models reported small transient vortical structures formed under the gradual free-surface rise immediately before the roller toe in breaking bores, and under the point where the free-surface turned to rise in undular bores (SIMON 2014, KHEZRI 2014). Figure 3-8 shows a sketch of small vortical structures found underneath a propagating breaking bore. The observed longitudinal acceleration and vertical deceleration were believed to be associated with the presence of these vortical structures, despite possible experimental errors.

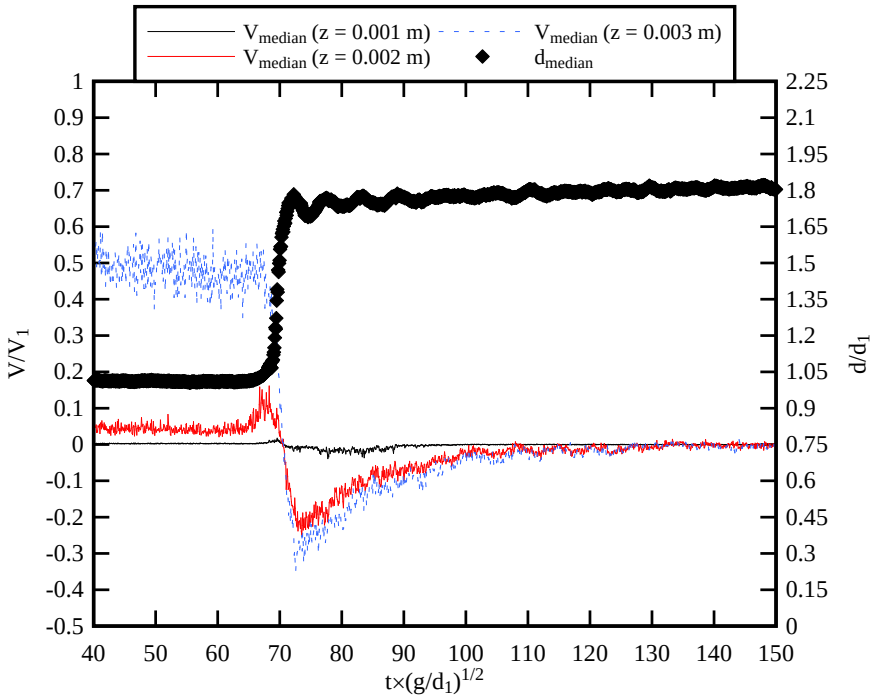

(A) Longitudinal velocity

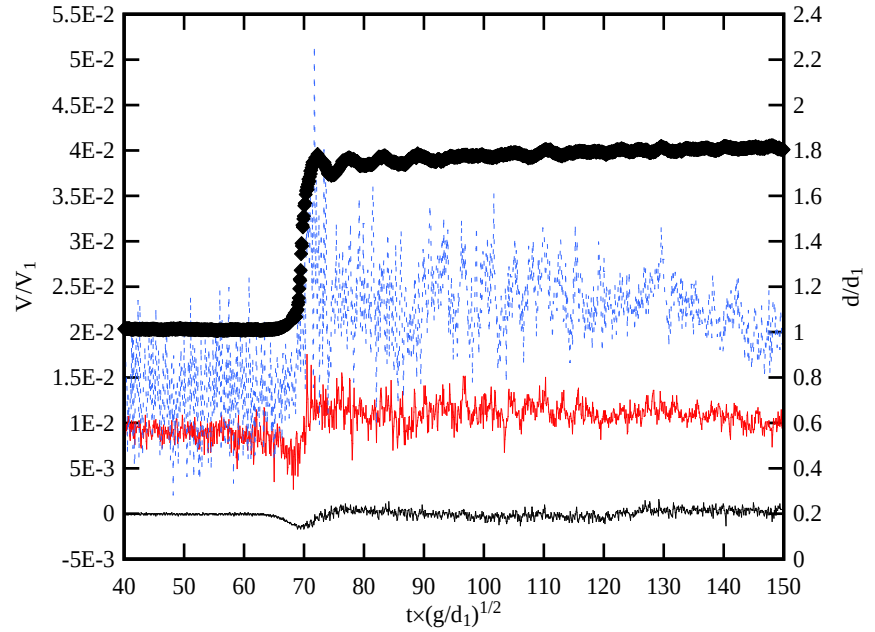

(B) Vertical velocity

Fig. 3-7 - Ensemble-averaged time-variations of longitudinal and vertical velocity components and

free-surface elevation at close vicinity of the channel bed - Transverse and vertical velocity offset by + 0.01 for the two higher elevations.

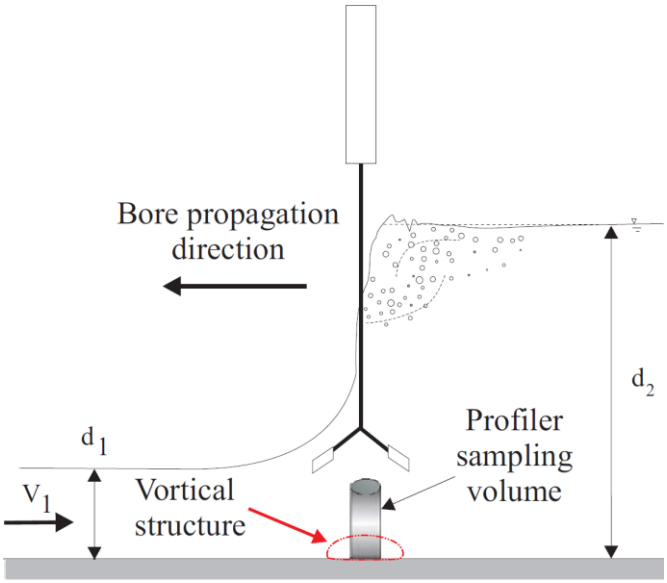

Fig. 3-8 - Sketch of small transient vortical structures beneath a propagating breaking bore, as detected by the Profiler probe (sketch not to scale).

Despite the similarities between the data collected by ADV and Profiler as discussed above, the present study also acknowledged a number of differences. First the Profiler measurements contained error in terms of velocity magnitudes at a number of locations: these data were meaningless and had to be removed from the dataset. Second the velocity fluctuations, in steady or unsteady flows, deviated from those measured by the ADV, except about the sweet spot of a sampling profile. Third, as presented in Table 3-1 and 3-2, the turbulent velocity characteristics measured by the Profiler agreed with the ADV measurements only in terms of order of magnitude, but not in terms of quantitative values. Overall, the Profiler showed higher velocity fluctuations for all velocity components compared to the ADV, except for the vertical velocity component. This suggested that the higher sensitivity of the Profiler in the measurement of velocity fluctuations was not due to the difference in sampling volumes between the two instruments, but more related to the geometrical arrangement of the receivers. Altogether the present study demonstrated the applicability of Vectrino II Profiler in turbulent flow measurements, but only with careful calibration and quality control of the data collected.

4. ENSEMBLE-AVERAGED REYNOLDS STRESSES

In a turbulent unsteady flow, the Reynolds stress component τ_{ij} would characterise the shear stress on the interface $dx_i \times dx_j$ of a small control volume with dimensions dx, dy and dz, where i, j = x, y or z. The Reynolds stress tensor, composed of all stress components, is a transport effect which is a result of the turbulent motion due to velocity fluctuations and subsequent increase of momentum exchange and mixing (PIQUET 1999). Following CHANSON and DOCHERTY (2012) and LENG and CHANSON (2015c), the Reynolds stress components and stress fluctuations were calculated using the ensemble-averaging (EA) method. In this section, the normal Reynolds stress components $\rho \times v_x \times v_x$, $\rho \times v_y \times v_y$, $\rho \times v_z \times v_z$ and the tangential Reynolds stress components $\rho \times v_x \times v_y$, $\rho \times v_y \times v_z$, $\rho v_x v_z$ were analysed based upon the velocity data collected using the Profiler.

Overall, the ensemble-averaged Reynolds stress data highlighted large shear stress magnitudes and large shear stress fluctuations at all elevations associated with the bore passage, for all flow conditions. The time-variations of the ensemble-median Reynolds stress components and corresponding shear stress fluctuations were comparable to previous ADV data (CHANSON 2010, CHANSON and DOCHERTY 2012, KHEZRI and CHANSON 2012a, LENG and CHANSON 2015c). Figures 4-1 and 4-2 present typical ensemble-averaged Reynolds stresses and associated fluctuations analysed from the ADV Vectrino II Profiler data for a breaking bore and an undular bore respectively.

For the range of investigated flow conditions (Table 2-2), all Reynolds stress components showed a marked increase in magnitudes and in fluctuations at all vertical elevations during and following the bore passage. Maximum stress magnitudes were reached typically at the same time as the maximum stress fluctuations were observed: that is, shortly after the arrival of the bore front. The tangential stress component $v_x \times v_z$ was usually negative, sometimes associated to consecutive double peaks with opposite signs. Comparing upper and lower water column data, the data at lower vertical elevations were associated with higher stress magnitudes and stress fluctuations, as well as more pronounced maxima, for all components. During the early flood tide immediately after the bore front, the shear stresses and shear stress fluctuations were smaller compared to those in the initially steady flow, except for the normal stress component $v_z \times v_z$ and tangential stress component $v_x \times v_z$, which sometimes showed high-level fluctuations even in the early flood tide (Fig. 4-1).

For the range of investigated undular bores, no marked peak in Reynolds stresses or stress fluctuations was observed, except for the normal stress component $v_x \times v_x$ at vertical elevations $z/d_1 < 0.2$. Instead a decrease in magnitudes of all Reynolds stress components was seen at $z/d_1 > 0.2$, as the free-surface started to rise, followed by rapid, high-frequency fluctuations in median stress levels beneath the whelps (after the first wave crest). The stress fluctuations varied in a quasi-

periodic manner, their period being equal to and out of phase with the quasi-periodic oscillation in free-surface, although with lesser regularity (Fig. 4-2). In the upper water column, the magnitudes and fluctuations of all shear stress components showed some decrease with increasing elevation, during both the initially steady flow before the bore, the rapid deceleration phase during the bore front passage and the early flood tide after the bore front.

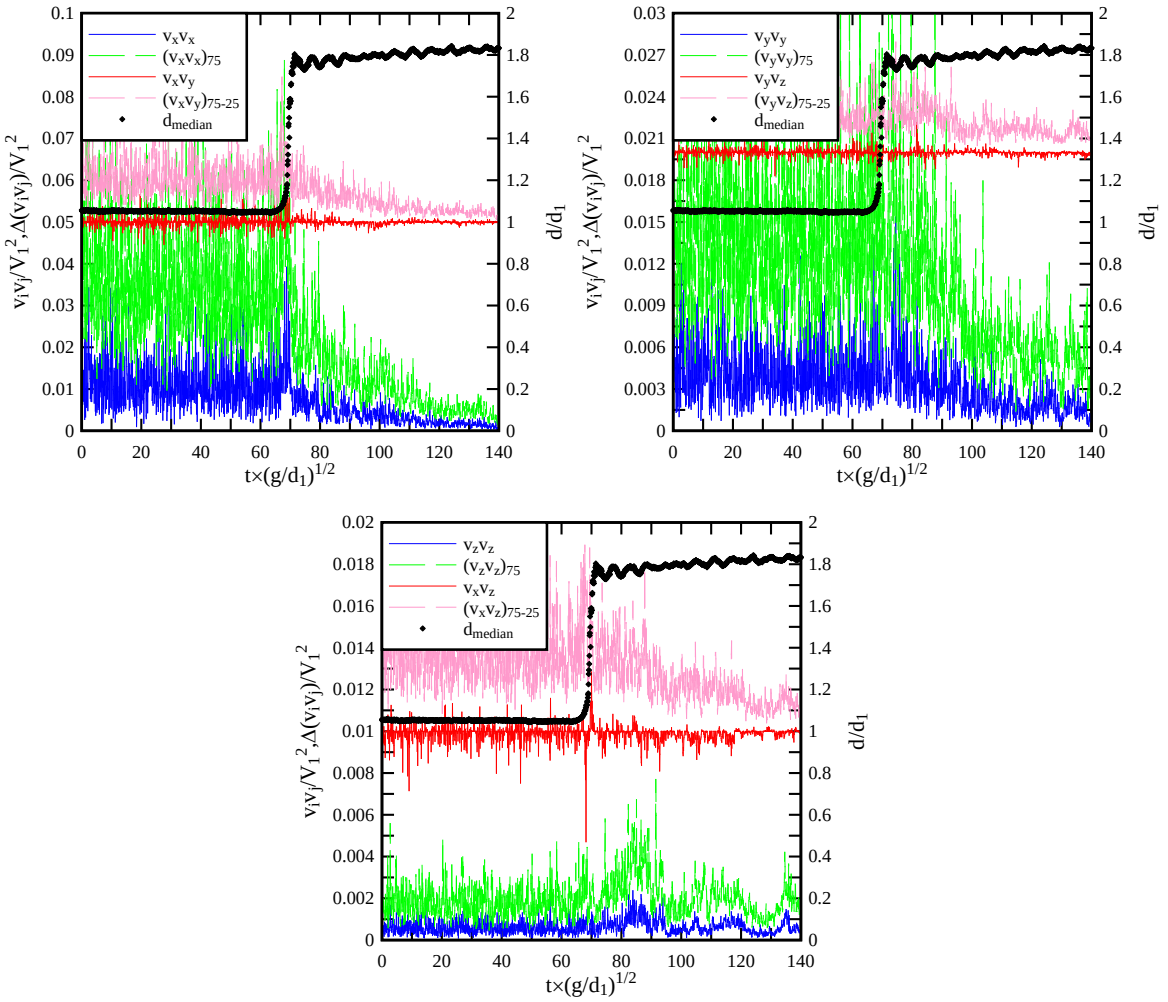

Fig. 4-1 - Ensemble-averaged time-variations of Reynolds stress components at vertical elevation z = 0.05 m in a velocity profiler from z = 0.015 m to 0.05 m - Flow conditions: Q = 0.103 m^3/s, Fr_1 = 1.6 - Tangential stresses offset by + 0.05, + 0.02 and + 0.01 for components $v_x \times v_y$, $v_y \times v_z$ and $v_x \times v_z$, respectively.

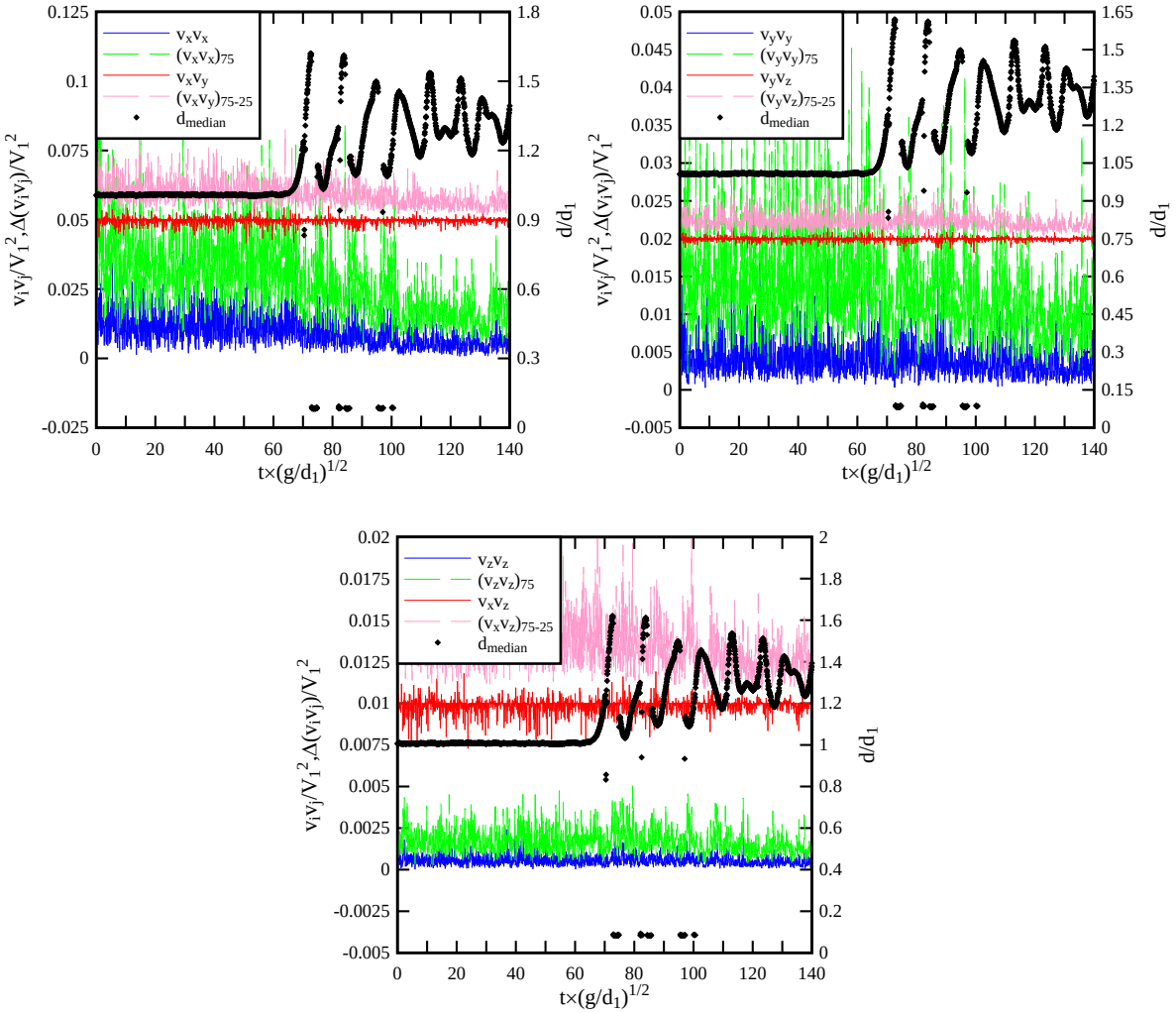

Fig. 4-2 - Ensemble-averaged time-variations of Reynolds stress components at vertical elevation z = 0.05 m in a velocity profiler from z = 0.015 m to 0.05 m - Flow conditions: Q = 0.099 m^3/s, Fr_1 = 1.2 - Tangential stresses offset by + 0.05, + 0.02 and + 0.01 for components $v_x \times v_y$, $v_y \times v_z$ and $v_x \times v_z$, respectively.

Previous ADV measurements highlighted maximum Reynolds stresses and stress fluctuations occurring shortly after the arrival of the bore front (LENG and CHANSON 2015c). The findings were consistent for all Reynolds stress components at all vertical elevations throughout the initial flow depth, for Froude numbers ranging from 1.2 to 2.2. In the present study, similar peaks in the ensemble-median Reynold stresses $(v_i v_j)_{max}$ and in the stress fluctuations $(v_i v_j)_{75\text{-}25,\ max}$, as well as time lags after the bore arrival time, were observed. Detailed data was tabulated in Table 4-1 (A) and (B). The time lag ΔT was defined as the time difference between the occurrence of the maximum shear stress magnitudes (or shear stress fluctuations) and the arrival time of the bore front. With data for which no obvious peak was visible, the results are marked by N/A in Table 4-1.

Overall, breaking bores with higher Froude numbers were associated with larger maximum Reynolds stresses and shear stress fluctuations at similar dimensionless elevations, compared to undular bores and breaking bores with lower Froude numbers. For bores with the same Froude number, larger maximum shear stresses and shear stress fluctuations at the higher vertical elevations, possibly linked to the large scale vortical structures generated in the wake of the bore front, next to the free-surface. The normal stress components were typically associated with more pronounced peaks in median shear stress and shear stress fluctuations, compared to the tangential stress components. The tangential stress component $v_x \times v_z$, which would tend to the bed shear stress in the close vicinity of the bed, showed negative maxima irrelevant of the Froude numbers. In terms of time lag, the maximum shear stress magnitudes and the maximum stress fluctuations occurred simultaneously, within ± 0.1 s.

The maximum shear stress, the maximum stress fluctuations and their time lags, measured by the Profiler, were in the same orders of magnitude as those recorded with the ADV. Herein the ensemble-median stresses measured by the Profiler for breaking bore with large Froude numbers were one order of magnitude larger than the critical threshold for sediment motion of both cohesive and non-cohesive materials ([1]). The instantaneous data and fluctuation data indicated even larger stress levels, in excess of 1 kPa, found under laboratory conditions. The results indicated that the bore propagation can easily scour a mobile bed as illustrated in laboratory by KHEZRI and CHANSON (2012b,2015).

[1] For fine sand particles, the Shields diagram gives a critical shear stress for sediment motion of 0.1 to 0.5 Pa (GRAF 1971, CHANSON 2004). In natural channels with cohesive sediments, field observations indicated a critical shear stress for sediment erosion between 0.1 Pa and 10 Pa (SANCHEZ and LEVACHER 2008, JACOBS et al. 2011).

Table 4-1 - Maximum ensemble-median Reynolds stresses, maximum ensemble-averaged Reynolds stress fluctuations and their associated time lags measured by Profiler for all flow conditions

(A) Maximum ensemble-median Reynolds stresses and associated time lags

Ref.	Q (m^3/s)	S_o	d_1 (m)	z/d_1	Surge type	Fr_1	$(v_xv_x)_{max}$ (m^2/s^2)	ΔT_{xx} (s)	$(v_xv_y)_{max}$ (m^2/s^2)	ΔT_{xy} (s)	$(v_yv_y)_{max}$ (m^2/s^2)	ΔT_{yy} (s)	$(v_yv_z)_{max}$ (m^2/s^2)	ΔT_{yz} (s)	$(v_zv_z)_{max}$ (m^2/s^2)	ΔT_{zz} (s)	$(v_xv_z)_{max}$ (m^2/s^2)	ΔT_{xz} (s)
1a	0.099	0	0.169	0.1	Breaking	1.6	0.016	0.860	0.003	0.580	0.007	1.350	N/A	N/A	0.002	1.260	N/A	N/A
1b	0.099	0	0.17	0.3	Breaking	1.5	0.027	0.380	N/A	N/A	0.009	1.040	N/A	N/A	0.002	2.360	-0.004	0.300
1c	0.099	0	0.17	0.7	Breaking	1.5	0.036	0.420	N/A	N/A	N/A	N/A	N/A	N/A	0.002	1.550	-0.003	0.410
2a	0.099	0	0.196	0.1	Undular	1.2	0.014	1.010	N/A	N/A	N/A	N/A	N/A	N/A	0.001	1.810	N/A	N/A
2b	0.099	0	0.197	0.3	Undular	1.2	N/A	N/A	N/A	N/A	N/A	N/A	N/A	N/A	N/A	N/A	N/A	N/A
2c	0.099	0	0.199	0.6	Undular	1.2	N/A	N/A	N/A	N/A	N/A	N/A	N/A	N/A	N/A	N/A	N/A	N/A
3a	0.099	0.0075	0.097	0.1	Breaking	2.1	0.095	0.930	N/A	N/A	N/A	N/A	N/A	N/A	0.012	0.940	-0.012	0.950
3b	0.099	0.0075	0.097	0.4	Breaking	2.1	0.100	1.640	N/A	N/A	N/A	N/A	N/A	N/A	0.016	2.270	-0.010	2.230

(B) Maximum Reynolds stresses fluctuations and associated time lags

Ref.	$(v_xv_x)_{75,\ max}$ (m^2/s^2)	$\Delta T_{xx,\ 75}$ (s)	$(v_xv_y)_{75\text{-}25,\ max}$ (m^2/s^2)	$\Delta T_{xy,\ 75\text{-}25}$ (s)	$(v_yv_y)_{75,\ max}$ (m^2/s^2)	$\Delta T_{yy,\ 75}$ (s)	$(v_yv_z)_{75\text{-}25,\ max}$ (m^2/s^2)	$\Delta T_{yz,\ 75\text{-}25}$ (s)	$(v_zv_z)_{75,\ max}$ (m^2/s^2)	$\Delta T_{zz,\ 75}$ (s)	$(v_xv_z)_{75\text{-}25,\ max}$ (m^2/s^2)	$\Delta T_{xz,\ 75\text{-}25}$ (s)
1a	0.040	0.960	0.013	1.290	0.022	1.680	0.006	1.340	0.004	1.260	0.006	1.010
1b	0.062	0.280	0.024	0.170	N/A	N/A	N/A	N/A	0.005	2.520	N/A	N/A
1c	1.836	0.400	0.015	0.380	0.013	2.120	0.004	1.520	0.005	1.820	0.090	0.470
2a	0.042	*1.750*	0.008	1.880	N/A	N/A	N/A	N/A	N/A	N/A	0.004	1.670
2b	N/A	N/A	N/A	N/A	N/A	N/A	N/A	N/A	N/A	N/A	N/A	N/A
2c	N/A	N/A	N/A	N/A	N/A	N/A	N/A	N/A	N/A	N/A	N/A	N/A
3a	0.536	1.020	N/A	N/A	N/A	N/A	N/A	N/A	0.087	0.940	0.055	1.020
3b	1.070	0.840	N/A	N/A	N/A	N/A	N/A	N/A	0.038	2.450	0.050	2.110

Note: *italic font* denoted suspicious data.

Discussion

For the ensemble-averaged normal Reynolds stress component τ_{xx}, a most distinctive maximum $(\tau_{xx})_{max}$ was observed during the tidal bore passage. Herein the vertical distributions of maximum ensemble-median stresses $\tau_{xx,max}$ and associated time lags ΔT_{xx} were analysed. Figure 4-3 shows the results in a dimensional form for all flow conditions. Overall, the data highlighted high median stress levels, ranging from 10 to 110 Pa, throughout the lower water column (Fig. 4-3). The maximum median stresses during the breaking bore with the highest Froude number were in general much larger than those of bores with smaller Froude numbers at all vertical elevations. For bores with lower Froude numbers (Fr_1 = 1.2 and 1.6), the maximum stress levels were close, fluctuating between 10 to 30 Pa for all vertical elevations.

For the bore with the highest Froude number (Fr_1 = 2.1), the variation in maximum stresses with vertical elevation was large. The results showed that some large median shear stress range could occur up to 50 Pa to 110 Pa within the boundary layer. Similarly, for all bore flow conditions, the vertical profile of the time lag showed some large range, from 0.2 s to 2 s, with data scatter of up to 1 s between elevations. These results must be considered with care and might not represent the true trend of maximum stress levels with vertical elevation, because the root mean square of the velocity signals of the Profiler was known to have errors (App. A). Therefore, the vertical distribution of the maximum Reynolds stresses could only provide information on the range and order of magnitude of shear stress levels and order of magnitude.

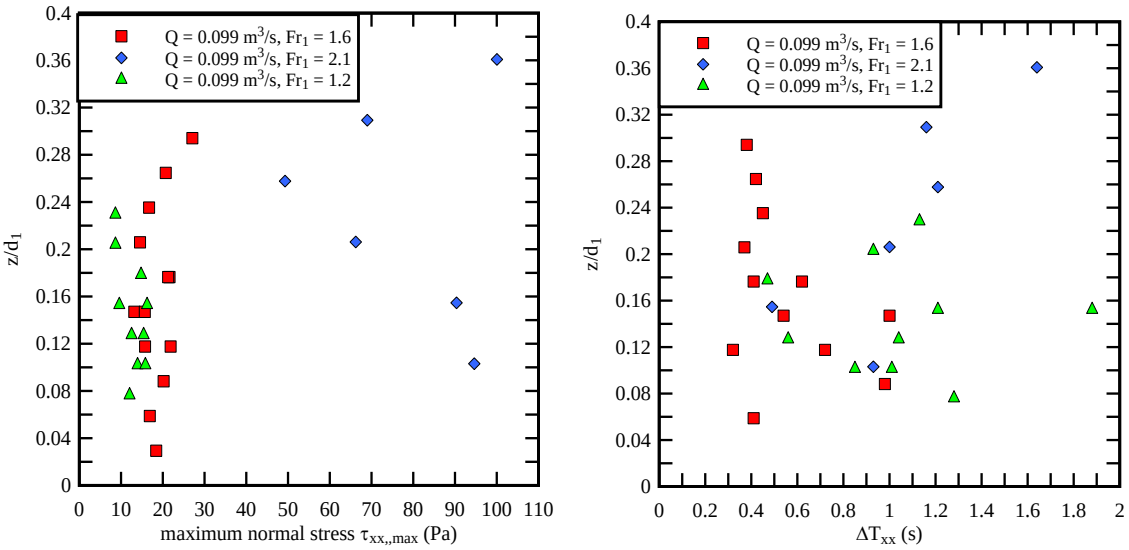

Fig. 4-3 - Vertical profile of maximum ensemble-median normal Reynolds stress $\tau_{xx,max}$ and the associated time lag ΔT_{xx} for all flow conditions.

The instantaneous Reynolds stress data was analysed to obtain the probability density functions of normal and tangential stresses over a short time period (within 3 s) before, during and after the bore passage. Selected flow conditions were examined in details and the results were compared to shear stress probability density functions analysed from ADV data for similar flow conditions (LENG and CHANSON 2015c). Figure 4-4 illustrates a typical comparison of the normal stress component $v_x \times v_x$ analysed from the Profiler and ADV data. The Profiler and ADV results were analysed using the same time span before, during and after the bore passage: i.e., about 3 s. Considering the difference in sampling rates between the Profiler and ADV (100 Hz versus 200 Hz), the Profiler data set contained approximately 7,500 data points, whereas the ADV data set contained about 15,000 data points.

Overall, the results showed close agreement between the PDF analysed from the Profiler and ADV measurements before, during and after the bore passage: e.g., for $v_x \times v_x$ levels up to 0.1 to 0.2 m^2/s^2 (Fig. 4-4), corresponding to shear stress levels of up to 100 to 200 Pa. Both the Profiler and ADV PDF data demonstrated marked peaks which were associated with very similar stress levels (~ 10 to 50 Pa) before, during and after the bore passage. For shear stress levels higher than 100 to 200 Pa, the Profiler data deviated from the ADV data, with higher probability densities observed for the Profiler data under a certain stress level. The reasons could be caused by some noise in the Profiler signals, which resulted in some large high-frequency velocity fluctuation and produced inaccuracies in the velocity fluctuations, hence stress data.

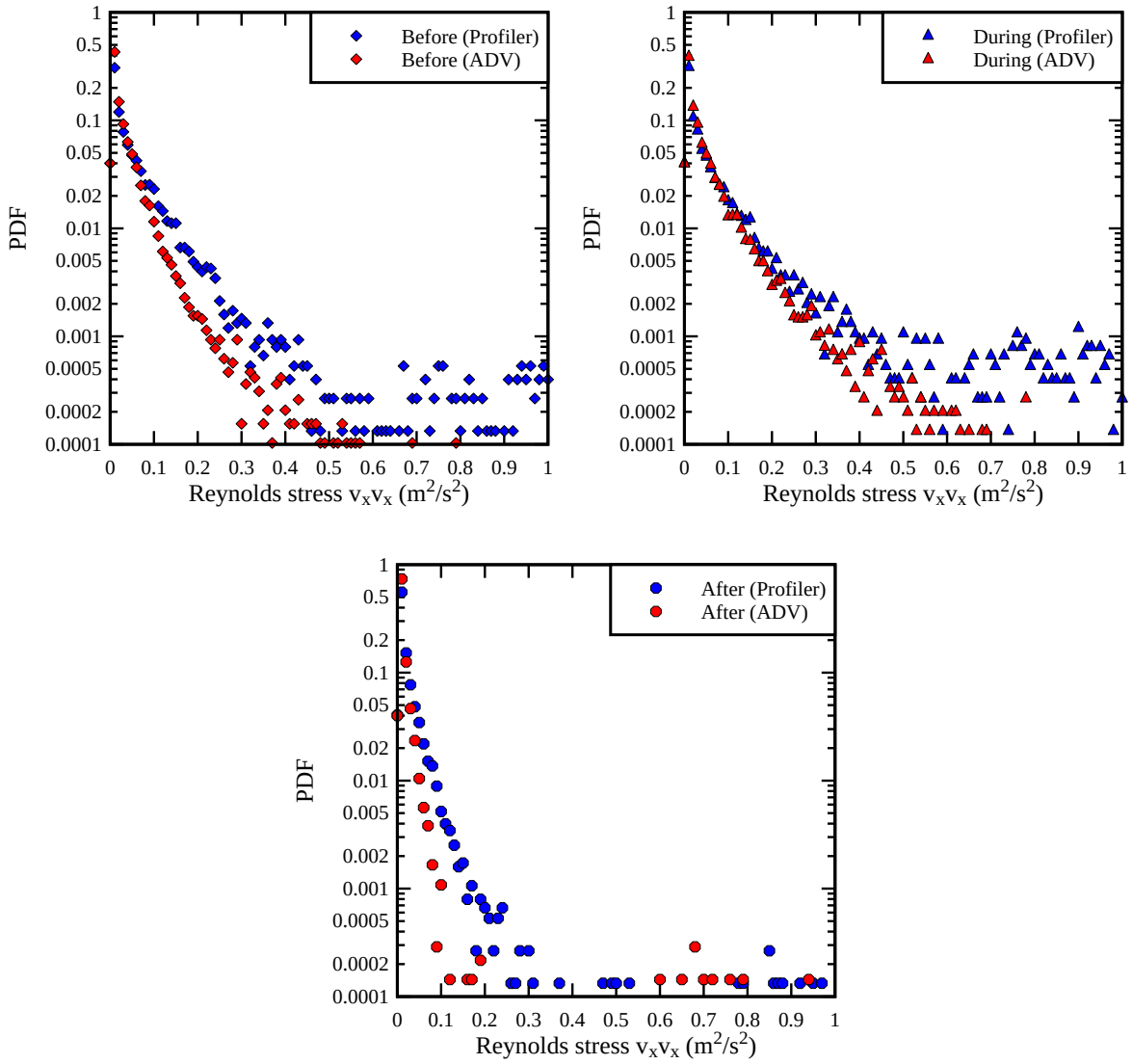

Fig. 4-4 - Probability density functions of normal Reynolds stress tensor $v_x \times v_x$ before, during and after a breaking bore passage - Comparison with ADV data for similar flow conditions: Q = 0.099 m^3/s, Fr_1 = 2.1, z/d_1 = 0.1 - Vertical axes in logarithmic scale.

5. TURBULENT TIME AND LENGTH SCALES

5.1 STEADY FLOW TIME AND LENGTH SCALES

The turbulent time and length scales include the Eulerian integral time scale T_E, the turbulent integral time scale T_i where i denoted the velocity component; i = x, y, z, and length scale L_i. In turbulent flows, the normalised auto-correlation function R_{ii} (τ) of the i-velocity fluctuations for single point measurements is defined as:

$$R_{ii}(\tau) = \frac{\overline{v_i(t) \times v_i(t+\tau)}}{\overline{v_i}^2} \qquad (5\text{-}1)$$

where τ is the time lag, v_i is the instantaneous velocity fluctuations defined as: $v_i = V_i - \overline{V_i}$, and $\overline{V_i}$ is the instantaneous ensemble-averaged median velocity component i. The auto-correlation function is unity for a time lag of zero and ranges between -1 and 1 for a non-zero time lag. Figure 5-1 shows typical autocorrelation functions calculated in steady flow for z = 0.001 m to 0.030 m, with 30 sampling points in total.

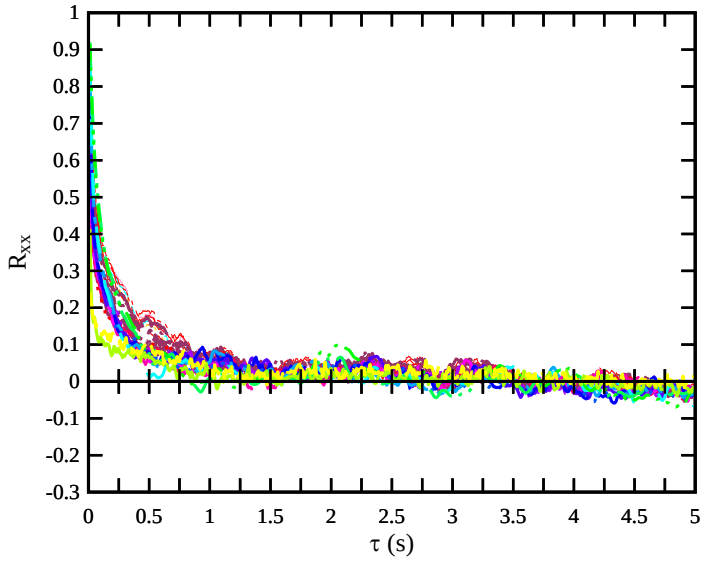

Fig. 5-1 - Autocorrelation functions of the steady flow longitudinal velocity - Coloured curves denoted autocorrelation functions for 30 points in a profile - Flow condition: Q = 0.099 m^3/s, Fr_1 = 1.6, z/d_1 = 0 to 0.17, Profiler located at x = 7.87 m.

The Eulerian integral time scale, also called auto-correlation time scale, is defined as:

$$T_{E,i} = \int_0^{\tau(R_{ii}=0)} R_{ii}(\tau) \times d\tau \qquad (5\text{-}2)$$

where R_{ii} is the normalised auto-correlation function of the turbulent velocity fluctuation v_i, and $R_{ii}(\tau) = 0$ denotes the first crossing of the autocorrelation function with the x-axis. The Eulerian

integral time scale $T_{E,i}$ is a measure of the longest connection in the turbulent behaviour of $v_i(\tau)$ (HINZE 1975, CHANSON 2014). It is also called macro time scale. Figure 5-2 shows typical vertical profiles of the Eulerian integral time scales of the longitudinal, transverse and velocity components in the initially steady flow. The results highlighted that the vertical velocity was associated with larger time scales for all elevations compared to the other two velocity components ($T_{E,y}/T_{E,x}$ ~ 0.2 to 1.0, $T_{E,z}/T_{E,x}$ ~ 2.0 to 3.3). Overall, the Eulerian integral time scales in steady flow were of an order of magnitude from 10^{-2} s to 10^{-1} s. The dimensionless Eulerian integral time scales $T_E \times (g/\delta)^{1/2}$ of the present study for all velocity components ranged from 0.06 to 1.0 in steady flow and they agreed well with the steady flow data of KOCH and CHANSON (2005).

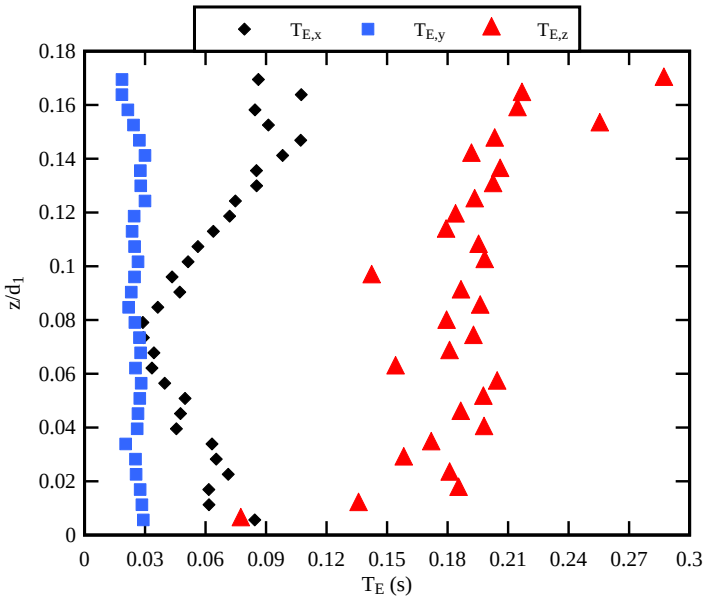

Fig. 5-2 - Eulerian integral time scale profile for longitudinal, transverse and vertical velocity autocorrelation functions in initially steady flow - Flow conditions: Q = 0.099 m^3/s, Fr_1 = 1.6, z/d_1 = 0 to 0.17, Profiler located at x = 7.87 m.

The turbulent integral time and length scales were calculated from the velocity data by cross-correlating the instantaneous velocity signals between two points located at elevations z_1 and z_2 separated by a vertical distance Δz, and measured simultaneously in a vertical profile. The cross-correlation function in terms of the velocity component i is calculated as:

$$R_{z1z2,i}(\tau) = \frac{\overline{v_{z1,i}(t) \times v_{z2,i}(t+\tau)}}{\sqrt{\overline{v_{z1,i}}^2 \times \overline{v_{z2,i}}^2}} \quad (5\text{-}3)$$

The turbulent integral length scale, which represents a characteristic vertical size of a large vortical structure found in the velocity direction i, is defined as:

$$L_{z,i} = \int_0^{\Delta z_{max}} (R_{z1z2,i})_{max} \times dz \quad (5\text{-}4)$$

where $(R_{z1z2,i})_{max}$ is the peak of the cross-correlation function between the two points z_1 and z_2, and Δz_{max} is the maximum vertical separation between two points in a profile. The turbulent integral time scale characterises the time scale (or lifespan) of a large vortical motion detected in the velocity direction i. This time scale is defined as:

$$T_{z,i} = \frac{1}{L_{z,i}} \times \int_0^{\Delta z_{max}} (R_{z1z2}, i)_{max} \times T_{z1z2,i} \times dz \quad (5\text{-}5)$$

where $T_{z1z2,i}$ is the integral of the cross-correlation function between the time lag associated with the peak correlation and the first intersection of the function with zero.

Figure 5-3 demonstrates typical cross-correlation functions of the longitudinal, transverse and vertical velocity components, calculated between a reference point and the other sampling points in a vertical profile in the initially steady flow. The reference point was taken as the upper point in a profile ([1]). For example, for a profile covering z = 0.001 to 0.030 m within the water depth, the reference point would be at z = 0.030 m. Table 5-1 presents the turbulent integral time and length scales calculated in steady flows measured by the Profiler at a range of vertical elevations, with a comparison to past experimental data by SIMON and CHANSON (2013) ([2]).

In the initially steady flow, the occurrence of the peaks in cross-correlation functions was related to the separation distance Δz. As the separation distance increased, the maximum cross-correlation decreased, while the time lag increased as the vertical distance between the two points increased. The shape of the cross-correlation functions was wider with smaller peaks for two points separated at larger vertical distances, compared to closer vertical separations. The cross-correlation functions calculated from the longitudinal velocity components were associated with larger areas underneath the curves, compared to the other two velocity components, for all vertical elevations and flow conditions. That is, the data corresponded to larger turbulent time and length scales. The turbulent length and time scales in the initially steady flow were between 0.01 m to 0.02 m and 0.01 s to 0.30 s, respectively, with larger time and length scales observed in the lower water column. The data highlighted that, in the initially steady flow, vortical structures of a typical size of 0.01 m to 0.02 m developed next to the channel bed, and disappeared within 0.3 s. The longitudinal time and length scales were in general larger than those in the transverse and vertical directions, with $L_{z,y}/L_{z,x} \sim 0.3$

[1] That is, the first data point in the profile.

[2] Note that SIMON and CHANSON (2013) considered a different approach. They used two Nortek™ ADV Vectrino+ units separated in the transverse direction Δy. The cross-correlation calculations were performed for six transverse separations only. For completeness, SIMON and CHANSON (2013) tested ADV configurations with longitudinal separation distance and as well as vertical separation distances. The ADV units interfered with each other and produced meaningless velocity signals for these two configurations.

to 0.8, $L_{z,z}/L_{z,x}$ ~ 0.6 to 0.8, $T_{z,y}/T_{z,x}$ ~ 0.01 to 0.27, and $T_{z,z}/T_{z,x}$ ~ 0.1 to 0.9.

In comparison, the longitudinal time and length scales for the present study were overall larger than those of a past data set (Table 5-1). Some were up to one order of magnitude larger. A reason could be that the previous experiments were performed in the transverse directions using two ADVs. The cross-correlation calculations were conducted for six transverse separations only, with one measurement for each separation. The present experiments were performed in the vertical direction, with 30 points sampled simultaneously giving 30 vertical separations. The finer spatial resolution and simultaneous sampling herein combined to give larger time and length scales. Another reason could be that the present experiments were performed in a much larger facility with higher flow rates.

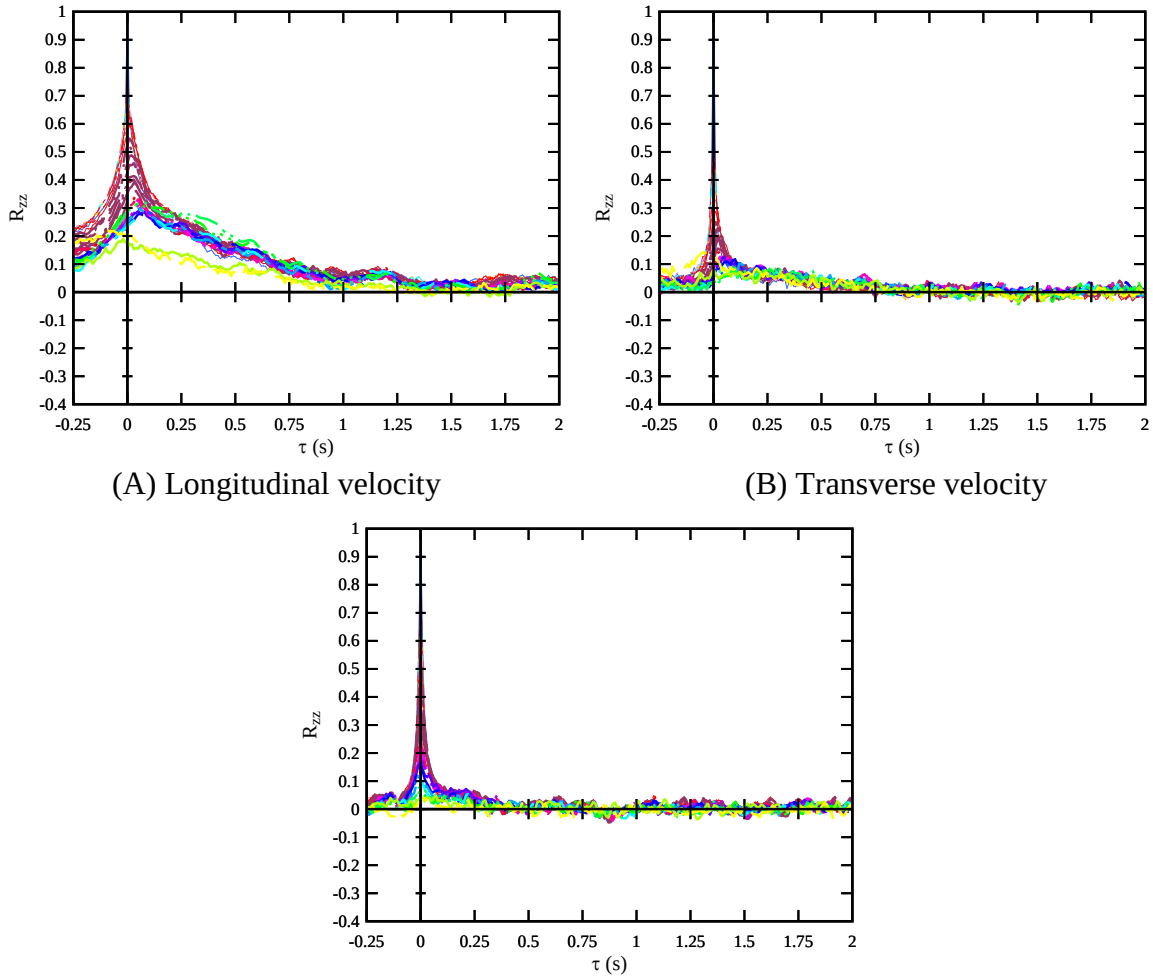

(A) Longitudinal velocity (B) Transverse velocity

(C) Vertical velocity

Fig. 5-3 - Cross-correlation functions of the steady flow velocity components - Coloured curves denoted cross-correlation functions at 30 points in a profile - Flow conditions: Q = 0.099 m^3/s, d_1 = 0.171 m, Fr_1 = 1.6, z/d_1 = 0 to 0.17, Profiler located at x = 7.87 m.

Table 5-1 - Turbulent time and length scales in steady flows

Reference	Q (m^3/s)	d_1 (m)	$(z/d_1)_{min}$	$(z/d_1)_{max}$	$L_{z,x}$ (m)	$T_{z,x}$ (s)	$L_{z,y}$ (m)	$T_{z,y}$ (s)	$L_{z,z}$ (m)	$T_{z,z}$ (s)	$L_{y,x}$ (m)	$T_{y,x}$ (s)	$L_{y,y}$ (m)	$T_{y,y}$ (s)
Present study	0.099	0.177	0.00	0.17	0.013	0.230	0.007	0.040	0.010	0.024	N/A	N/A	N/A	N/A
			0.17	0.34	0.013	0.172	0.007	0.040	0.011	0.025	N/A	N/A	N/A	N/A
			0.56	0.73	0.009	0.066	0.007	0.019	0.019	0.050	N/A	N/A	N/A	N/A
	0.099	0.215	0.00	0.14	0.013	0.261	0.004	0.014	0.009	0.021	N/A	N/A	N/A	N/A
			0.56	0.70	0.008	0.045	0.006	0.013	0.019	0.038	N/A	N/A	N/A	N/A
SIMON & CHANSON (2013)[1]	0.053	0.112	0.11	--	N/A	N/A	N/A	N/A	N/A	N/A	0.004	0.040	0.006	0.018
			0.27	--	N/A	N/A	N/A	N/A	N/A	N/A	0.006	0.056	0.010	0.020
			0.45	--	N/A	N/A	N/A	N/A	N/A	N/A	0.006	0.031	0.010	0.017
			0.63	--	N/A	N/A	N/A	N/A	N/A	N/A	0.005	0.011	0.009	0.013

Note: [1]: ADV point measurements collected at a fixed vertical elevation and over different transverse separations Δy.

The maximum cross-correlation function $R_{zz,\,max}$ at some optimum time lag $\tau(R=R_{max})$ was analysed and plotted against the dimensionless vertical separation distance $\Delta z/d_1$, where Δz was measured from the topmost point of a profile (i.e. reference point). Typical data are presented in Figure 5-4, where the legend indicates the relative vertical elevation of the reference point z/δ, where δ is the boundary layer thickness. Results both inside and outside the developing boundary layer are shown. Altogether, the maximum cross-correlation function inside and outside of the boundary layer decreased with increasing separation distance, in a fashion comparable to the experimental findings of FAVRE et al. (1957). Inside the boundary layer, the maximum cross-correlation function decreased sharply as $\Delta z/d_1$ increased from 0 to 0.06, then kept decreasing albeit in a much smoother manner as $\Delta z/d_1$ increased further. Outside of the boundary layer, the maximum cross-correlation function showed a similar trend as the separation distance increased, although with smaller magnitudes overall. This differed from the findings of FAVRE et al. (1957), who observed larger magnitudes in maximum cross-correlation functions outside the boundary layer. A reason of the inconsistency could be caused by the Profiler itself, which exhibited better signal correlations and data quality within the boundary layer (Appendix A).

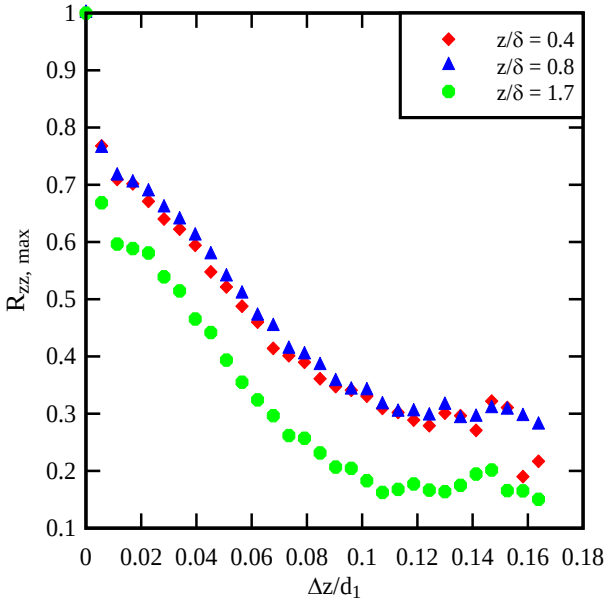

Fig. 5-4 - Maximum cross-correlation functions as functions of separation distance inside (z/δ = 0.4 and 0.8) and outside (z/δ = 1.7) of the developing boundary layer - Flow conditions: Q = 0.099 m^3/s, d_1 = 0.171 m, Fr_1 = 1.6, Profiler located at x = 7.87 m.

5.2 UNSTEADY FLOW TIME AND LENGTH SCALES

5.2.1 Auto-correlation data analyses

The auto-correlation functions of all velocity components were calculated for each sampling point. The calculations were performed in terms of three flow phases: (1) the initially steady flow before bore arrival, (2) the rapidly-varied flow region during the bore passage or deceleration phase, and (3) the unsteady flow region after the bore front passage or early flood tide. Figure 5-5 shows typical auto-correlation functions R_{xx} of the longitudinal velocity component over different flow regions, measured at different vertical elevations z. Overall, for all velocity components and flow conditions, the auto-correlation functions exhibited a bell shape, regardless of the flow phases. The early flood tide phase was associated with largest positive areas under curves compared to the other two flow phases while the rapid deceleration phase was characterised by large negative areas under curves with time lag τ greater than 0.1 s.

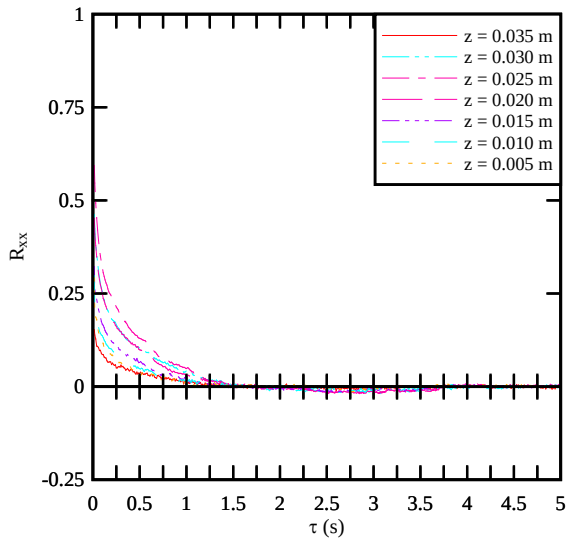

(A) Initially steady flow

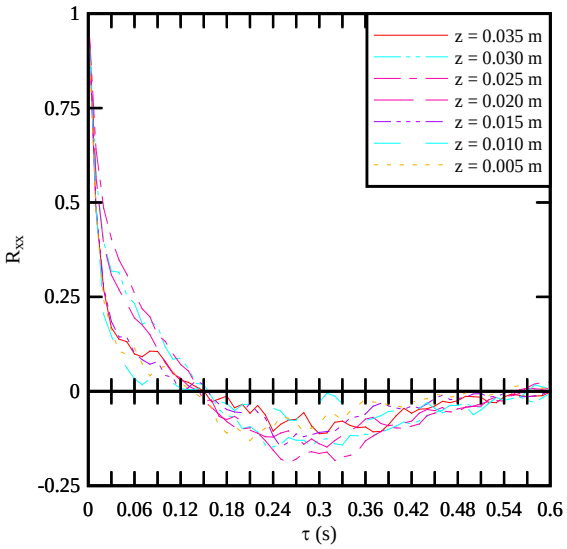

(B) Deceleration phase

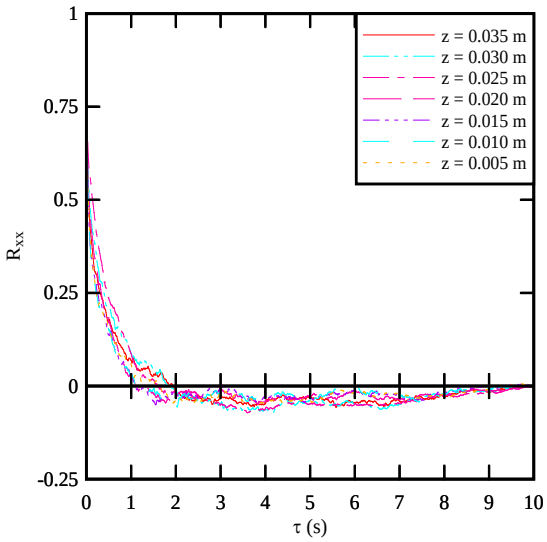

(C) Early flood tide

Fig. 5-5 - Typical auto-correlation functions of the longitudinal velocity over different phases - Flow conditions: Q = 0.099 m_3/s, Fr_1 = 1.6, z/d_1 = 0 to 0.207.

The Eulerian integral time scale T_E was computed based upon the auto-correlation functions, applied to the instantaneous velocity fluctuation data. Figure 5-6A presents typical vertical profiles of the Eulerian integral time scale in the longitudinal velocity direction for the initially steady, rapid deceleration and early flood tide phase. Their shape was not meaningful as highlighted in Figure 5-6B. Figure 5-6B presents two vertical profiles of the Eulerian integral time scale, for two overlapping sampling profile z/d_1 = 0.006 to 0.207 and z/d_1 = 0.092 to 0.289 in the steady flow region. Within the overlapping range, the data highlighted major differences by the two profiles. This was caused by instrumental errors, seen for example in the Profiler velocity signal RMS, which affected all velocity fluctuations. At this stage, the present data could only represent the

orders of magnitude and range of the auto-correlation time scales, but should not be considered in terms of absolute quantitative values.

The results suggested that, for all velocity components and flow conditions, the Eulerian time scales ranged from an order of magnitude of 10^{-2} s to 10^{-1} s, corresponding to a dimensionless range of $T_E \times (g/d_1)^{1/2} = 10^{-2}$ to 1. In the initially steady flow, the time scales in the initially steady flow region were comparable to previous laboratory studies (SIMON and CHANSON 2013, CHANSON and TOI 2015). The early flood tide phase was associated with some large time scale. This is illustrated in Table 5-1 (columns 14 to 16) showing the time scale ratio of before to after the bore. For all velocity components, the auto-correlation time scales were consistently larger after the tidal bore, in the early flood tide, inclusive of the deceleration phase and early flood tide in the present study, compared to in the end ebb tide (initially steady flow, in the present study). The present results were consistent with past field studies (Table 5-2). The data further showed no clear trend in terms of relative vertical elevation and Froude number. The auto-correlation time scales in the longitudinal velocity direction were generally larger than those of the other velocity components (Fig. 5-7, Table 5-2), with $T_{E,y}/T_{E,x}$ ~ 0.3 to 0.8 and $T_{E,z}/T_{E,x}$ ~ 0.7 to 1.5. The results implied that the experimental flow was anisotropic, which agreed with previous laboratory and field studies.

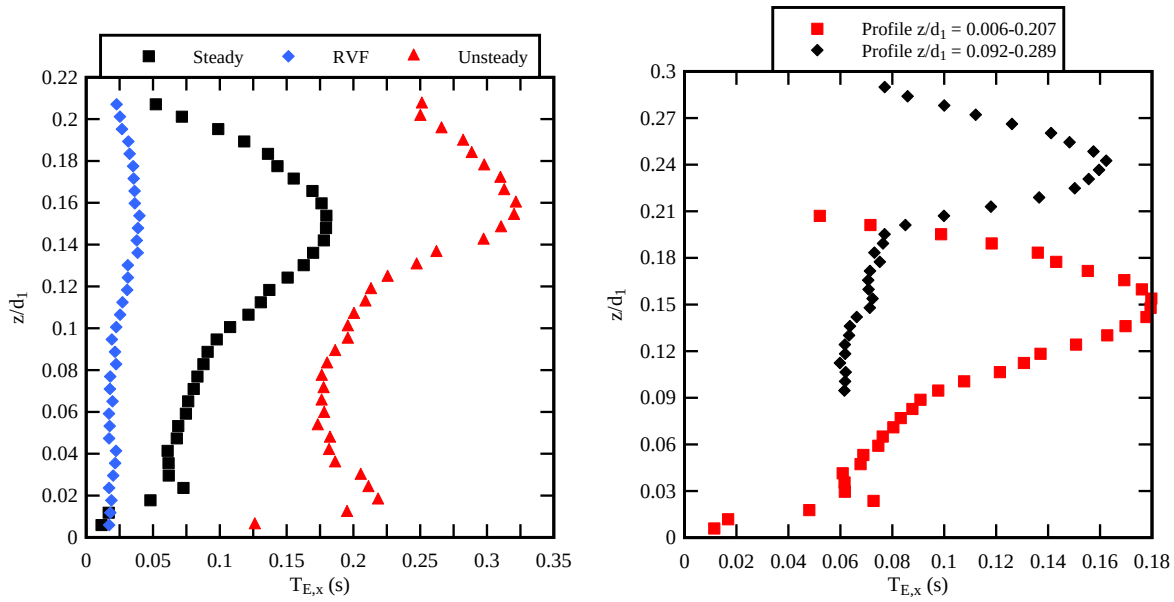

(A, Left) Eulerian auto-correlation time scale of the longitudinal velocity component for the three flow phases for z/d_1 = 0.006 to 0.207

(B, Right) Eulerian auto-correlation time scale for two overlapping vertical profiles z/d_1 = 0.006 to 0.207 and z/d_1 = 0.092 to 0.289 during the initially steady flow

Fig. 5-6 - Eulerian auto-correlation time scale profile of the longitudinal velocity component during steady and unsteady flows - Flow conditions: Q = 0.099 m^3/s, Fr_1 = 1.6.

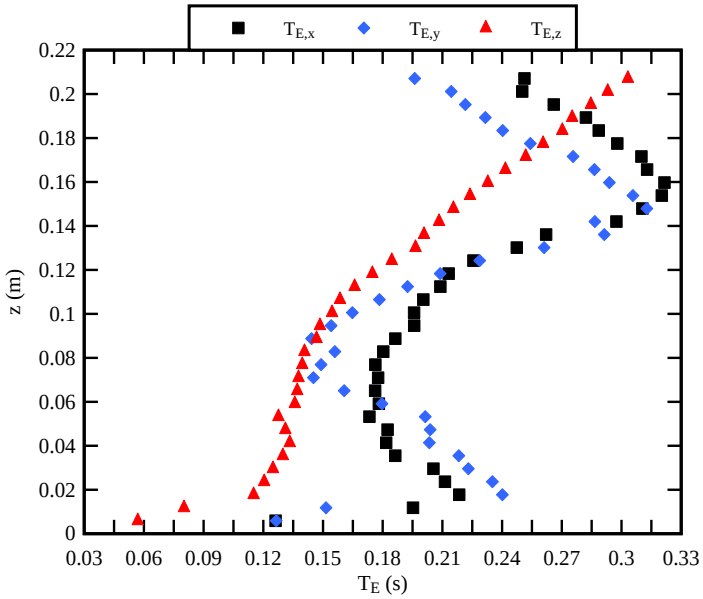

Fig. 5-7 - Eulerian integral time scale profile of the longitudinal, transverse and vertical velocity components over the unsteady flow region; Flow conditions: Q = 0.099 m^3/s, Fr_1 = 1.6, z/d_1 = 0.006 to 0.207.

5.2.2 Integral time and length scales

The cross-correlation functions were calculated between one reference point (the top most point of a single profile) and other points in the same sampling profile for each velocity component, based upon the instantaneous velocity fluctuations v_i, with i = x, y or z. As the flow was rapidly-varying during and following the propagation of the bore front, it would be meaningless to cross-correlate the velocity signals in the rapidly-varied and unsteady flow regions. Herein the turbulent integral time and length scales in the vertical flow direction were derived from the ensemble-averaged cross-correlation functions, and the results are presented in terms of three main flow phases: (1) the initially steady flow before bore arrival, (2) the deceleration phase during the bore passage, and (3) the early flood tide immediately after the bore front passage. Figure 5-8 shows a definition sketch highlighting the three regions. For the initially steady flow, the analysis was performed for the first 60 s of the data sets. The rapid deceleration phase was taken from the start of the free-surface rise, corresponding to the first instance when the first derivative of the water depth became non-zero, to the instance of the minimum streamwise velocity reached at the end of the longitudinal deceleration. All velocity data were analysed within this duration typically ranging from 0.5 s to 2 s. The analysis in the early flood tide, or unsteady flow region, was performed for 10 s, immediately following the end of the deceleration phase. The methodology was applied consistently to all flow conditions.

Table 5-2 - Auto-correlation time scales in tidal bores - Comparison between laboratory and field data

Reference	Site	Instrument	Sampl. rate Hz	Fr_1	d_1 ([1]) m	z/d_1	$T_{E,y}/T_{E,x}$			$T_{E,z}/T_{E,x}$			Ratio After to Before			Remark
							End ebb tide	Rapid deceleration	Early flood tide	End ebb tide	Rapid deceleration	Early flood tide	T_{Ex}	T_{Ey}	T_{Ez}	
(1)	(2)	(3)	(4)	(5)	(6)	(7)	(8)	(9)	(10)	(11)	(12)	(13)	(14)	(15)	(16)	(17)
REUNGOAT et al. (2014)	Garonne River	Sontek microADV	50	1.02	2.91	0.646	--	--	--	--	--	--	21.7	--	--	Field data
REUNGOAT et al. (2015)	Garonne	Nortek Vectrino+	200	1.27	2.05	0.522	0.39	--	0.46	0.39	--	0.09	9.7	11.3	2.33	Field data
Present study	Laboratory	Nortek Vectrino II Profiler	100	1.6	0.17	0.006-0.73	0.36	0.65	0.81	0.83	1.14	1.10	7.1	16.1	11.2	Average values
				1.2	0.199	0.005-0.63	0.32	0.71	0.34	1.11	1.49	0.67	1.68	2.28	1.88	
				2.1	0.097	0.01-0.36	-- ([2])	-- ([2])	--	1.45	0.91	0.75	9.4	-- ([2])	10.1	

Notes: ([1]): water depth at ADV; ([2]): For $Fr_1 = 2.1$, there is no V_y data, because the receivers for V_y component were affected by in the wake behind the receivers: and all velocity characteristics in the y-direction under this flow configuration were deemed erroneous and not considered.

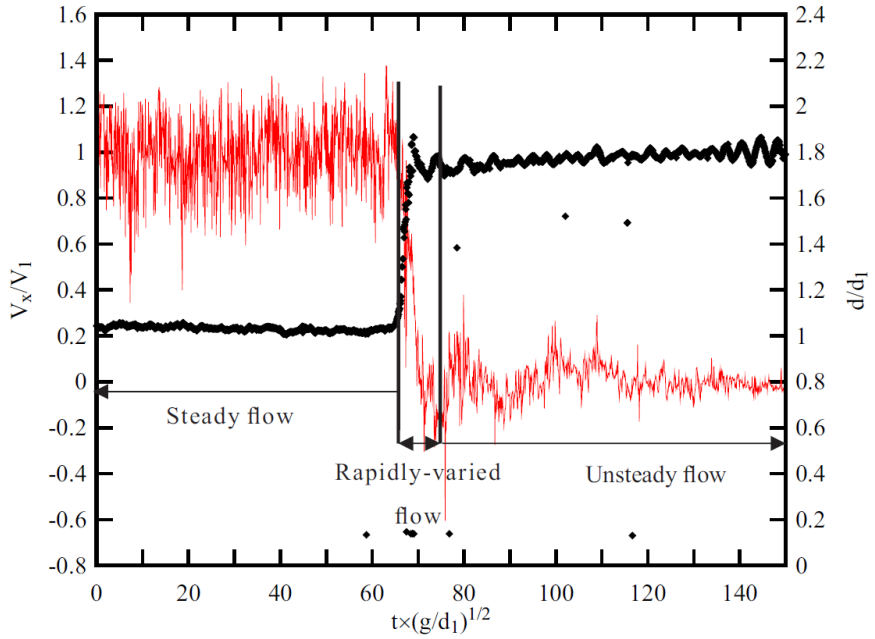

Fig. 5-8 - Definition sketch of different flow phases in the turbulent integral scale analysis, with 6,000 data included in the initially steady flow, between 50 to 200 data in the rapid deceleration phase, and 1,000 data included in the early flood tide phase (unsteady flow).

The ensemble-averaged correlation functions in the steady flow region for all flow conditions exhibited similar shapes and orders of magnitudes as those analysed using the instantaneous velocity data (Section 5.1), although the absolute values of maximum cross-correlations were typically lower than for analyses using the instantaneous fluctuation data. Typical ensemble-averaged cross-correlation functions of the longitudinal velocity during the rapidly-varied and unsteady flow regions for bores of two Froude numbers are presented respectively in Figures 5-9A and 5-9B. The results highlighted some difference in terms of shapes of the cross-correlation functions, compared to the steady flow region, and between different Froude numbers. During the deceleration phase (Fig. 5-9A), all cross-correlation functions showed a quasi-symmetrical shape, with two local minima on each side of the marked maximum. The absolute values of the local minima were less than that of the maximum, for all Froude numbers. The absolute maximum correlation occurred at positive time lags during the initially steady and deceleration phases, and these time lags increased with increasing distance from the reference point (Fig. 5-9A). This suggested that some vortical structures were formed at higher vertical elevations, and tended to dissipate towards the bed. During the early flood tide, however, the time lags became negative for breaking bores with Fr_1 = 1.6, indicating that vortical structures were formed next to the channel bed and advected upwards (Fig. 5-9B, left). For breaking bores with high Froude number (Fr_1 = 2.1), the time lags were almost zero, hinting that large vortical structures, possibly exceeding the length of the profile, were formed and detected almost simultaneously by all sampling points along

a profile. In undular bore (Fr_1 = 1.2), the cross-correlation functions during the early flood tide showed a quasi-symmetrical shape, with periodic variations for the positive and negative time lags (Fig. 5-9B, right). The time lags corresponding to the maximum cross-correlations for undular bore were positive throughout the three flow phases.

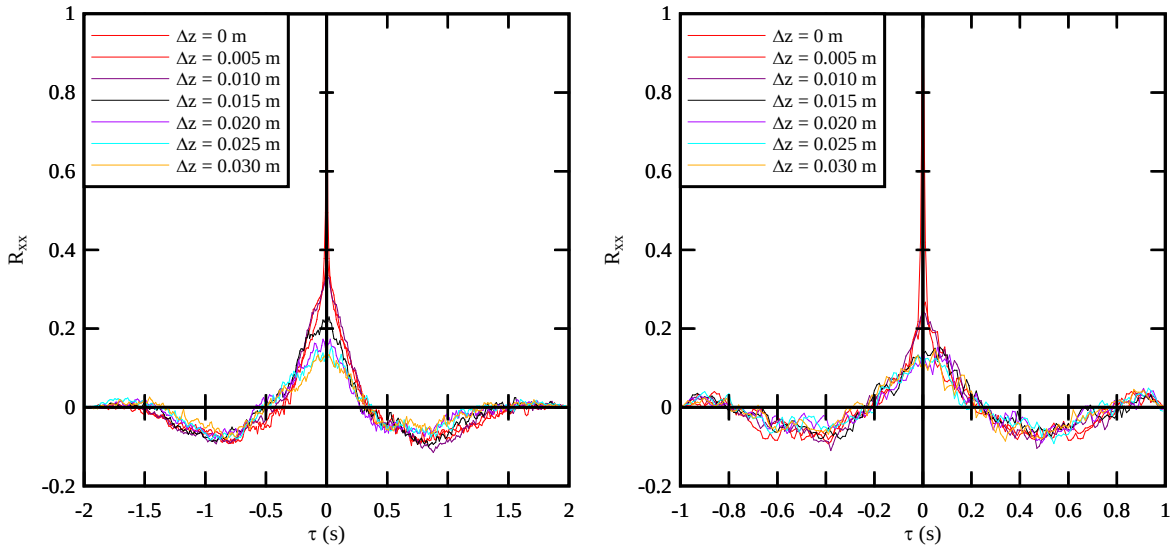

(A) Deceleration phase (left Fr_1 = 1.6, right Fr_1 = 1.2)

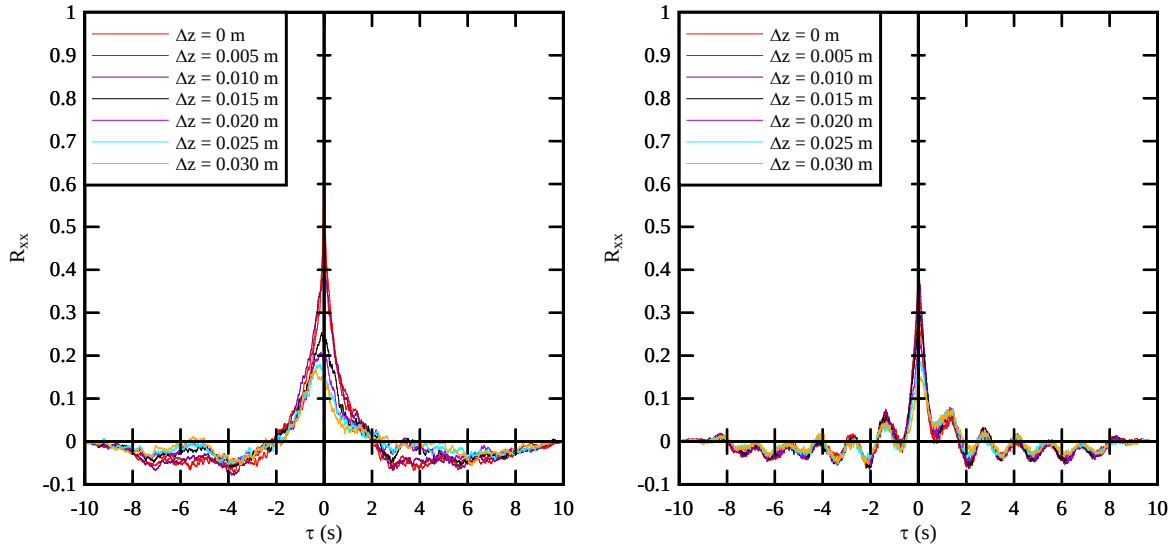

(B) Early flood tide (left: Fr_1 = 1.6; right: Fr_1 = 1.2)

Fig. 5-9 - Ensemble-averaged cross-correlation functions of the longitudinal velocity component for the rapid deceleration phase (rapidly-varied flow) and the early flood tide (unsteady flow) - Flow conditions: Q = 0.099 m^3/s at two Froude numbers Fr_1 = 1.2 and 1.6.

Table 5-3 summarises the turbulent integral time and length scales for the longitudinal, transverse and vertical velocity components for all flow conditions during different flow phases. The results are compared to a previous laboratory study (SIMON and CHANSON 2013). Overall the data

highlighted that the propagation of tidal bores in an open channel flow was an anisotropic turbulent process, with the turbulent time and length scales being much larger with the longitudinal and vertical velocity components than in the transverse component: that is, $L_{z,y}/L_{z,x}$ ~ 0.1 to 0.9 and $T_{z,y}/T_{z,x}$ ~ 0.1 to 0.6. The present study demonstrated that a majority of turbulent time and length scales in the vertical velocity direction were larger than those in the longitudinal velocity direction, with $L_{z,z}/L_{z,x}$ ~ 1.1 to 7.3 and $T_{z,z}/T_{z,x}$ ~ 1.1 to 14.4, for all the flow conditions. Physically, this would suggest that the vertical size and lifespan of the vortical structures were larger in the vertical direction compared to those in the longitudinal directions. Visual observations in breaking bores highlighted indeed large helicoidal structures, elongated mostly along the vertical direction, which existed both in the roller and the aerated flow regions following the roller (Fig. 5-10). The experimental results could be representations of these vortical structures. Note however that earlier observations of neutrally-buoyant particle trajectories suggested flatter structures in undular bores (CHANSON and TAN 2010,2011).

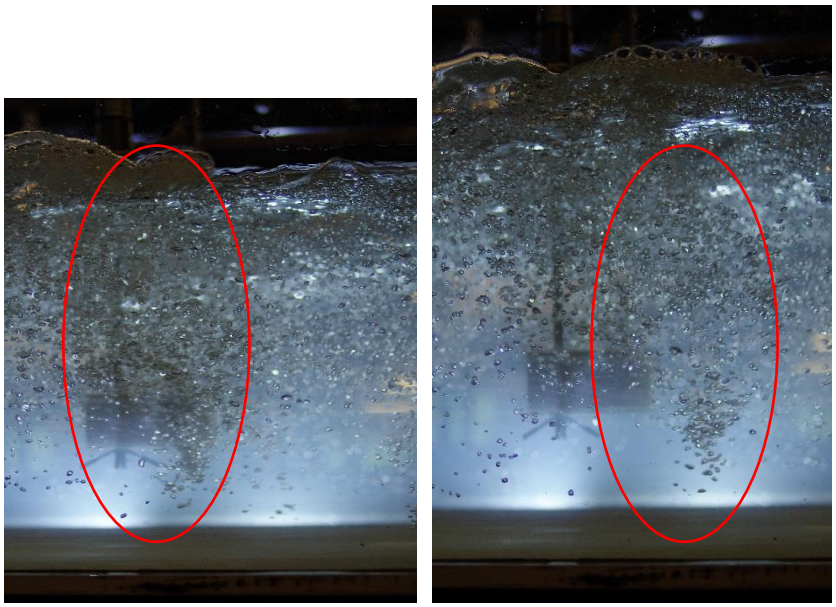

Fig. 5-10 - Photographs of vertical vortices formed in the aerated flow region following the breaking bore roller; Flow conditions: Q = 0.099 m^3/s, Fr_1 = 2.1, photograph taken on 14/04/2015.

Table 5-3 - Unsteady turbulent integral time and length scales for all velocity components and flow conditions

					Steady		Deceleration		Early flood tide		Steady		Deceleration		Early flood tide		Steady		Deceleration		Early flood tide	
Present study	Q (m^3/s)	Fr_1	d_1 (m)	$(z/d_1)_{max}$	$L_{z,x}$ (m)	$T_{z,x}$ (s)	$L_{z,x}$ (m)	$T_{z,x}$ (s)	$L_{z,x}$ (m)	$T_{z,x}$ (s)	$L_{z,y}$ (m)	$T_{z,y}$ (s)	$L_{z,y}$ (m)	$T_{z,y}$ (s)	$L_{z,y}$ (m)	$T_{z,y}$ (s)	$L_{z,z}$ (m)	$T_{z,z}$ (s)	$L_{z,z}$ (m)	$T_{z,z}$ (s)	$L_{z,z}$ (m)	$T_{z,z}$ (s)
	0.099	1.6	0.169	0.207	0.007	0.073	0.009	0.040	0.010	0.210	0.004	0.011	0.004	0.014	0.009	0.217	0.009	0.021	0.009	0.026	0.015	0.226
	0.099	1.6	0.173	0.289	0.007	0.067	0.010	0.019	0.009	0.207	0.004	0.006	0.005	0.012	0.008	0.142	0.010	0.020	0.008	0.018	0.018	0.343
	0.099	1.6	0.170	0.735	0.003	0.006	0.009	0.010	0.009	0.181	0.003	0.003	0.005	0.005	0.008	0.111	0.013	0.027	0.015	0.019	0.020	0.301
	0.099	1.2	0.196	0.199	0.005	0.062	0.007	0.018	0.010	0.118	0.003	0.007	0.004	0.005	0.005	0.025	0.008	0.018	0.008	0.013	0.012	0.037
	0.099	1.2	0.197	0.254	0.005	0.050	0.006	0.022	0.009	0.080	0.003	0.005	0.003	0.004	0.004	0.016	0.008	0.018	0.008	0.022	0.012	0.036
	0.099	1.2	0.199	0.628	0.002	0.003	0.004	0.005	0.007	0.038	0.003	0.004	0.004	0.005	0.004	0.010	0.016	0.048	0.016	0.032	0.018	0.061
	0.099	2.1	0.097	0.361	0.003	0.010	0.004	0.014	0.006	0.101	--	--	--	--	--	--	0.004	0.005	0.006	0.018	0.013	0.095

					Early flood tide		Early flood tide	
SIMON and CHANSON (2013)[1]	Q (m^3/s)	Fr_1	d_1 (m)	$(z/d_1)_{max}$	$L_{y,x}$ (m)	$T_{y,x}$ (s)	$L_{y,y}$ (m)	$T_{y,y}$ (s)
	0.053	1.6	0.112	0.110	0.004	0.038	0.007	0.039
				0.270	0.007	0.058	0.010	0.049
				9.450	0.006	0.050	0.010	0.051
				0.630	0.007	0.051	0.009	0.037
	0.053	1.3	0.112	0.110	0.005	0.042	0.006	0.033
				0.270	0.006	0.053	0.010	0.032
				9.450	0.008	0.062	0.010	0.027
				0.630	0.008	0.055	0.012	0.025

Note: [1]: ADV point measurements collected at a fixed vertical elevation and over different transverse separations Δy, calculation based upon velocity fluctuations.

The early flood tide phase was associated with large time and length scales, compared to those during the initially steady flow and deceleration phases. The early flood tide time scales were an order of magnitude higher than the steady flow and rapid deceleration time scales in the lower water column, regardless of velocity directions and initial flow conditions. The time and length scales seemed to decrease with increasing vertical elevations, and be possibly related to the initial flow depth.

The present study compared well with a past laboratory data (SIMON and CHANSON 2013) in terms of orders of magnitude, except for time scales during the early flood tide phase for breaking bores: then, the present time scales were an order of magnitude larger. In terms of quantitative results, both the turbulent integral time and length scales were larger compared to this past study. A reason could be that the present experiments were performed in a much larger facilities with higher Reynolds numbers. Furthermore, previous experimental data was collected by point measurements using two ADVs, separated at 6 transverse intervals, with 5 experiments repeated for each interval. Herein the study was performed in the vertical direction by sampling simultaneous 35 points, each two adjacent points separated at 1 mm, and repeated 25 times. The present spatial resolution was much finer, and the correlations between velocity signals were expected to be higher, as all points were sampled at the same time.

6. CONCLUSION

New unsteady velocity measurements were conducted to study the turbulent characteristics of tidal bores in a relatively large-size laboratory facility using a Nortek^{TM} ADV Vectrino II Profiler equipped with a fixed stem and down-looking head. The Profiler recorded instantaneous velocities in a vertical profile of 35 mm high, consisting of 35 velocity sampling points in total. The Profiler was sampled at 100 Hz, and the longitudinal, transverse and vertical velocity components were recorded simultaneously for all 35 sampling points. The free-surface elevations were also measured simultaneously using a series of acoustic displacement meters (ADMs) located at different longitudinal positions along the channel centreline. The ADMs were sampled 100 Hz, synchronised with the Profiler. Both undular and breaking bores were investigated with Froude numbers ranging from 1.2 to 2.1. An ensemble-averaged measurement technique was used. All experiments were repeated 25 times and results ensemble-averaged. The number of repeats was determined by a sensitivity analysis.

Preliminary steady and unsteady velocity measurements using the Profiler showed a close agreement with previous experimental results obtained using a Nortek^{TM} ADV Vectrino+ for the same flow conditions (LENG and CHANSON 2015c), in terms of the instantaneous median velocity and velocity fluctuations, instantaneous median Reynolds stresses and shear stress fluctuations, longitudinal velocity recirculation, longitudinal velocity deceleration, etc. The instantaneous velocity fluctuations and Reynolds stress fluctuations were of the same order of magnitude between the Profiler and ADV results. The Profiler data showed that the longitudinal velocity profile within the inner region of the turbulent boundary layer followed the log law before, during and after the passage of tidal bores. The Eulerian time scale, turbulent time and length scales in the vertical direction were computed for steady flows and rapidly-varied unsteady flows associated with tidal bores. The results indicated that the propagation of tidal bores in an open channel flow is an anisotropic process, with larger time and length scales in the longitudinal and vertical directions. The time and length scales were of an order of magnitude between 1 ms and 100 ms, and 10^{-3} m and 10^{-1} m respectively, similar to previous laboratory and field data. Some instrumental error was observed. Outside the boundary layer, the Profiler tended to produce errors in terms time-averaged velocity data and velocity fluctuations for a number of points in a profile. Even at vertical elevations where the time-averaged velocity was meaningful, the vertical distribution of the velocity fluctuations contained errors.

Overall, the study demonstrated that the propagation of tidal bores is a highly unsteady turbulent process, and the performance of Vectrino II Profiler in such an unsteady turbulent flow was satisfactory, provided that a careful validation was undertaken for all Profiler outputs.

7. ACKNOWLEDGEMENTS

The authors thank Dr Bruce MACVICAR (University of Waterloo, Canada) and Dr Heide FRIEDRICH (University of Auckland, New Zealand) for their detailed review of the report and valuable comments.

The authors thank Professor Pierre LUBIN (University of Bordeaux, France) and Dr Hang WANG (The University of Queensland, Australia) for their personal involvement, contribution and comments. The authors also thank Dr Bruce MACVICAR (University of Waterloo, Canada) and Professor Colin RENNIE (University of Ottawa, Canada) for sharing their expert advice. The authors acknowledge the technical contribution of Dr Jan BECKER (Federal Waterways Engineering and Research Institute, Germany) and Gangfu ZHANG (The University of Queensland, Australia) in the data post-processing program. The authors also acknowledge the technical assistance of Jason VAN DER GEVEL, Stewart MATTHEWS and Dr Van Thuan NGUYEN (The University of Queensland). The financial support through the Australian Research Council (Grant DP120100481) is acknowledged.

APPENDIX A. PRELIMINARY EXPERIMENTS USING VECTRINO II PROFILER

A.1 PRESENTATION

New experiments were conducted using a Nortek Vectrino+ acoustic Doppler velocimeter (Serial number P21419, Hardware ID VNO 0436) and an ADV Vectrino II Profiler (Serial number P27338, Hardware ID VNO 1366) in both steady and unsteady flows. The aim of the experiments was to test the quality of the data recorded by the Vectrino Profiler, by comparing the velocity profile data obtained with the Profiler to velocity data measured by the ADV. The Vectrino II Profiler is a high-resolution acoustic Doppler velocimeter used to measure instantaneous velocity in a wide variety of applications from the laboratory to the Ocean (Nortek 2012). The basic measurement technology is coherent Doppler processing, which is characterised by accurate data and no appreciable zero offset (Nortek 2012). Previous experimental studies using a Vectrino Profiler included those by CRAIG et al. (2011), ZEDEL and HAY (2011) and MACVICAR et al. (2014). The above studies found advantages as well as issues associated with the deployment of an ADV Vectrino II Profiler in turbulent flows.

The Profiler was equipped with a fixed stem and a down-looking head, with one central emitter and four receivers, capable of recording velocity components in the longitudinal, transverse and vertical directions. Herein the velocity characteristics were sampled simultaneously for a 30 mm profile, with 30 sampling points throughout the profile using downward-facing receivers and emitter. The sample profile was set to be 45 mm away from the downward-facing emitter (Figure A-1). Hence there was a physical limitation on the highest elevation where the Profiler was able to work in the water column.

An acoustic Doppler velocimeter was used to check the quality of the Profiler data. The acoustic Doppler velocimeter (ADV) was a Nortek™ Vectrino+, equipped with a three-dimensional side-looking head, capable of measuring three velocity components (longitudinal, transverse and vertical) at a single point within the water column. The velocity range was ±1.0 m/s and the sampling rate was 200 Hz. The data accuracy was 1% of the velocity range. The ADV was set up with a transmit length of 0.3 mm and a sampling volume of 1.5 mm height.

The ADV and Profiler were mounted side by side at the same longitudinal location x = 7.87m, where x was measured from the upstream end of the experimental channel (Fig. A-1). The ADV control volume was at approximately the same vertical elevation of the mid-point of the Profiler control volume. The Profiler emitter was centred on the channel centreline, with a transverse separation distance of 0.085 m between control volumes of the ADV and Profiler. The two velocimeters were connected to two separate data acquisition systems, and the data acquisitions

were synchronised together such that the two velocimeters started data recording at the same time. The sampling rates for ADV and Profilers were respectively 200 Hz and 100 Hz. The unsteady free-surface variations were measured by a series of acoustic displacement meters (ADMs), sampled simultaneously with the ADV and Profiler at 200 Hz on the channel centreline. Figure A-1 shows dimensioned side and top views of the experimental channel and instrument setup.

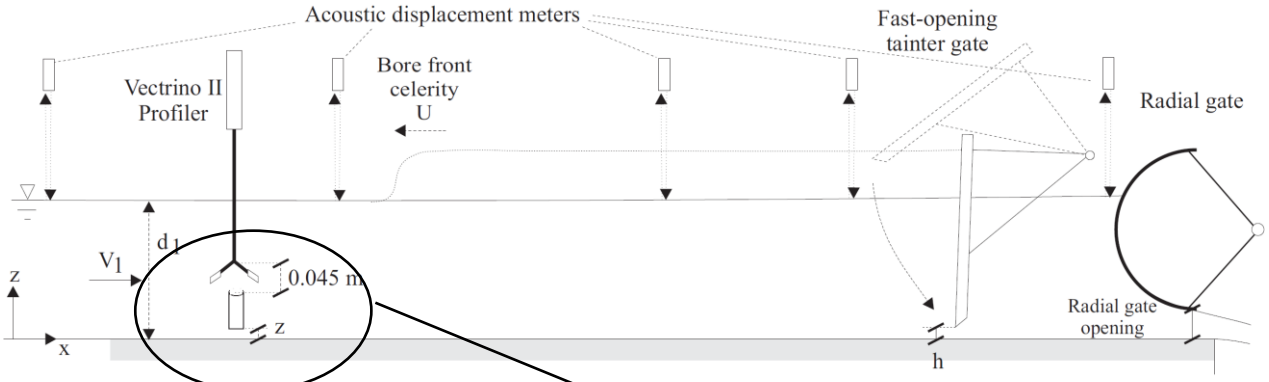

(A) Side view of the experimental channel

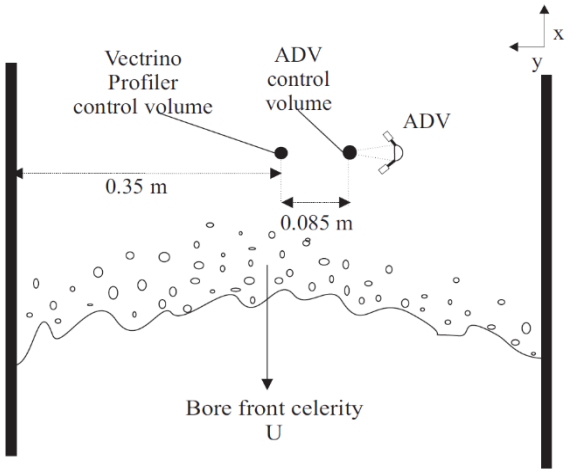

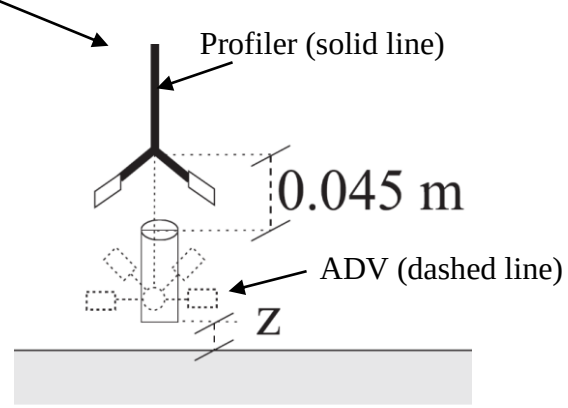

(B, Left) View in elevation (thick black line indicates channel side walls)

(C, Right) Details of the relative vertical elevations of the ADV and Profiler

Fig. A-1 - Sketches of the experimental channel and instrument setup.

The Profiler output data were saved as MATLAB files and post-processed using the MATLAB program VTMT version 1.1, designed and written by Jan BECKER from Federal Waterways Engineering and Research Institute (BAW), Karlsruhe (Germany). In steady flows, the post-processing included the removal of data with average correlation values less than 90% and average signal to noise ratio less than 5 dB. In addition, the phase-space thresholding technique developed by GORING and NIKORA (2002) was applied to removal spurious points in the data set. In the unsteady flows, the above post-processing technique was not applicable (NIKORA 2004, *Person. Comm.*, CHANSON 2008,2010, KOCH and CHANSON 2009), and the data was output directly for

analysis.

Various flow discharges from 0.055 m^3/s to 0.100 m^3/s were tested in the steady and unsteady flow experiments. The channel was horizontal ($S_o = 0$) and a complete Tainter gate closure (h = 0) was used to generate breaking bores during the unsteady flow experiments. The velocity measurements were performed at a number of vertical elevations z throughout the water column, with ADV and Profiler sampling simultaneously. The experimental flow conditions are summarised in Table A-1.

Table A-1 - Experimental flow conditions of the steady flow Profiler tests

Date	x (m)	Q (m^3/s)	d_1 (m)	Fr_o	Radial gate opening (m)	z (m)	Instrumentation
8/01/2015	7.87	0.100	0.177	0.60	N/A	0.001-0.130	ADV & Profiler
13/01/2015	7.87	0.085	0.161	0.60	N/A	0.001-0.096	ADV & Profiler
13/01/2015	7.87	0.071	0.144	0.59	N/A	0.001-0.090	ADV & Profiler
13/01/2015	7.87	0.100	0.215	0.45	0.112	0.001-0.150	ADV & Profiler
13/01/2015	7.87	0.086	0.211	0.40	0.090	0.001-0.150	ADV & Profiler
15/01/2015	7.87	0.071	0.21	0.33	0.670	0.001-0.150	ADV & Profiler
16/01/2015	2	0.100	0.19	0.55	N/A	0.001-0.120	ADV & Profiler
16/01/2015	2	0.055	0.201	0.27	0.05	0.001-0.150	ADV & Profiler

Notes: x: longitudinal location of velocity sampling point, measured from the upstream end of the experimental channel; Q: water discharge; d_1: initially steady flow water depth at velocity sampling point; Fr_o: initially steady flow Froude number; z: vertical elevation of velocity sampling point.

A.2 COMPARATIVE RESULTS IN STEADY FLOW

Figure A-2 presents the steady flow profile of the longitudinal velocity V_x and velocity fluctuations, characterised by the standard deviations of the three velocity components (v_x', v_y' and v_z'), with a comparison between the ADV and Profiler results. The data showed a close agreement between the velocity magnitudes and fluctuations recorded by the Profiler and those measured by the ADV. However some outlying points occurred slightly above the outer edge of the boundary layer. The occurrence of these suspicious points were consistent in terms of the velocity directions. That is, if the longitudinal velocity showed outlying data at some particular vertical elevations, similar outliers would be observed at the same vertical elevations in both transverse and vertical velocity components. Figure A-2 also highlights larger difference in vertical velocity fluctuations measured by the ADV and Profiler, compared to the fluctuations in the other two velocity components. This could be caused by the effect of the bed proximity on the receiver for the vertical velocity

component ([1]).

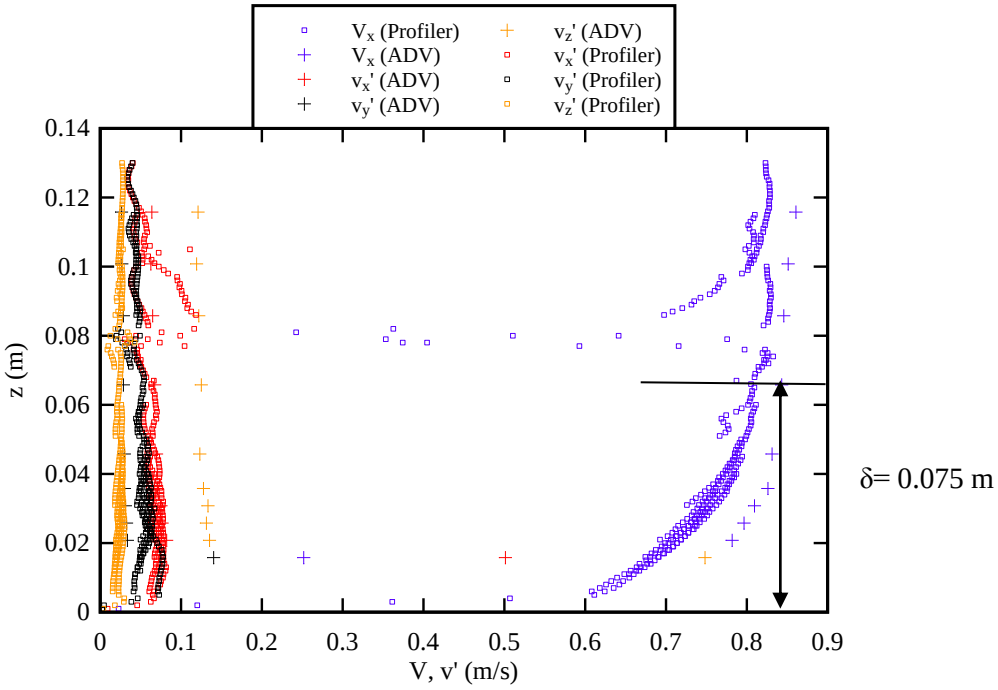

Fig. A-2 – Vertical profile of the time-averaged longitudinal velocity and velocity fluctuations in steady flow: a comparison between ADV and Profiler data - Q = 0.100 m^3/s, d_1 = 0.177 m, x = 7.87 m.

Figure A-3 presents the time-variations of instantaneous longitudinal velocity in an unsteady flow, measured at a profile where obvious outliers were observed in steady flows. The ADV data, marked by a black dashed line, was deemed to be reasonably accurate to characterise accurately the velocity field. Other curves were selected from the 30 points in a single profile measured by the Profiler. For the elevations associated with unrealistic velocity values in steady flows (z = 0.082, 0.083, 0.084, 0.085, 0.086, 0.087 m), the data also exhibited values deviating substantially from the ADV results, as seen in the steady flow region in Figure A-3. The results suggested no difference in terms of data quality between steady and unsteady flows. However, after the passage of the bore, which was highlighted by the sudden deceleration of the longitudinal velocity, the deviation between ADV and Profiler data became less significant, but is was unclear if this indicated any improvement of Profiler data quality after the passage of a bore.

[1] A number of studies showed that, with the ADV Vectrino+, the vertical velocity component V_z data might be affected adversely by the bed proximity for z < 0.030 m (CHANSON and DOCHERTY 2012). This was associated with unusually large vertical velocity fluctuations throughout most of the water column (CHANSON 2010, CHANSON and DOCHERTY 2012, LENG and CHANSON 2015c).

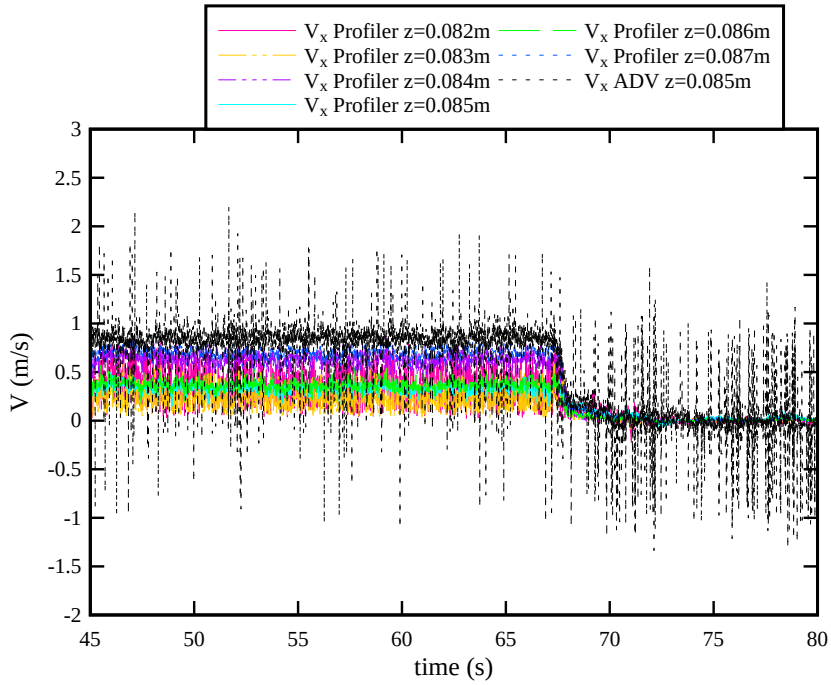

Fig. A-3 - Instantaneous longitudinal velocity variations as functions of time measured by the ADV and Profiler - Selected Profiler data were sampled in one profile.

Further scrutiny into the data suggested the following findings:

- The locations of the error points in a single profile at a fixed vertical elevation were consistent and can be reproduced by repeating experiments at this elevation, whether the flow was steady or unsteady.
- A single profile could be free of any error points in terms of the time-averaged velocity, and this is often associated with profiles inside the boundary layer.
- Change of flow conditions (discharge, initial water depth, bed slope etc.) may change the amount and locations of the error points.
- Overall, the locations of the error points were either at the outer edge of the boundary layer, or above the outer edge of the boundary layer. Within the experimental flow conditions of the present study, the Profiler gave good approximation in the time-averaged velocity profiler within the turbulent boundary layer.
- The locations of the error points in a single velocity profile measured by the Profiler were completely random and could be discontinuous. That is, the error points could occur at the bottom, middle or top of the profile. They could occur as the top five points in the profile, or the first, second and fifth points in the profile.
- The locations of the error points were not consistent with their vertical elevations in the water column. For example, for a single profile detecting the range z = 0.03-0.06 m, error

could occur at z = 0.0045 m but did not necessarily to occur at the same elevations for a single profile detecting the range z = 0.004-0.007 m.

A number of measuring parameters of the ADV Profiler were modified to investigate their effect on the proportion of erroneous measurements. The tests were conducted for a water discharge of Q = 0.100 m^3/s with zero bed slope, at three vertical elevations z = 0.065 m, 0.085 m and 0.1 m. Steady flow velocity profiles were tested by changing one parameter at a time. The modified parameters and range of modifications were listed in Table A-2. Overall the results suggested that, for the range of parameters tested, little effect was observed in terms of the proportion of error points.

Figures A-4 to A-6 present vertical velocity profiles and velocity fluctuations for the experiments performed at x = 7.87 m, with comparisons between the ADV and Profiler data. For measurements conducted without the downstream radial gate (Fig. A-4A, A-5A & A-6A), the Profiler results showed consistently some error points above the outer edge of the boundary layer for all discharges. Within the boundary layer, the ADV and Profiler data were quite close. More experiments were conducted with a downstream radial gate to increase the initial water depth to examine data quality further above from the boundary layer outer edge (Fig. A-4B, A-5B & A-6B). The results highlighted error points above a vertical elevation which was two times the boundary layer thickness for all flow conditions, except for the highest flow discharge.

Table A-2 - Modified parameters and ranges of modifications in the steady flow tests of ADV Vectrino II Profiler

Parameter	Range
Velocity range (m/s)	0.5, 1, 1.5, 2
Ping algorithm	Minimum interval, maximum interval, adaptive
Sampling rate (Hz)	50, 100
Cell size (mm)	1, 2, 4
Detection range (mm)	45-74, 40-69, 40-50, 40-60
Seeding concentration (g/L)	0, 100 g per 5 litres

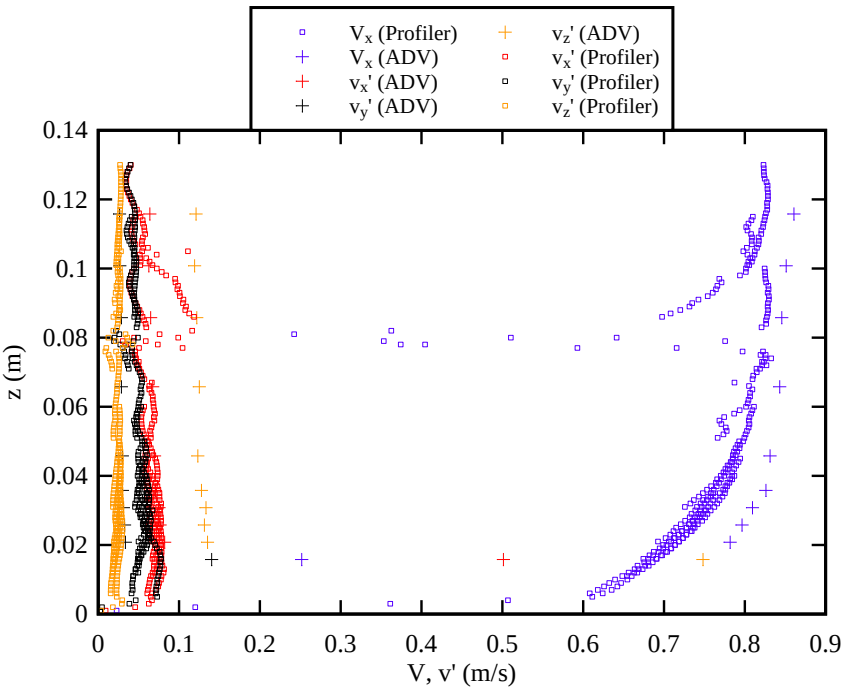

(A) d_1 = 0.177 m, radial gate fully open

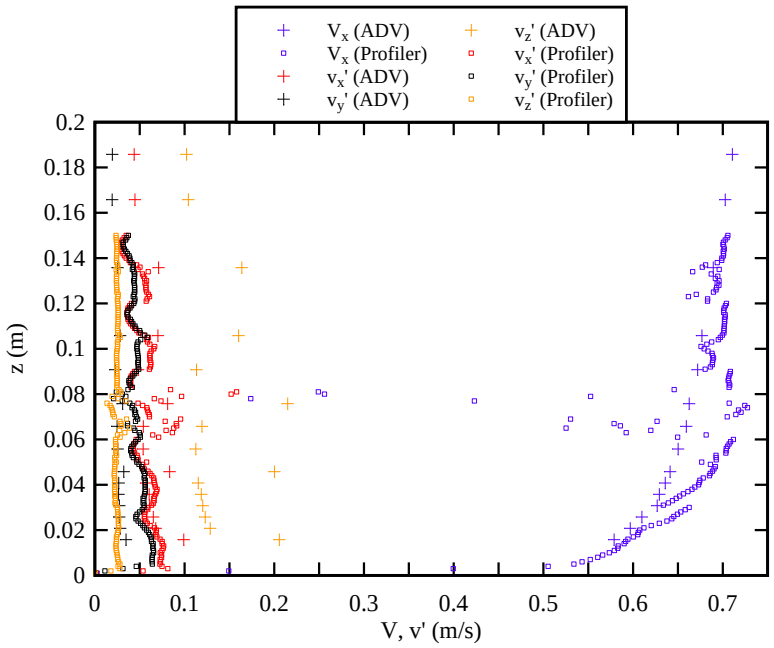

(B) d_1 = 0.215 m, radial gate opening = 0.112 m

Fig. A-4 - Time-averaged velocity profile of the longitudinal velocity and velocity fluctuations in steady flow: a comparison between ADV and Profiler data for Q = 0.100 m^3/s, x = 7.87 m.

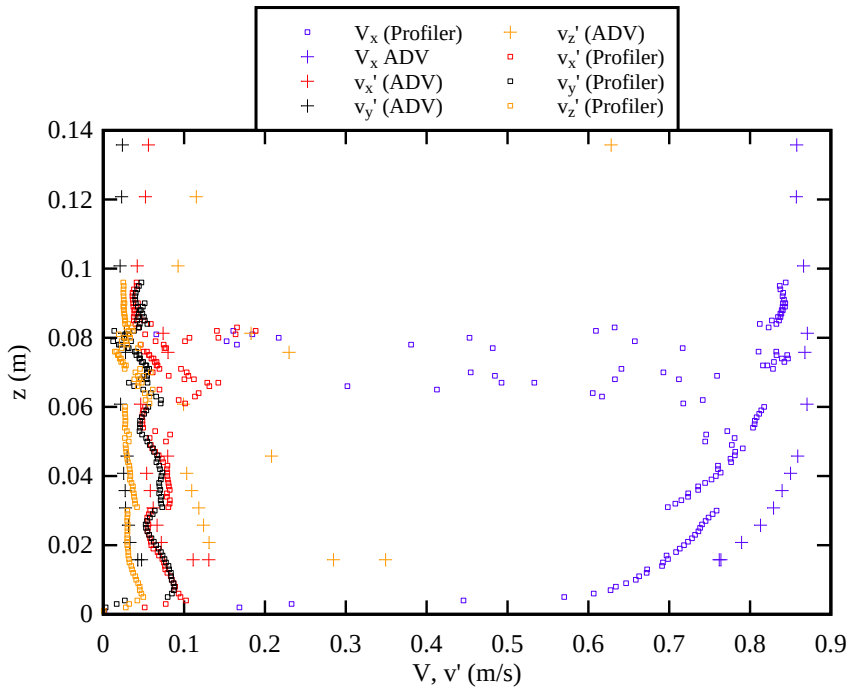

(A) d_1 = 0.161 m, radial gate fully open

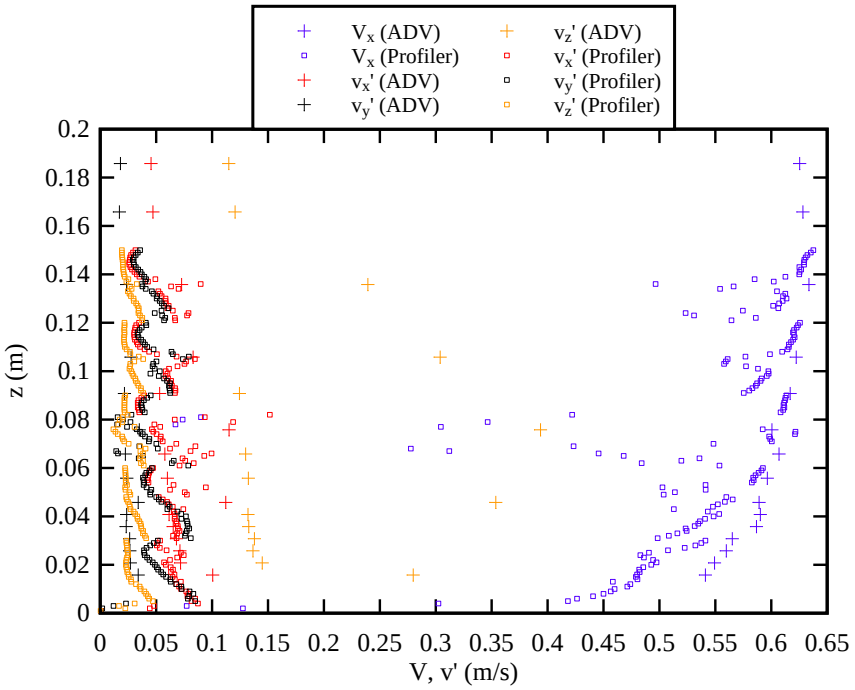

(B) d_1 = 0.211 m, radial gate opening = 0.09 m

Fig. A-5 - Time-averaged velocity profile of the longitudinal velocity and velocity fluctuations in steady flow: a comparison between ADV and Profiler data for Q = 0.085 m^3/s, x = 7.87 m.

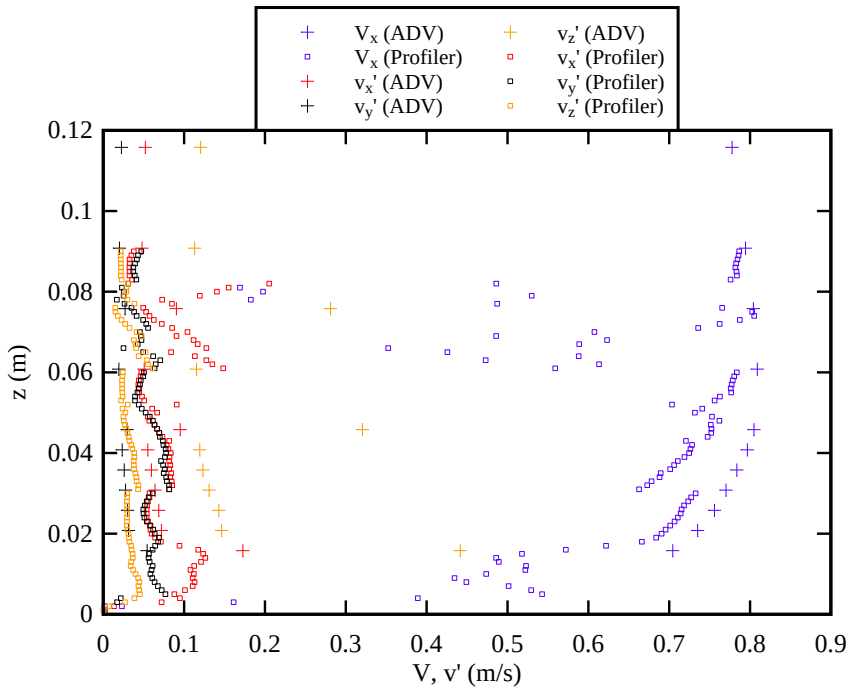

(A) d_1 = 0.144 m, radial gate fully open

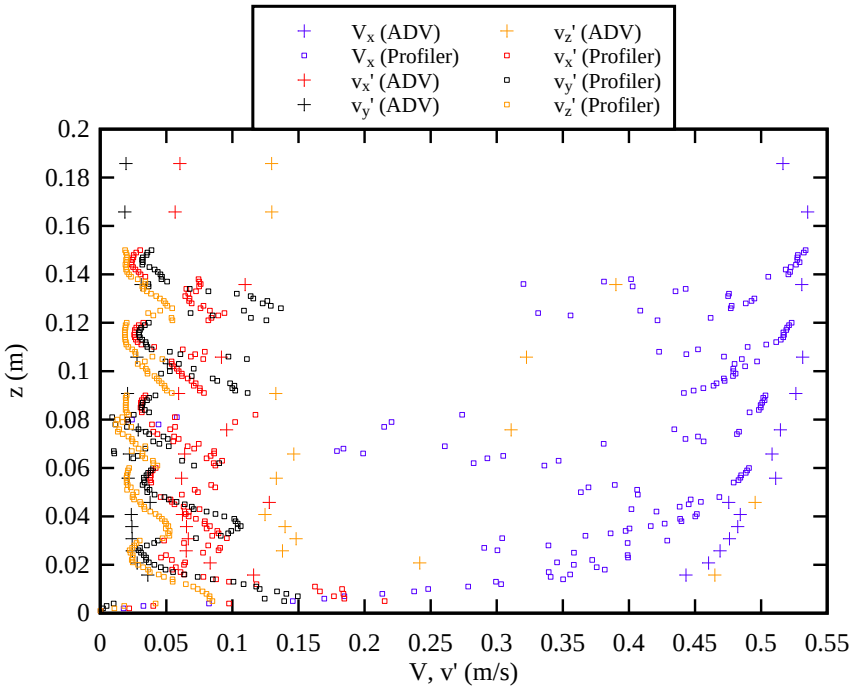

(B) d_1 = 0.21 m, radial gate opening = 0.067 m

Fig. A-6 - Time-averaged velocity profile of the longitudinal velocity and velocity fluctuations in steady flow: a comparison between ADV and Profiler data for Q = 0.071 m^3/s, x = 7.87 m.

Further experiments were conducted near the upstream end of the channel at x = 2 m to examine the effect on the occurrence of error points with a thinner boundary layer. Figure A-7 shows the vertical velocity profile and fluctuations measured by the ADV and Profiler, in which the ADV data clearly highlighted a boundary layer thickness of approximately 0.02 m for both discharges of 0.100 m^3/s

and 0.055 m^3/s. Although the boundary layer thickness was significantly thinner, compared to measurements done at x = 7.87 m, the results suggested no obvious difference in the occurrence of the error points, both in terms of locations and quantity, for a discharge Q = 0.100 m^3/s (Fig. A-7A & A-4). Altogether, the findings indicated that the presence of the error points in the Profiler measurements may not be directly related to the turbulent mixing at the vicinity of the boundary layer outer edge, but more related to the flow discharge, channel geometry and vertical elevation. Importantly all data highlighted comparatively accurate recordings close to the channel bed within the boundary layer thickness regardless of flow discharge depth and boundary layer characteristics.

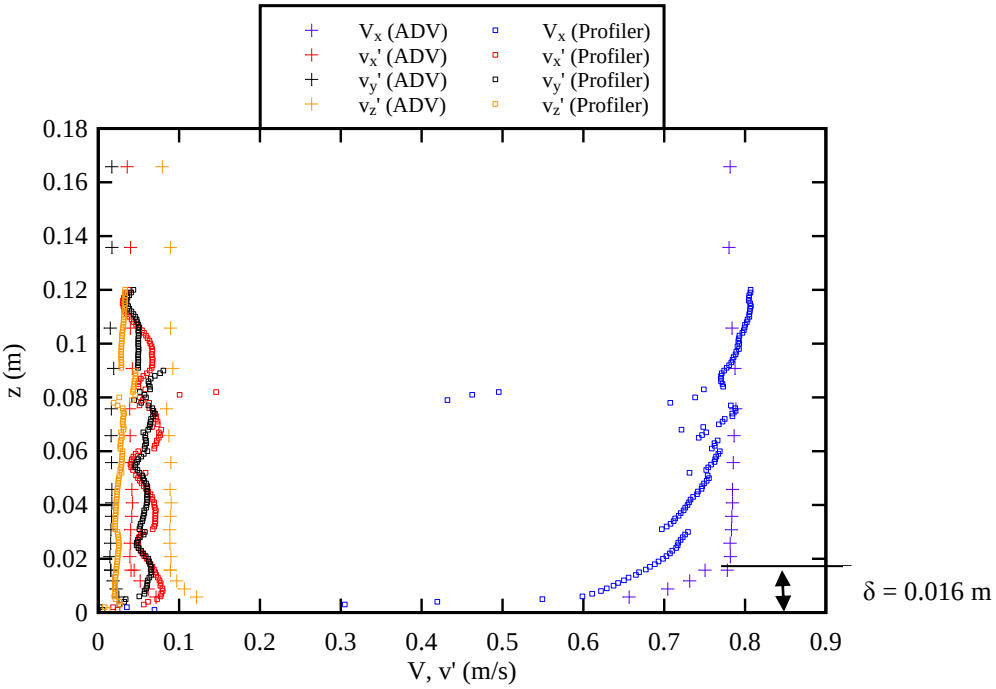

(A) Q = 0.100 m^3/s, d_1 = 0.190 m, radial gate fully open

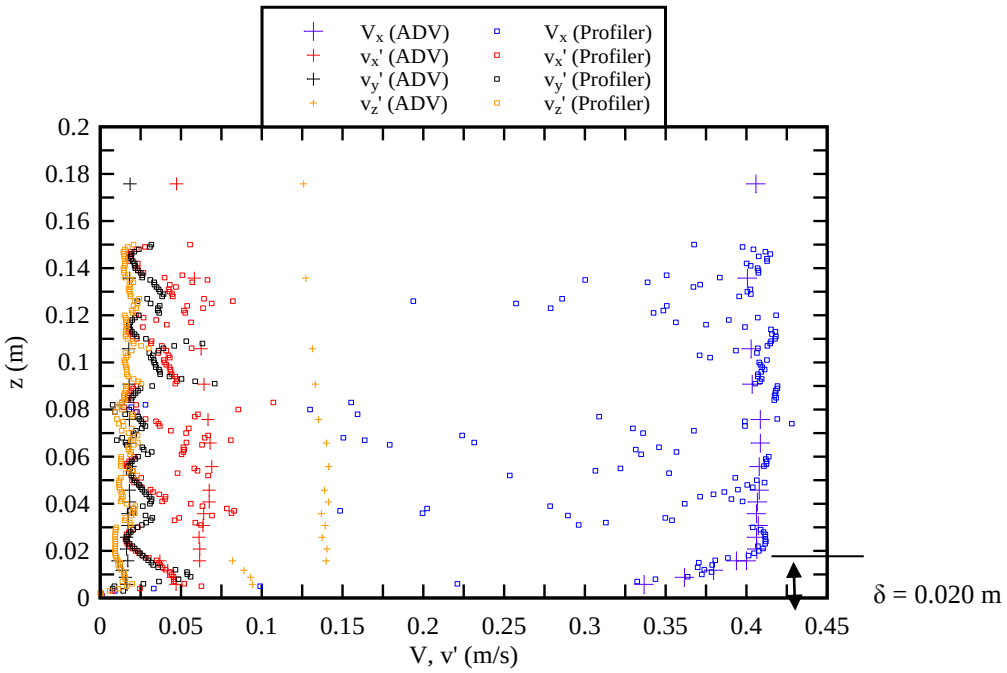

(B) Q = 0.055 m^3/s, d_1 = 0.201 m, radial gate opening = 0.05 m

Fig. A-7 - Time-averaged velocity profile of the longitudinal velocity and velocity fluctuations in steady flow: a comparison between ADV and Profiler data for x = 2.0 m.

A.3 INTERACTIONS BETWEEN ADV AND PROFILER

The interactions between the ADV and Profiler were studied when both units were sampled simultaneously relatively close to each other. Four ways of setting up the ADV and Profiler were tested and steady flow measurements were performed at the same vertical elevations for the four setups using both instruments, sampled simultaneously or separately. In the first setup, the ADV and Profiler were mounted side by side at the same longitudinal location x = 8.5 m, where x was measured from the upstream end of the experimental channel. The transverse distance between control volumes measured by the two instruments was 0.085 m. The emitter of the ADV was facing the control volume detected by the Profiler. The setup, despite the change in longitudinal location x, was the same as illustrated in Figure A-1B. In the second setup, the ADV head was rotated by 180º, with the ADV emitter facing away from the Profiler. For the third and fourth setups, the ADV unit was further separated longitudinally from the Profiler unit (see below).

In the first stup, the interactions between instruments were tested by collecting and repeating measurements under three sets of conditons: (a) Profiler sampling only, (b) ADV sampling only and (c) Profiler and ADV sampling simultaneously. The flow conditions consisted of a water discharge Q = 0.102 m^3/s, zero bed slope (S_o = 0) and no radial gate (fully-opened) for all steady flow measurements. The initial steady flow water depth at the sampling location was d_1 = 0.175 m. Each single Profiler measurement covered a vertical range of 0.015 m to 0.05 m above the channel

bed, composed of 35 sampling points. This specific range was chosen because the Profiler measurements were deemed to be of best quality. The ADV measurements were conducted throughout the water column.

Figure A-8 and A-9 show comparisons in terms of the ADV signal amplitude and signal to noise ratio (SNR) of the ADV data when working with and without the Profiler. With the profilers, the results highlighted marked increase in ADV signal amplitude (from 10 to 50 counts) for all beams at distance from 100 mm to the emitter and beyond. The signal amplitude at the control volume (50 mm from the emitter) however showed little variation. The SNR at the ADV control volume was significantly lower when sampling with the Profiler (from 25 to 13 dB), with beam 1 denoting the longitudinal direction having a higher SNR than the other beams when the Profiler is on. The amplitude and SNR of the Profiler showed similar differences when working with and without the ADV. The findings indicated some two-way interactions occurring between the two velocimeters.

The vertical velocity profiles of the longitudinal, transverse and vertical velocity components recorded by the Profiler and ADV were compared for the three sampling circumstances. The time-averaged velocity magnitudes, standard deviation and skewness were presented in Figures A-10 to A-12. Overall, the results showed identical vertical velocity profiles for all three velocity components measured by both instruments, sampling simultaneously or separately. The Profiler data, when sampling alone, resembled closely the ADV data (sampling alone) in terms of shape of the longitudinal velocity profile. However the data were approximately 7% lower in terms of velocity magnitudes. The longitudinal velocity recorded by the Profiler, when sampling together with the ADV, deviated further from that of the ADV data sampled alone, mostly in the lower two thirds and upper one tenth of the profile. Compared to the longitudinal velocity, the transverse and vertical velocity components were less affected by the interferences between the ADV and Profiler units.

The standard deviation of the velocity data recorded by Profiler only showed some 'periodic' trend as a function of elevation for the longitudinal and transverse velocity components. This periodic shape of the velocity data was preserved when the Profiler was working together with the ADV, although with some fluctuations at the bottom of the profile. The shape and value of the velocity standard deviation measured by the Profiler were not comparable to those of the ADV, sampling together or separately. The standard deviation of the vertical velocity component measured by the Profiler alone showed an identical shape to that of the ADV measurements sampled-alone, with much less magnitudes. However, when sampling together, the standard deviation of the vertical velocity was adversely affected by the instrument interaction and showed a periodic shape similar to the other two velocity components recorded by the Profiler.

The skewness of all three velocity components was overall zero throughout the vertical profiler as

measured by the ADV alone, indicating a normal Gaussian distribution with no skew. The skewness of the transverse and vertical velocity components recorded by the Profiler alone resembled closely the skewness of the ADV data sampled-alone, although with some fluctuations. The fluctuations were larger when sampling together with the ADV, but the values were overall within ± 0.5. The skewness in the longitudinal direction, however, showed a parabolic shape as highlighted by the Profiler data, sampled alone or with the ADV. The Profiler data implied a strong right-skewness in the longitudinal velocity component. The skew was amplified when sampling together with the ADV, possibly due to the interactions between instruments.

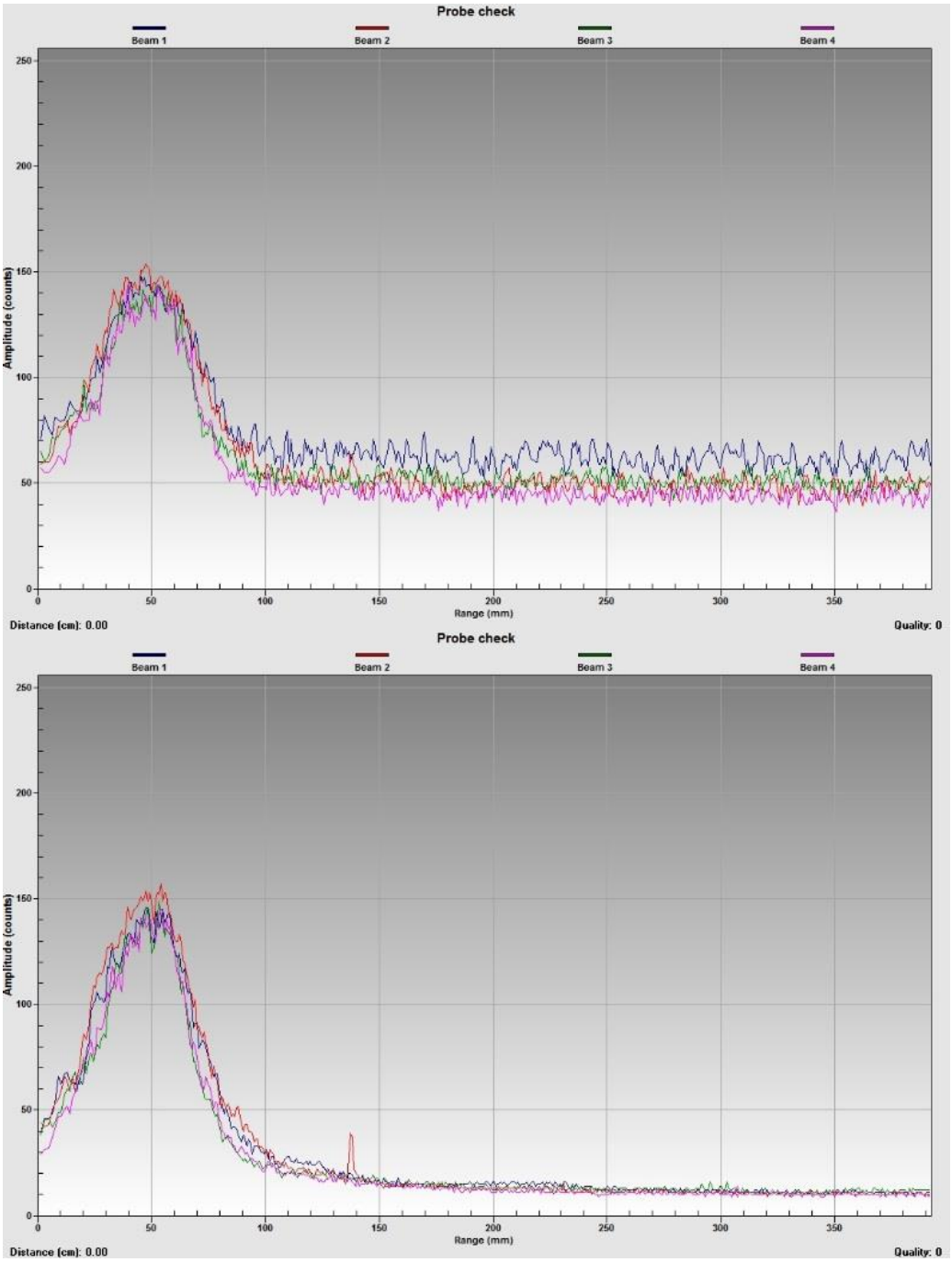

Fig. A-8 - Signal amplitude of ADV: a comparison between signal quality with (top) and without

(bottom) the Profiler sampling at the same time.

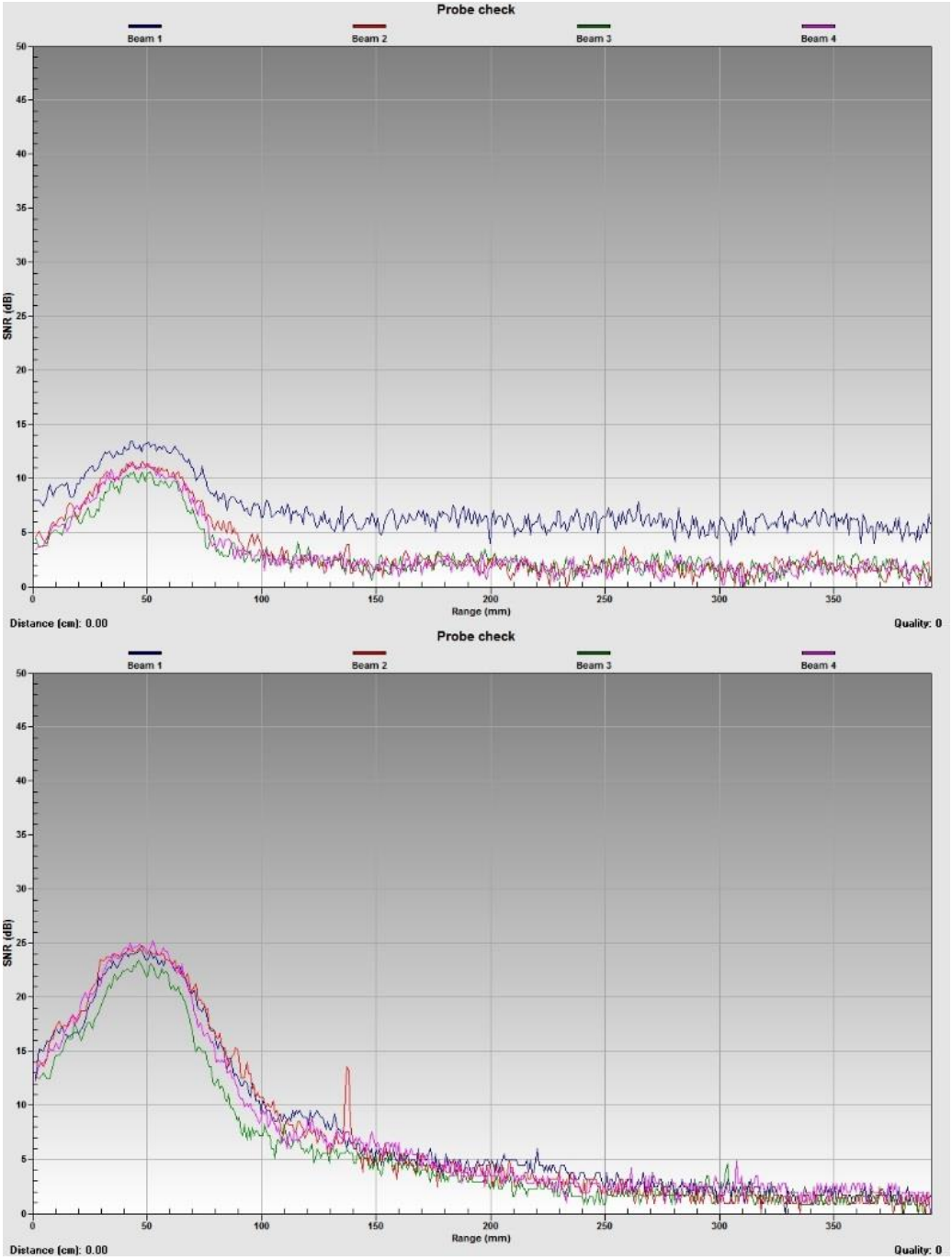

Fig. A-9 - Signal to noise ratio (SNR) of ADV: a comparison between signal quality with (top) and without (bottom) the Profiler sampling at the same time.

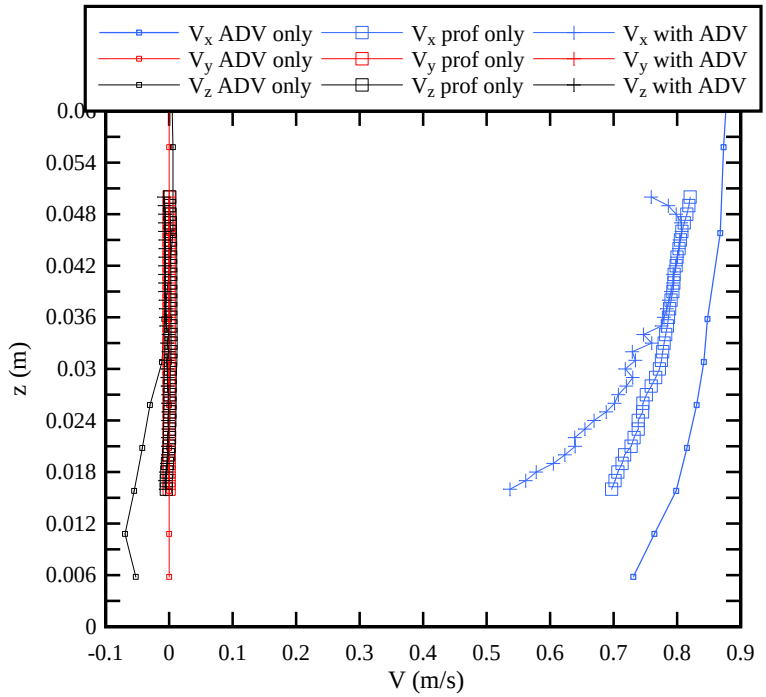

Fig. A-10 - Time-averaged longitudinal, transverse and vertical velocity profiles measured by Profiler sampling alone (denoted “prof only”) and sampling with the ADV (denoted “with ADV”), compared to ADV measurements sampling alone (denoted “ADV only”).

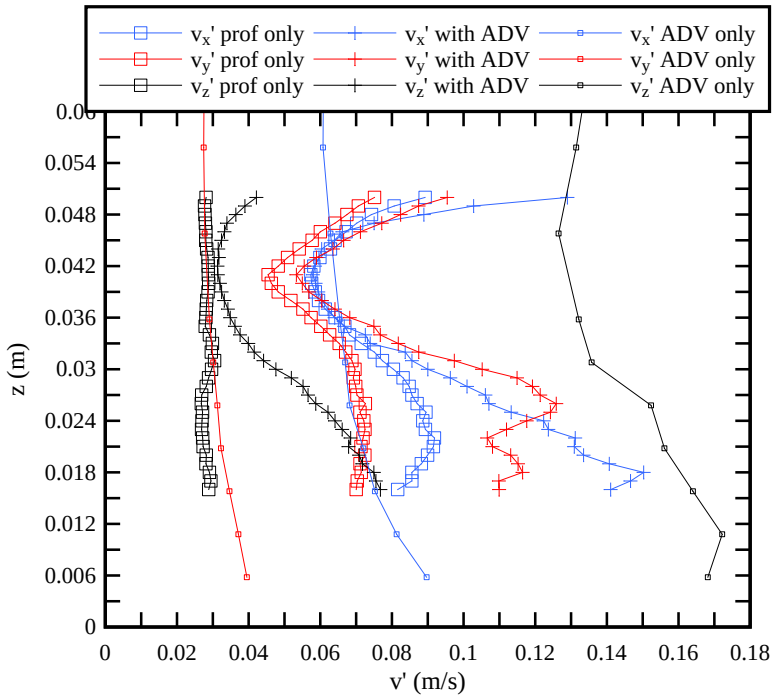

Fig. A-11 - Standard deviations of longitudinal, transverse and vertical velocity components measured by Profiler sampling alone (denoted “prof only”) and sampling with the ADV (denoted “with ADV”), compared to ADV measurements sampling alone (denoted “ADV only”).

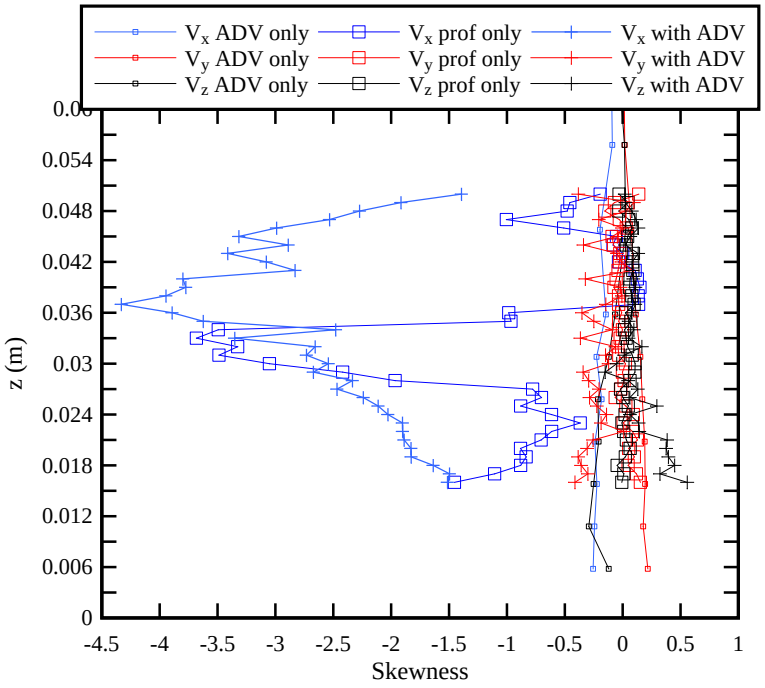

Fig. A-12 - Skewness of longitudinal, transverse and vertical velocity components measured by Profiler sampling alone (denoted "prof only") and sampling with the ADV (denoted "with ADV"), compared to ADV measurements sampling alone (denoted "ADV only").

The minimisation of the interactions between ADV and Profiler was tested in three other setups, in addition to the first setup. In the second setup, denoted Setup 2, the ADV was rotated 180º with its emitter facing the right side wall (Fig. A-13A). The distance between the control volumes of the ADV and Profiler was 0.185 m. In the third setup, the ADV was moved to x = 7.93 m, with a transverse distance of 0.125 m from the ADV probe to the Profiler probe to avoid the wake created by the ADV probe impacting on the Profiler control volume (Fig. A-13B & A-13C). The ADV emitter faced the right side wall, creating a transverse distance of 0.175 m between the two control volumes. The fourth setup was similar to the third setup, only with the ADV emitter rotated 180º to face the Profiler control volume. Figure A-13 illustrates these experimental setups. The three velocity components with the associated standard deviations and skewness were measured by the two instruments simultaneously sampling. The results were presented in Figures A-14 to A-16.

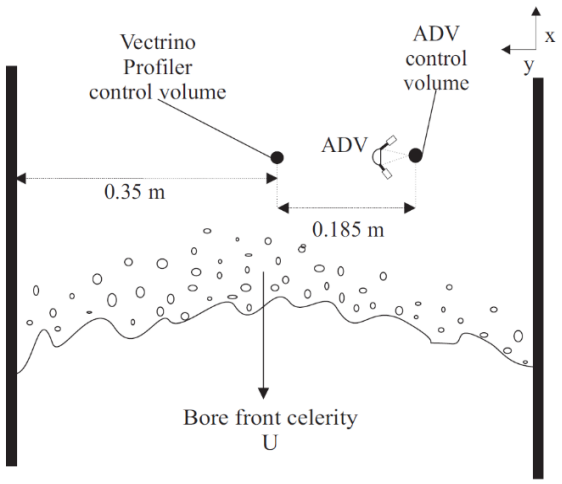

(A) Top view of Setup 2

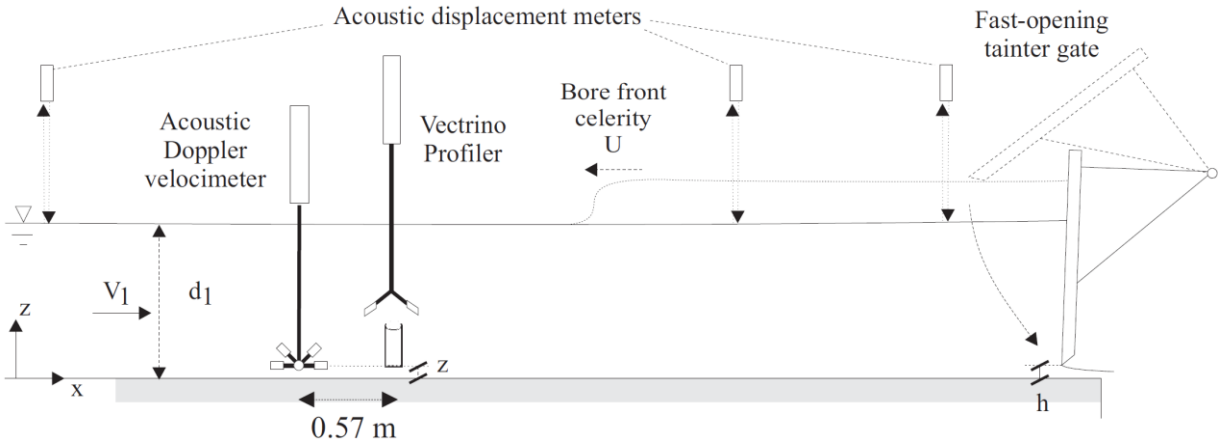

(B) Side view of Setup 3 and Setup 4

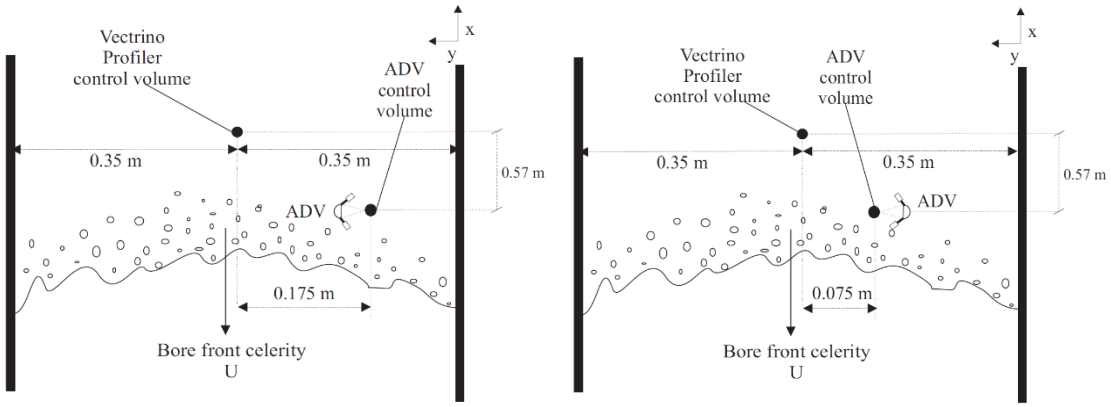

(C) Top views of Setup 3 and Setup 4

Fig. A-13 - Sketches of different experimental setups.

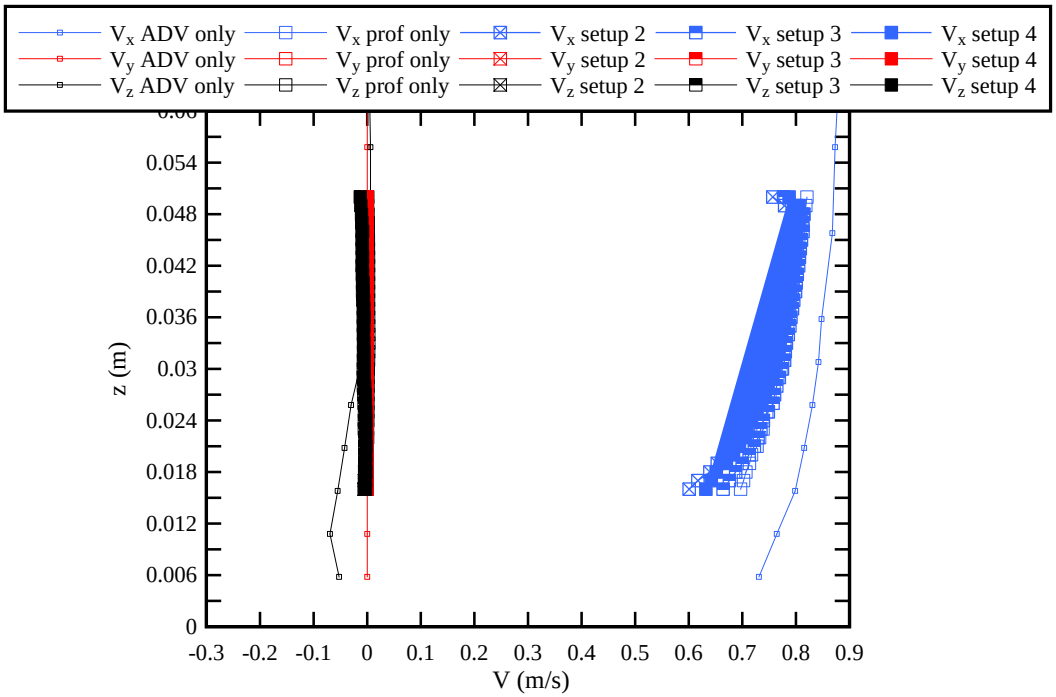

Fig. A-14 - Time-averaged longitudinal, transverse and vertical velocity profiles measured by Profiler sampling alone (denoted "prof only"), sampling with ADV using Setups 2, 3 and 4 (denoted "setup 2/3/4") compared to ADV measurements sampling alone (denoted "ADV only").

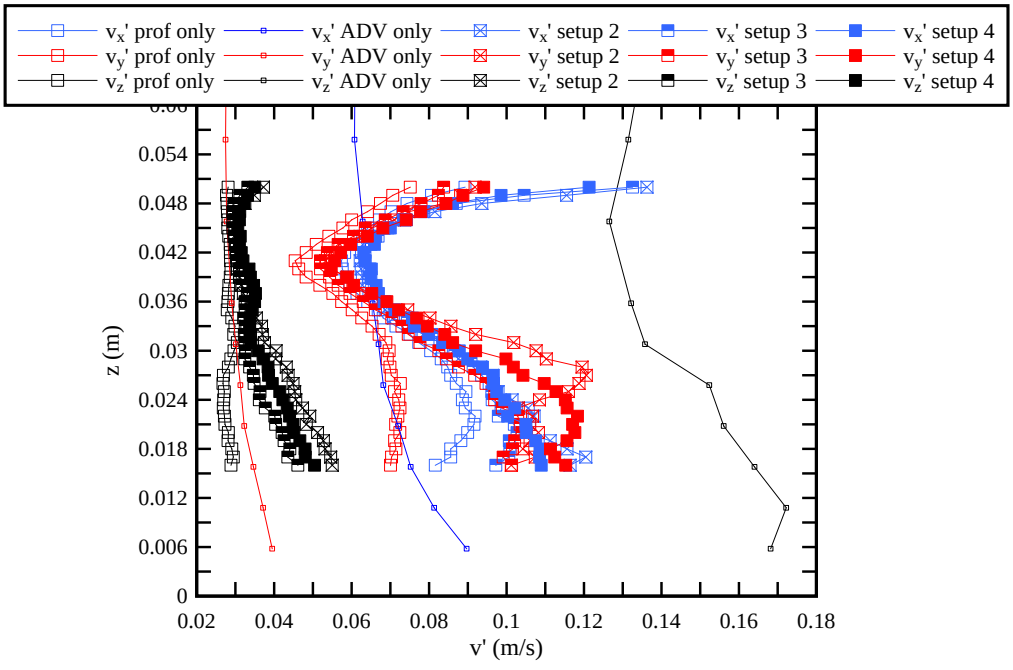

Fig. A-15 - Standard deviations of longitudinal, transverse and vertical velocity profiles measured by Profiler sampling alone (denoted "prof only"), sampling with ADV using Setups 2, 3 and 4 (denoted "setup 2/3/4") compared to ADV measurements sampling alone (denoted "ADV only").

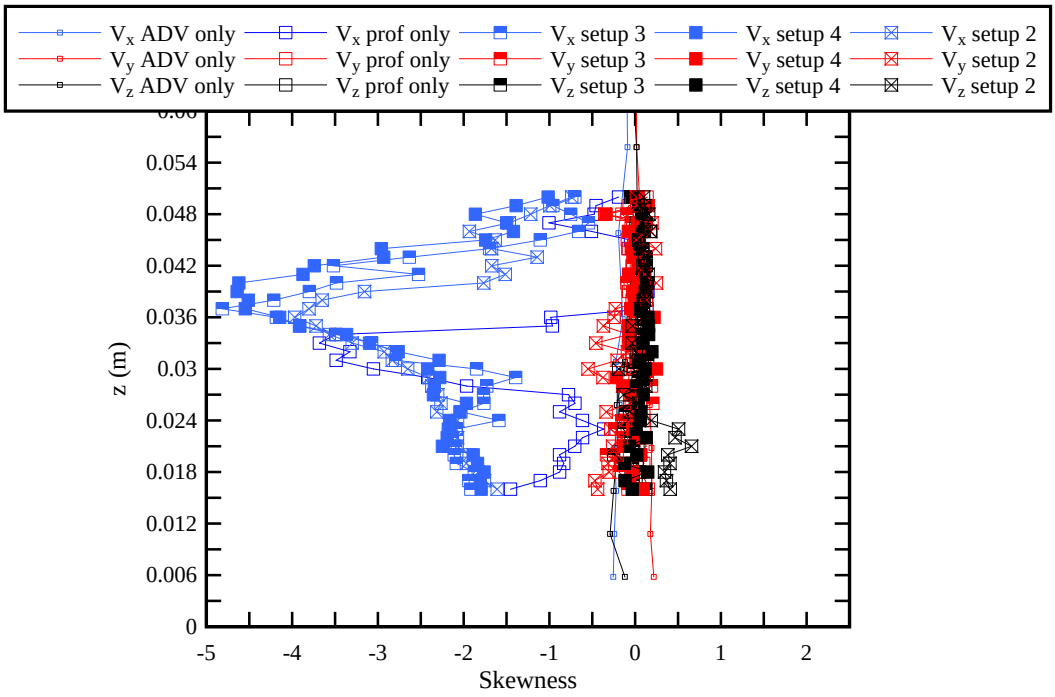

Fig. A-16 - Skewness of longitudinal, transverse and vertical velocity profiles measured by Profiler sampling alone (denoted "prof only"), sampling with ADV using Setups 2, 3 and 4 (denoted "setup 2/3/4") compared to ADV measurements sampling alone (denoted "ADV only").

The time-averaged longitudinal velocity profiler highlighted that Setup 3 produced data which was closest to that recorded by the Profiler sampling on its own, while Setup 2 showed the largest deviation, compared to 3 and 4. However, compared to the first setup, the Setups 2, 3 and 4 overall produced data that were in closer agreement to that of the Profiler sampled on its own. The standard deviations and skewness showed a similar order in terms of similarity to the sampled-alone Profiler data.

A.4 CONCLUSION

In summary, the preliminary tests of the new Vectrino Profiler highlighted the following findings:

- Some error points existed in the sampling profile, for which the recorded velocity values were not meaningful. The error points were typically associated with a sample profile located outside the outer edge of the boundary layer, and disappeared when measurements were taken within the developing boundary layer.
- The locations of the error points in a single profile at a fixed vertical elevation were consistent and can be reproduced by repeating experiments at this elevation, whether the flow was steady or unsteady.

- The locations of the error points in a single velocity profile were random and discontinuous. The locations of the error points were not consistent with their vertical elevations in the water column.
- The presence of the error points in the Profiler measurements was more related to the flow discharge and vertical elevation rather than the turbulent flow properties.
- There were interactions between ADV and Profilers when both instruments were sampled simultaneously. However, these interactions were not the cause of the error points in the Profiler. The interactions had more impacts on the velocity fluctuations. The velocity fluctuations at the upper and lower portions of the profiler were most adversely affected.
- The interactions between the instruments and impacts on the data quality can be reduced by simply rotating the ADV emitter by 180º to face the side wall instead of facing the Profiler control volume. Further improvements can be achieved by moving the ADV longitudinally and transversely away from the Profiler.

APPENDIX B. SENSITIVITY ANALYSIS OF VECTRINO II PROFILER ENSEMBLE-AVERAGED MEASUREMENTS

B.1 PRESENTATION

A sensitivity analysis was performed to study the ensemble-average turbulent fluctuating characteristics measured by the Nortek^{TM} acoustic Doppler velocimeter (ADV) Vectrino II Profiler in terms of the number of ensemble-averaged repeats required for a single set of flow conditions. The ADV Vectrino II Profiler was tested against a Nortek^{TM} ADV Vectrino+. The experiments were performed with two configurations, one with both Profiler and ADV sampling at the same time, and the second one with the Profiler only, the ADV unit being physically absent. The results of the sensitivity analysis are presented in the form of the unsteady turbulent fluctuating characteristics and their scatter as functions of the number of repeats.

Three characteristic unsteady turbulent fluctuating properties were examined. These were the maximum longitudinal velocity fluctuations occurring shortly after the passage of the bore, the time lag for the maximum longitudinal velocity fluctuation to occur after the bore passage and the longitudinal recirculation velocity (Fig. B-1). The longitudinal velocity fluctuations were quantified as the difference between the third and first quartile of the total ensemble (V_{75}-V_{25}). For Gaussian distribution of an ensemble around its mean, (V_{75}-V_{25}) would be equal to 1.3 times the standard deviation. The maximum velocity fluctuations $(V_{75}\text{-}V_{25})_{max}$ were found to occur shortly after the passage of the bore, and time lag of this maximum fluctuation Δt_V was quantified as the delay in relative to the time when the free-surface elevation started to rise up. The longitudinal recirculation velocity V_{recirc} marked the minimum velocity reached at the end of the longitudinal deceleration, which was generally negative for the experimental flow condition. This negative velocity indicated a region of flow reversal and recirculation beneath the bore. A definition sketch of the above fluctuating properties was illustrated in Figure B-1. Previous experimental analysis suggested that these properties were characteristics associated with the turbulent flow nature, and were strongly linked with time and magnitude of the maximum turbulent shear stress (LENG and CHANSON 2015c). Thus the sensitivity analysis focused on these properties.

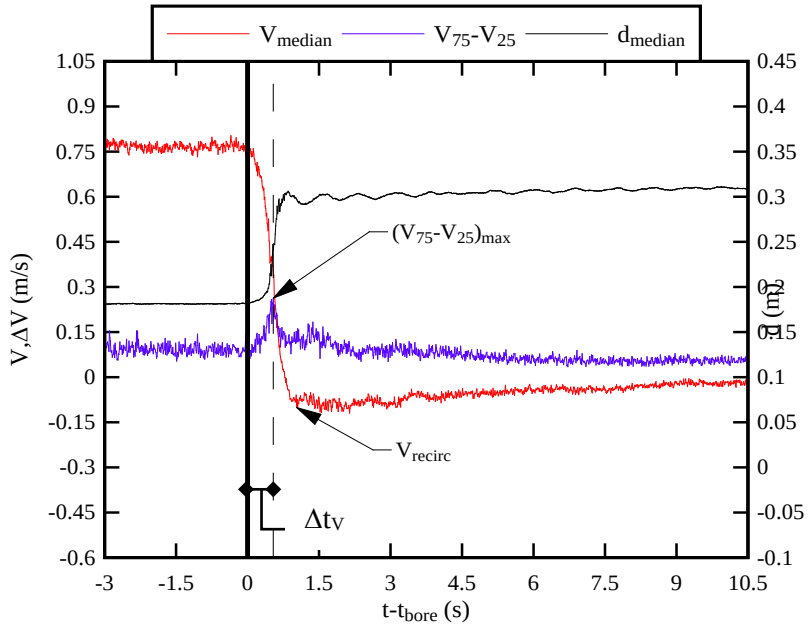

Fig. B-1 – Definition sketch of the characteristic unsteady turbulent fluctuating properties.

B.2 EXPERIMENTAL FACILITY AND SETUP

B.2.1 Instrumentations

The Profiler was a Nortek™ acoustic Doppler velocimeter Vectrino II Profiler (Serial number P27338, Hardware ID VNO 1366), capable of measuring instantaneous water velocity in a wide variety of applications from the laboratory to the Ocean (Nortek 2012). The basic measurement technology is coherent Doppler processing, which is characterised by accurate data and no appreciable zero offset (Nortek 2012). The Profiler was equipped with one central emitter and four receivers, able to record velocity components in the longitudinal, transverse and vertical directions. The Profiler had a downward looking head with all receivers and emitter facing downwards, sampling a vertical profile of 35 mm in height. The 35 mm profile contained 35 sampling points, each with a 1 mm high cell size, and the velocity characteristics were sampled simultaneously for these 35 points at 100 Hz. The first point of the sample profile was set to be 40 mm away from the downward-facing emitter. Detailed settings of the main parameters used to configure the Profiler are presented in Figure B-2.

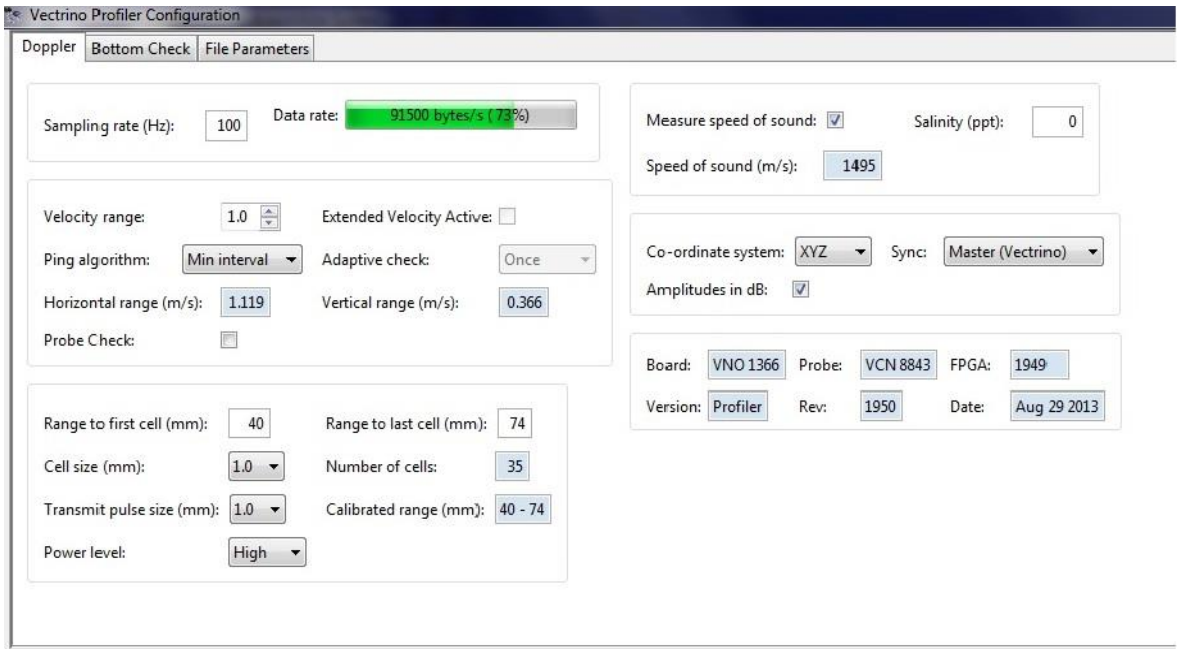

Fig. B-2 - Measuring parameter configurations of the Vectrino Profiler for the sensitivity analysis.

An acoustic Doppler velocimeter was used in the experiments to check the quality of the Profiler data. The acoustic Doppler velocimeter (ADV) was a Nortek™ ADV Vectrino+ (Serial number P21419, Hardware ID VNO 0436), equipped with a three-dimensional side-looking head, capable of measuring three velocity components (longitudinal, transverse and vertical) at a single point within the water column. The velocity range was ±1.0 m/s and the sampling rate was 100 Hz for the ADV. The data accuracy was 1% of the velocity range. The ADV was set up with a transmit length of 0.3 mm and a sampling volume of 1.5 mm height.

The unsteady water depths were recorded with a series of acoustic displacement meters. A Microsonic™ Mic+35/IU/TC unit was located at x = 18.17 m immediately downstream of the Tainter gate. Further three acoustic displacement meters Microsonic™ Mic+25/IU/TC were located at x = 17.81 m, 7.93 m, and 8.5 m. All acoustic displacement meters (ADMs) were calibrated against the pointer gauge measurements in steady flows. The ADMs, ADV and Profiler were synchronised within ± 10 ms, and they were sampled simultaneously at 100 Hz using a high-speed data acquisition system.

B.2.2 Experimental setup and flow conditions

Two sets of ensemble-averaged velocity measurements were conducted using the Profiler: one with the Profiler sampling alone (setup 1) on the channel centreline at x = 8.5 m where x was measured from the channel upstream end, and the other one with the Profiler sampling simultaneously with an acoustic Doppler velocimeter (ADV) (Fig. B-3A). In the second setup, the ADV was mounted at x

= 7.93 m, with a transverse distance of 0.125 m from the channel centreline towards the right side wall to avoid the wake impacting on the Profiler control volume (Fig. B-3B & B-3C). The ADV emitter faced the right side wall, creating a transverse distance of 0.175 m between its control volume and the sampling profile of the Profiler. This instrument setup was selected because it produced data which were least affected by the signal interference between the two instruments when both instruments were sampling simultaneously at a relatively close distance, based upon previous experimental findings (see Appendix A). This setup corresponded to "Setup 3" in Appendix A, and is denoted "Setup 2" in this appendix, for the ease of consistency within this appendix. Figure B-3 illustrates an overview of the experimental channel and the two facility setups, respectively.

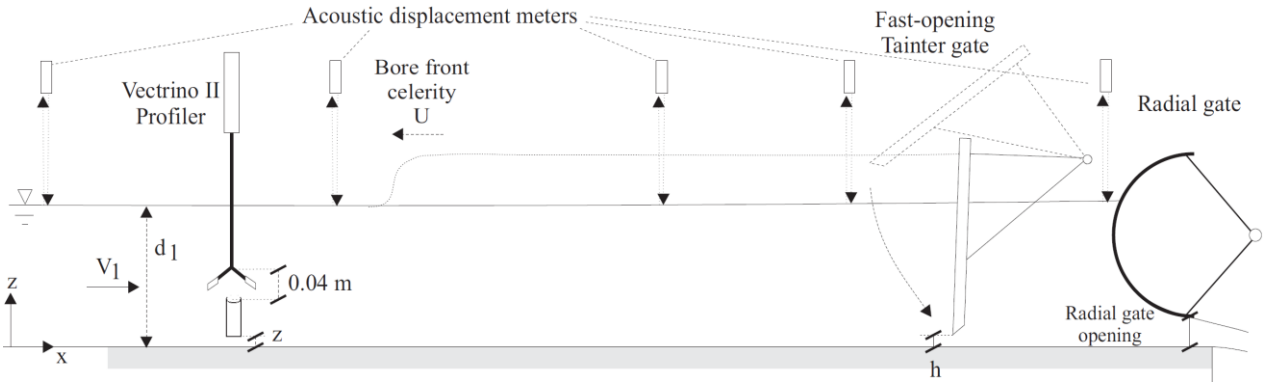

(A) Setup 1 (Profiler working alone) side view

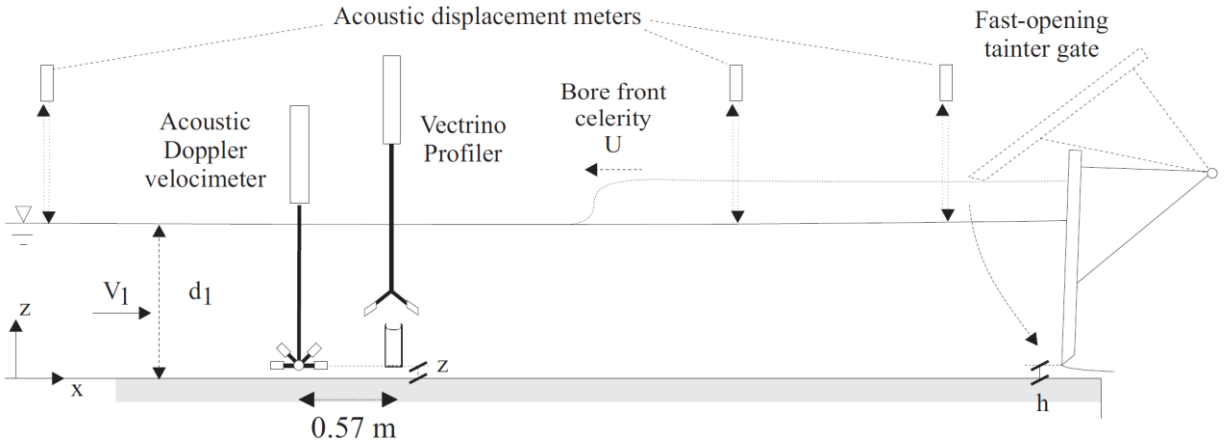

(B) Setup 2 (Profiler working with ADV) side view

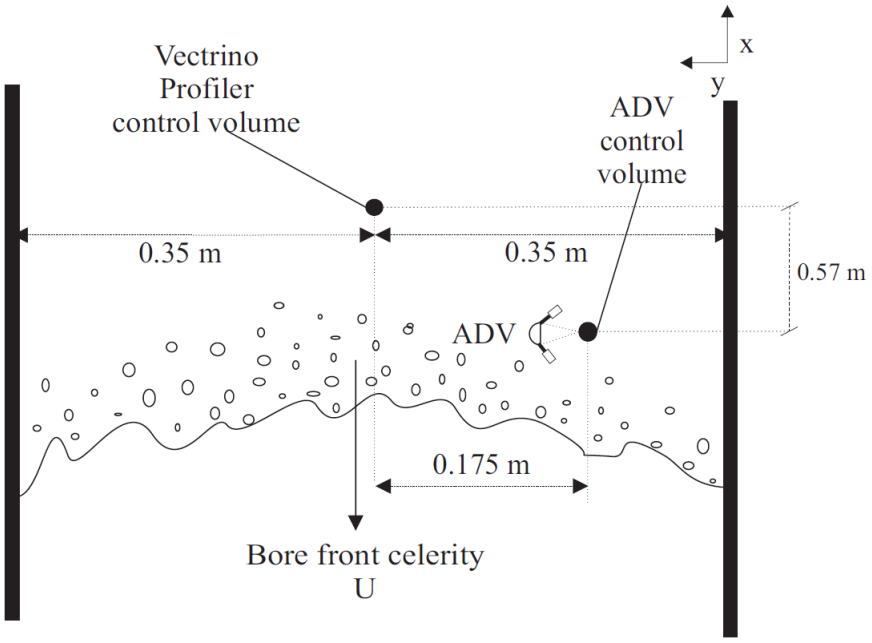

(C) Setup 2 (Profiler working with ADV) viewed in elevation

Fig. B-3 - Sketches of experimental channel and instrument setup.

Ensemble-averaged velocity and free-surface measurements were carried out for a water discharge of 0.101 m^3/s on a horizontal bed (S_o = 0). Breaking bores were generated by closing rapidly and completely the downstream Tainter gate (opening under gate h = 0) and propagated upstream, with a bore Froude number Fr_1 = 1.58. The gate closing time was within 0.2 s which was quick enough to have no effect on the upstream propagation of the tidal bores. The Profiler sampling profile in both setups covered a vertical range of z = 0.015 m to 0.050 m, where z was the vertical elevation within the water column measured from the surface of the channel bed. The vertical elevation of the ADV control volume in setup 2 was at z = 0.021 m. This vertical elevation was selected based upon the error analysis of the Profiler data for this experimental flow condition, at which best data accuracy and few spurious points were detected.

B.2.3 Methodology

The experiments were repeated 50 times for each of the two setups. The results were ensemble-averaged over the total 50 runs, as well as over 35 runs with some data overlapping, 25 runs, 15 runs, 10 runs and 5 runs with no data overlapping. Since a time-average is not meaningful in an unsteady turbulent flow as the hydrodynamic shock, short-term fluctuations must be treated separately (CHANSON and DOCHERTY 2012). The bore propagation was repeatable and reproducible in the current experimental setup. The free-surface and velocity characteristics were analysed by repeating the experiment for a number of times and obtaining the median of the

instantaneous data (i.e. the ensemble-average) at a point at an instant, which can be used to represent the mean property of the relevant parameters (DOCHERTY and CHANSON 2010). The synchronisation between different runs for a single flow condition was critical. This was done by taking the ADM located downstream of the gate as a reference. When the gate was closed, it generated a negative surge propagating downstream, which was characterised as a sudden drop of water elevations, at the same time as the generation of the bore. Hence, all 50 runs were synchronised according to the time at which the leading edge of the negative surge reached the ADM downstream of the gate. Mathematically, this time is equal to the instance at which the first derivative of the free-surface elevation with respect to time become none-zero.

Figure B-4 showed an example of the time-variations of the longitudinal velocity at the same vertical elevation measured by the Profiler, obtained from 50 instantaneous runs. All runs were synchronised together, and highlighted by the coloured lines. The black solid line denoted the median free-surface elevation at the velocity sampling point (x = 8.5 m), ensemble-averaged from 50 runs. Herein t_{bore} on the horizontal axis denotes the time at which the ensemble-averaged median free-surface elevation immediately upstream of the bore roller started to rise at x = 8.5 m.

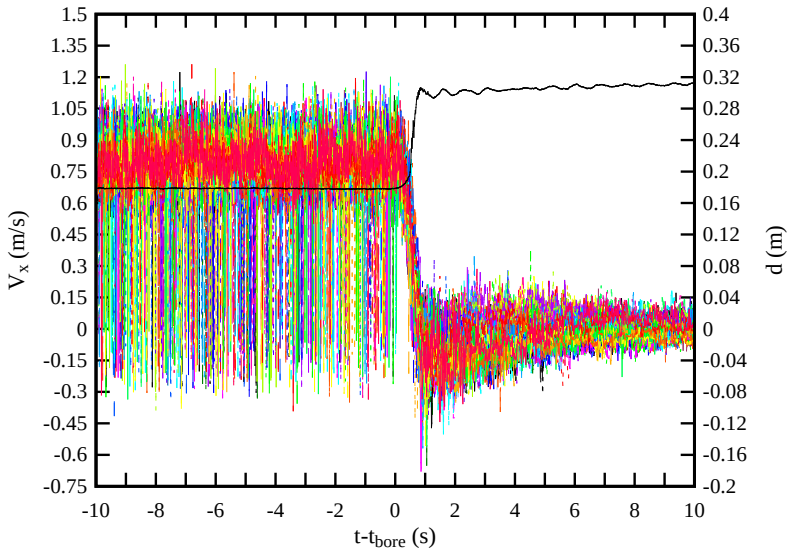

Fig. B-4 - Time-variations of instantaneous longitudinal velocity of 50 runs (coloured curves) and ensemble-averaged median water depth (black solid curve), all synchronised- Flow conditions: Q = 0.101 m^3/s, S_o = 0, no radial gate, h = 0 m, z = 0.033 m - Profiler sampling only.

B.3 DISCUSSION

Instantaneous profile of the time variations of velocity components in the longitudinal, transverse and vertical directions measured by the Profiler were illustrated in Figures B-5A, B-5B and B-5C

respectively. The coloured curves highlighted the unsteady time-variations of the three velocity components at 35 vertical elevations within one profiler. The solid black line denoted the instantaneous free-surface variations at the location of the Profiler. Overall, the velocity data measured at 35 different points throughout one profile showed consistent variations as the bore passed. The longitudinal velocity components decelerated almost simultaneously with the rise of free-surface associated with the bore passage. The transverse velocity at all measuring points fluctuated in a similar manner as the bore propagated and the vertical velocity showed a sharp acceleration followed by a deceleration, which was recorded at the same time by all measuring points.

The Profiler data showed a close agreement with the ADV velocity data measured at a single point. Figure B-6 presents the ensemble-averaged time-variations of the longitudinal velocity measured by the ADV (left) and Profiler (right) at a similar vertical elevation, both calculated based upon the total 50 runs. Herein t_{bore} on the horizontal axis denotes the time at which the ensemble-averaged median free-surface elevation immediately upstream of the bore roller started to rise at their respective velocity sampling locations for Profiler and ADV. The results showed close agreement in terms of shape and magnitude of the ensemble-median velocity variations measured by the two instruments. The velocity fluctuations in terms of (V_{75}-V_{25}) produced by both instruments showed marked peaks in the velocity fluctuations shortly after the passage of the bore front ($t-t_{bore} > 0$). The Profiler data seemed to show a more pronounced recirculation zone in comparison to the ADV data, as highlighted by negative velocity of larger magnitudes reached at the end of the longitudinal deceleration, indicating a stronger flow reversal. Altogether, the time-variations of the unsteady velocity measured by the Profiler, instantaneous or ensemble-average, were very similar to that measured by the ADV for all three components.

Table B-1 compared the turbulent fluctuating characteristics measured by Profiler in two setups, ensemble-averaged over the total 50 runs, to that measured by the ADV at similar vertical elevations, sampling with Profiler in setup 2 and alone (ensemble-average measurements made in 2014 with 25 runs). The results showed a close agreement between the Profiler data, working alone or with the ADV, and the ADV data, working alone or with the Profiler, at a given elevation. This indicated that the Profiler was suitable to conduct high frequency measurements in highly unsteady turbulent flows and capturing rapidly fluctuating characteristics with good accuracy, provided that the measurements were taken at a vertical elevation where no spurious points existed throughout the profile.

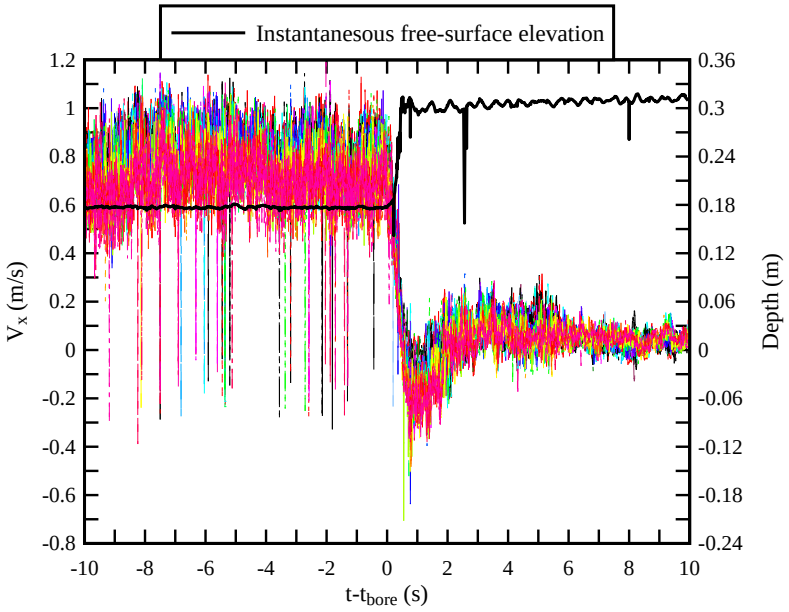

(A) Longitudinal velocity V_x

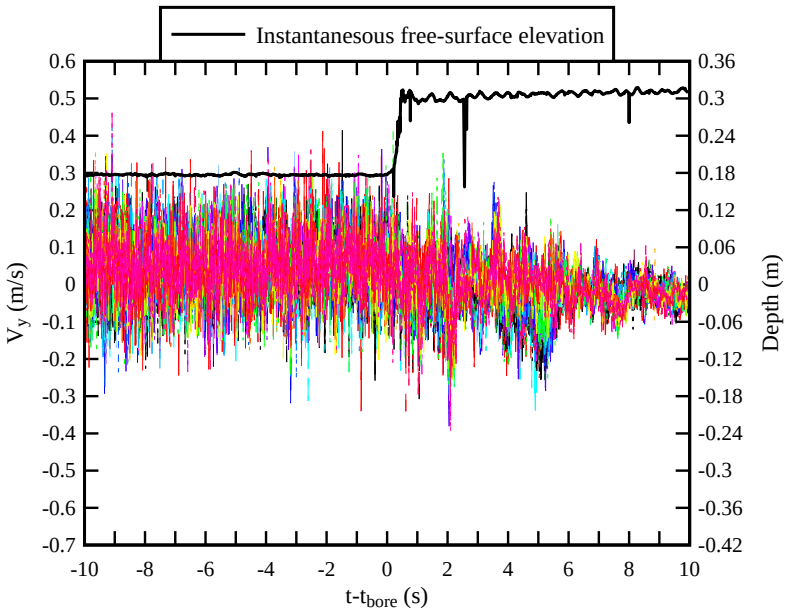

(B) Transverse velocity V_y

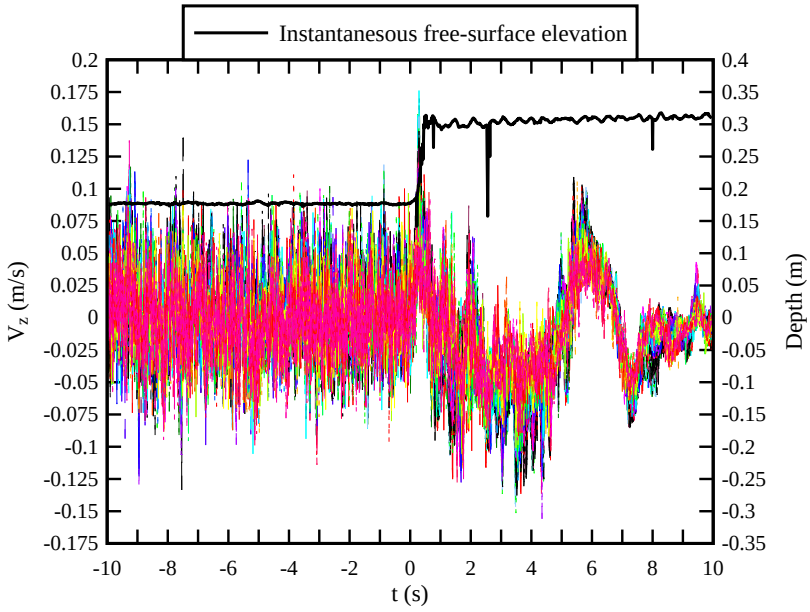

(C) Vertical velocity V_z

Fig. B-5 - Instantaneous profile of the time-variations of longitudinal (A), transverse (B) and vertical (C) velocity components for 35 sampling points (coloured curves); black solid line denoted instantaneous free-surface elevation at x = 8.5 m - Flow conditions: Q = 0.101 m^3/s, S_o = 0, no radial gate, h = 0 m, z = 0.015 - 0.050 m - Profiler sampling only (setup 1).

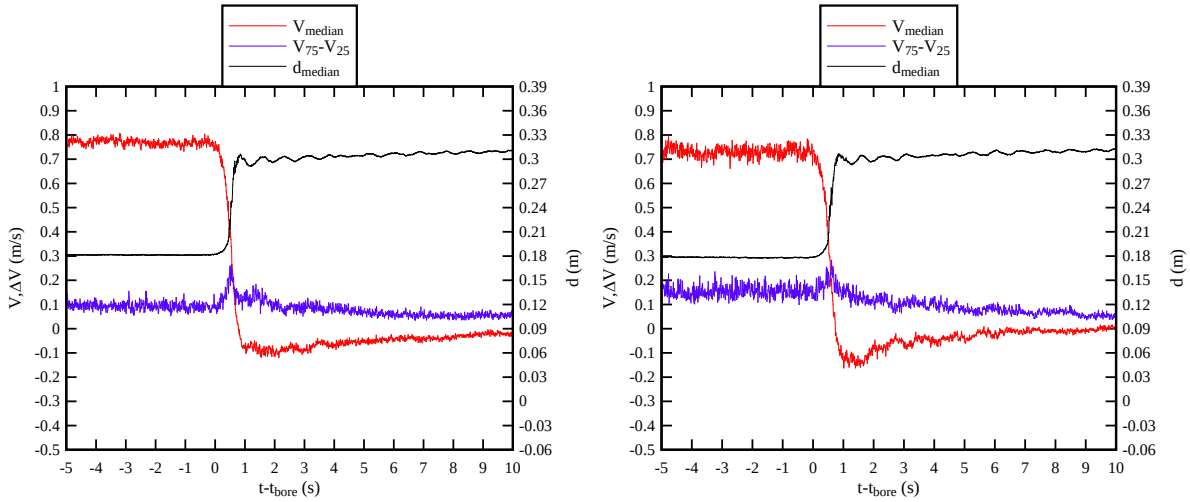

Fig. B-6 - Ensemble-averaged time-variations of the longitudinal velocity and free-surface elevation at the velocity sampling point: comparison between ADV data (left, working with Profiler in Setup 2) and Profiler data (right, working alone), both calculated from 50 runs - Flow conditions: Q = 0.101 m^3/s, S_o = 0, no radial gate, h = 0 m, z = 0.021 m for ADV and 0.015 - 0.050 m for Profiler.

Table B-1 - Comparison of turbulent fluctuating characteristics between instruments and setups

Instrument and setup	z (m)	$(V_{75}-V_{25})_{max}$ (m/s) Ensemble-averaged	Δt_V (s) Ensemble-averaged	V_{recirc} (m/s) Ensemble-averaged
Profiler with ADV Setup 2	0.023	0.305	0.52	-0.146
ADV Setup 2	0.021	0.263	0.54	-0.119
Profiler alone (Setup 1)	0.023	0.282	0.61	-0.162
ADV_2014 [1]	0.018	0.215	0.61	-0.239

Remarks: [1] ADV measurements collected in 2014 at x = 8.5 m on channel centreline for the same flow conditions; Results were ensemble-averaged over 25 runs.

The longitudinal velocity data at 7 vertical elevations (1 in 5 measuring points out of the total 35 points in a profile) were analysed to examine the effect of number of runs on the turbulent fluctuating characteristics $(V_{75}-V_{25})_{max}$, Δt_V and $V_{recirc.}$ Figures B-7 and B-8 present respectively the results obtained from two setups, each with a comparison between two vertical elevations (z = 0.048 m and z = 0.018 m). A complete data set was presented in the results in section B.5.

All three turbulent characteristics showed asymmetrical envelopes of data distribution as the number of runs of the total ensemble varied from 50 down to 5. The maximum fluctuations calculated based upon 50 runs tended to be smaller than the average of the results calculated from 35 or 25 runs. The time delay Δt_V obtained from a total ensemble of 50 runs was very close to the average of the time delay obtained from 35 and 25 runs, with 25 runs producing results that were closer to that of the 50 runs at some elevations. The magnitude of the recirculation velocity tended to decrease on average as the number of runs increased. For results calculated from an ensemble of less than 20 runs, the data scattered over a range of up to 4 times the magnitude of the ensemble-averaged results from 50 runs, which were deemed inaccurate in representing the turbulent fluctuating properties in the actual flow.

The asymmetrical shape of the data envelope observed for all three characteristics could be a result of the highly unsteady nature of the flow when varying rapidly with the bore passage. The longitudinal deceleration took place in typically less than 0.8 s, a period within which the flow was highly unsteady and intensive turbulent mixing occurred in a quasi-random manner. The time of occurrence of the peak velocity fluctuation was different, although only by a few milliseconds, in every single run, and the recirculation velocity, defined as the minimum velocity reached at the end of the deceleration phase, occurred at different time as well. Hence, when ensemble-averaging over a large number of runs, the maximum velocity fluctuation and recirculation velocity tended to be attenuated and thus less than the average of its subsamples. The number of runs therefore need to be large enough to accurately represent the turbulent fluctuating quantities in the rapidly varied flow,

at the same time not too large so that the attenuation is minimised. Therefore, 25 and 35 runs are considered most suitable for further ensemble-average velocity measurements using the Profiler, with 25 runs being selected simply because of time limitations.

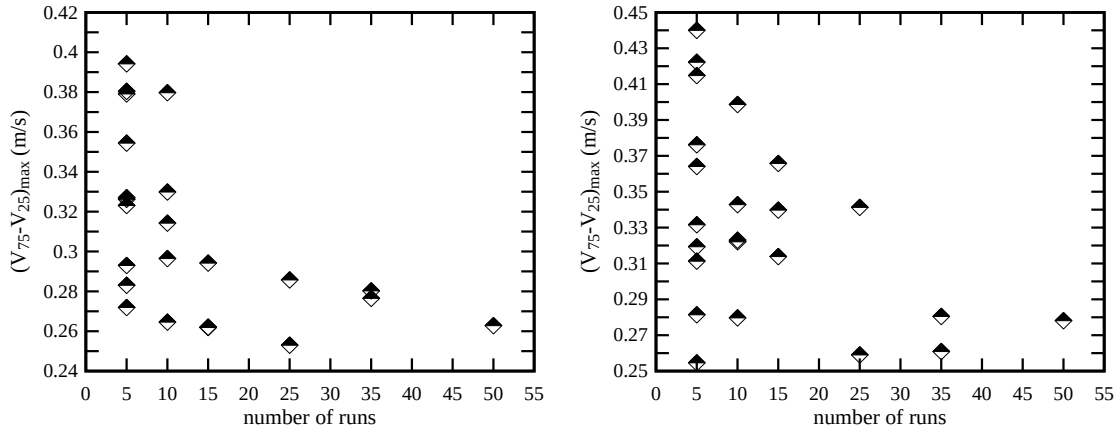

(A) Maximum longitudinal velocity fluctuations at z = 0.048 m (left) and z = 0.018 m (right)

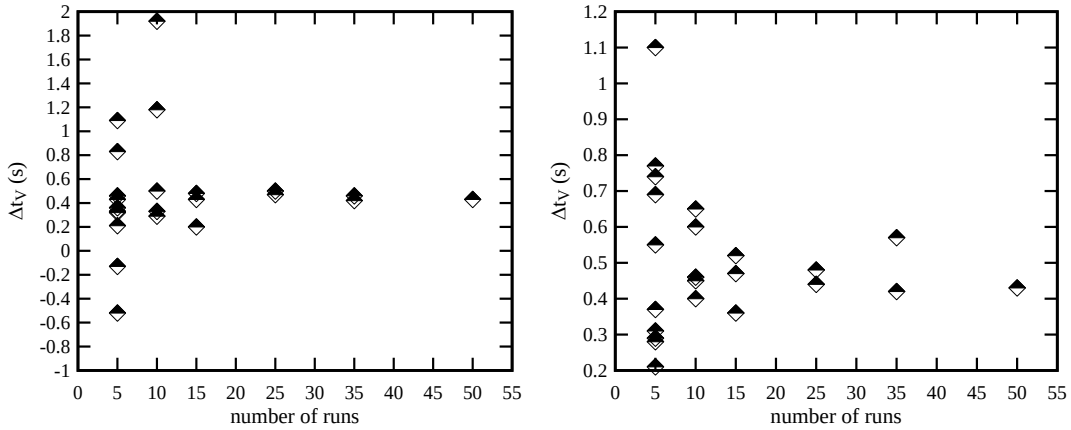

(B) Time lag at z = 0.048 m (left) and z = 0.018 m (right)

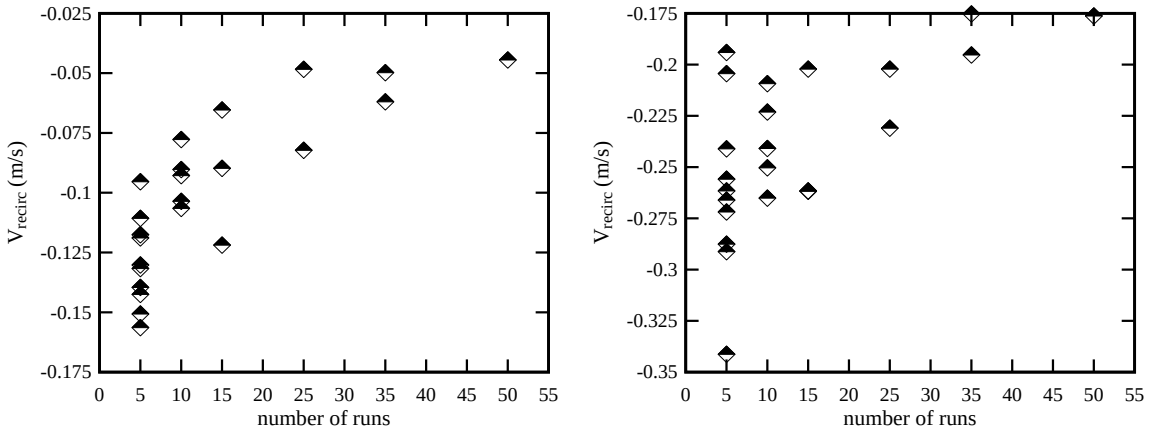

(C) Longitudinal recirculation velocity at z = 0.048 m (left) and z = 0.018 m (right)

Fig. B-7 - Sensitivity analysis of the maximum longitudinal velocity fluctuations, the time delay and the longitudinal recirculation velocity at two vertical elevations: comparison between ensemble-averaged results over different number of runs; Profiler sampling with ADV in Setup 2.

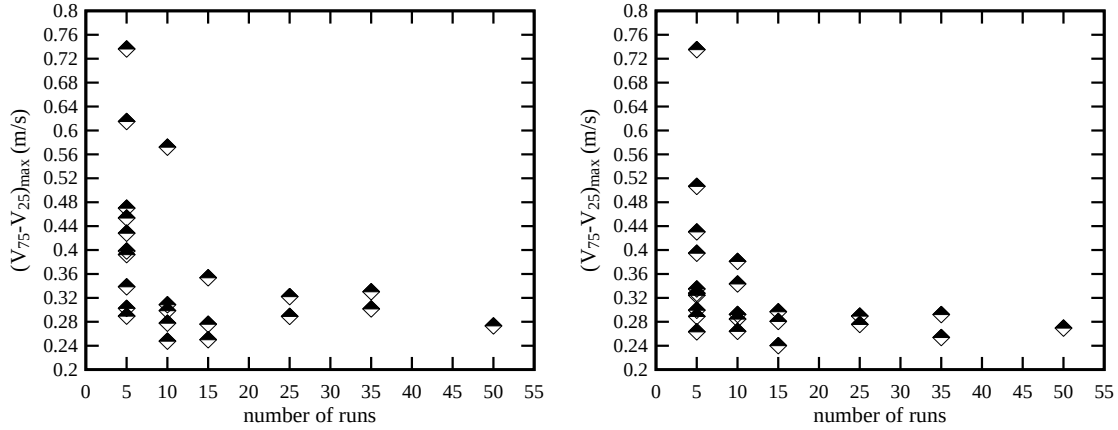

(A) Maximum longitudinal velocity fluctuations at z = 0.048 m (left) and z = 0.018 m (right)

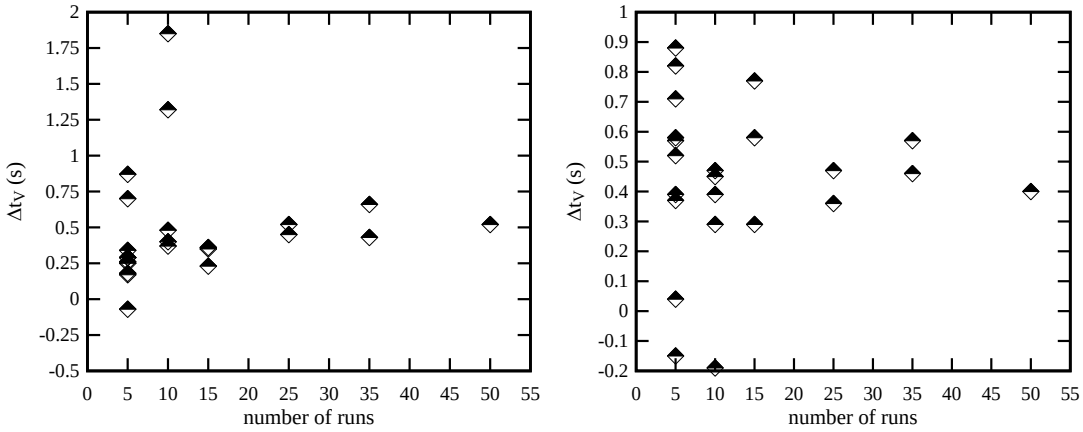

(B) Time lag at z = 0.048 m (left) and z = 0.018 m (right)

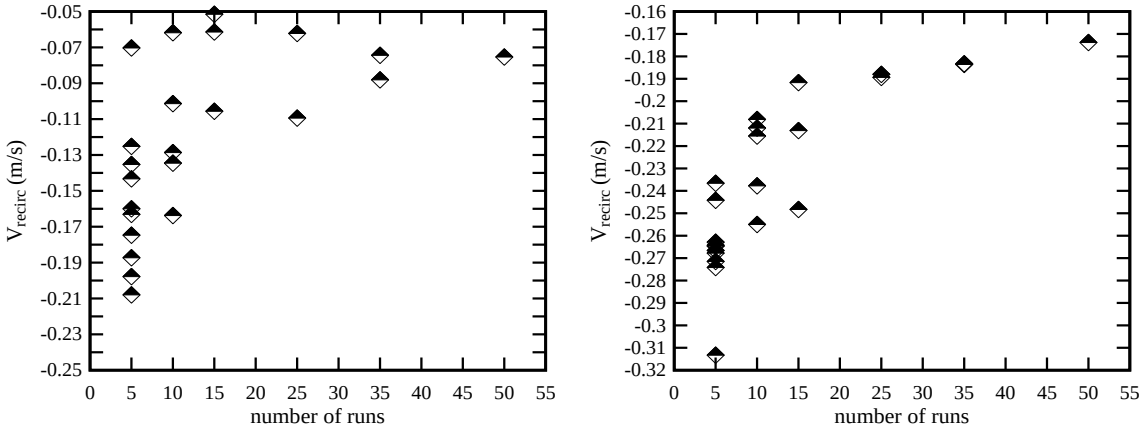

(C) Longitudinal recirculation velocity at z = 0.048 m (left) and z = 0.018 m (right)

Fig. B-8 - Sensitivity analysis of the maximum longitudinal velocity fluctuations, the time delay and the longitudinal recirculation velocity at two vertical elevations: comparison between ensemble-averaged results over different number of runs; Profiler sampling alone (Setup 1).

Comments

A fundamental challenge is the turbulence charaterisation in very-rapidly-varied unsteady flows,

such tidal bores. Phase-averaging may be easily applied in periodic flows (CANTWELL 1976, PERRY and WATMUFF 1981), but the technique is unsuitable to very-rapidly-varied flows. Instead the very-rapidly-varied unsteady flow experiments must be repeated in a carefully controlled manner for the results to be ensemble-averaged (BRADSHAW 1971, KIM and MOIN 1986). Herein a sensitivity analysis was conducted by repeating each experiment 50 times. The results implied that the data were basically independent of the number of experiments for a minimum of 25 runs. For comparison, PERRY et al. (1980) required 10 samples for convergence of their phase-averaged data, SLEATH (1987) used records with 50 cycles, while LENG and CHANSON (2015d) needed a minimum of 15-20 runs to characterise accurately expansion waves in open channels.

In the main study, each experiment was conducted 25 times, and it is acknowledged that the number of repeated runs was somehow limited.

B.4 CONCLUSION

Ensemble-average unsteady velocity measurements were conducted using an ADV Vectrino II Profiler (Profiler) in two instrument setups—with or without the simultaneous sampling of an acoustic Doppler velocimeter (ADV). A total of 50 runs were performed for each setup and a sensitivity analysis was carried out based upon the ensemble-averaged data set. Ensemble-averaged velocity data measured using the Profiler highlighted close agreements with the data recorded using the ADV. That is, Profiler and ADV data showed very similar trends and magnitudes of time-variations of all three velocity components, magnitudes and time of occurrence of the unsteady turbulent characteristics. Little difference in terms of the magnitudes and occurrence time of the turbulent characteristics was observed between setups, and comparing to previous ensemble-averaged ADV results.

The sensitivity analysis showed an asymmetrical envelope for the scatter of all unsteady turbulent characteristics with respect to number of runs. A total of 25 runs was selected as the most desirable number of runs to conduct further ensemble-average measurements using the Profiler, as it was large enough to represent accurately the turbulent characteristics, yet not too large to attenuate the turbulent characteristics. The result was consistent with the relevant literature.

B.5 RESULTS

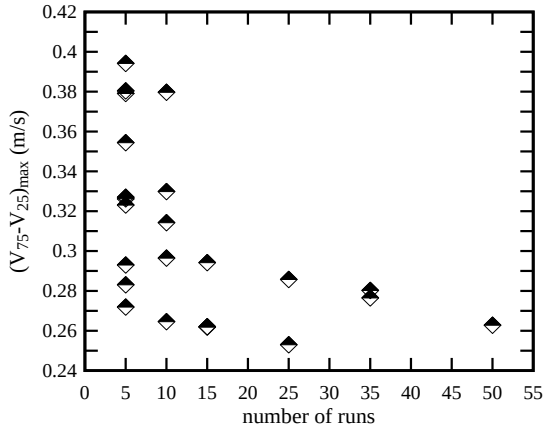

(A) z = 0.048 m

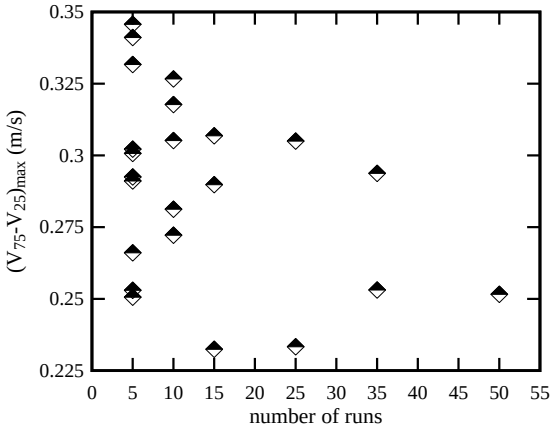

(B) z = 0.043 m

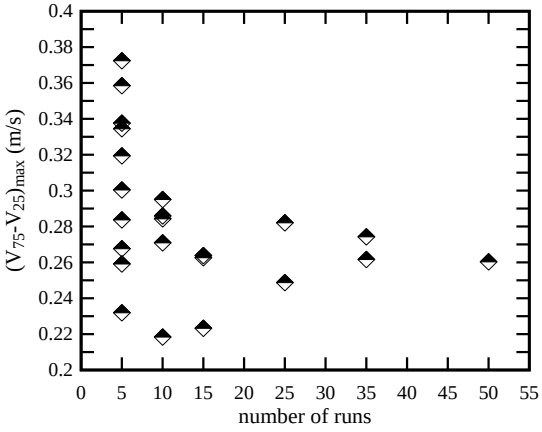

(C) z = 0.038 m

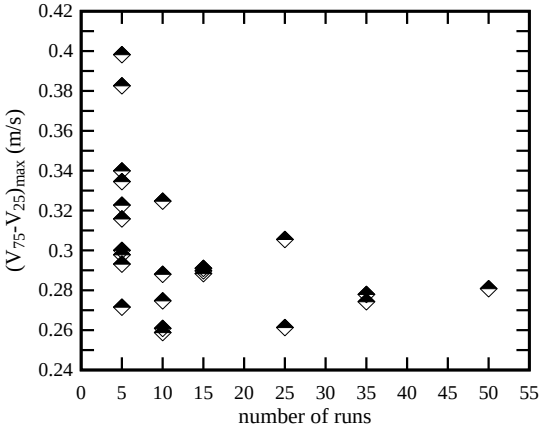

(D) z = 0.033 m

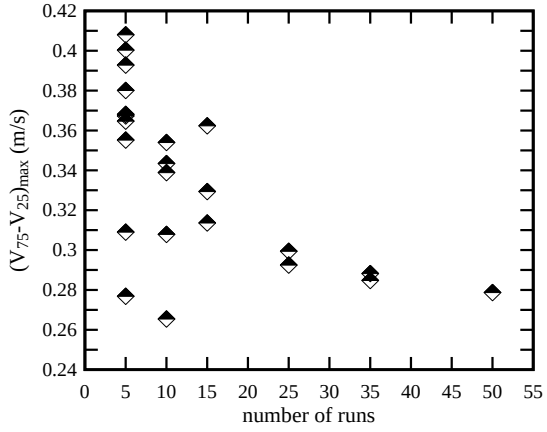

(E) z = 0.028 m

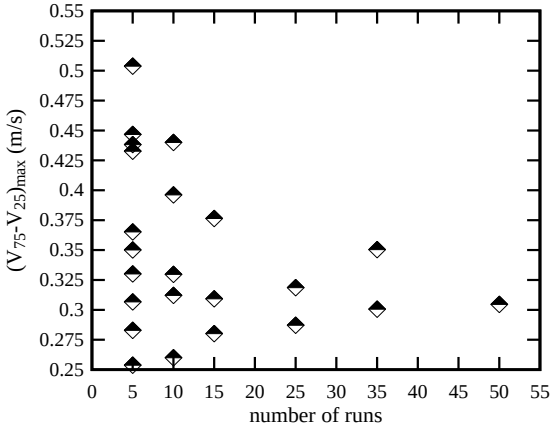

(F) z = 0.023 m

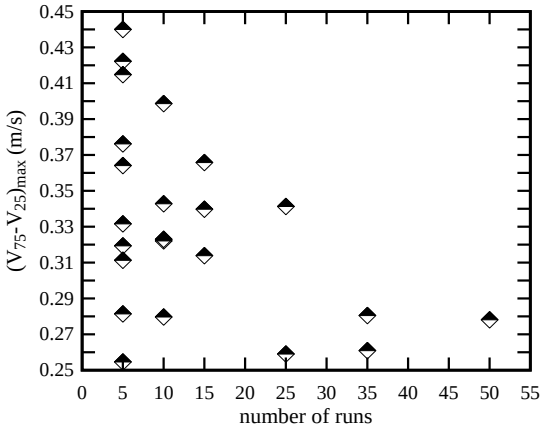

(G) z = 0.018 m

Fig. B-9 - Sensitivity analysis of the maximum longitudinal velocity fluctuations: comparison between ensemble-averaged results over different number of runs; Profiler sampling with ADV in Setup 2.

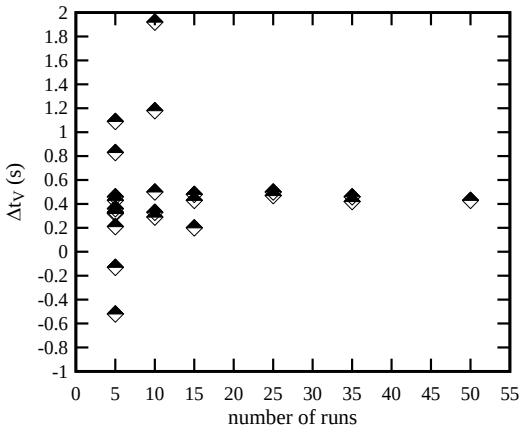

(A) z = 0.048 m

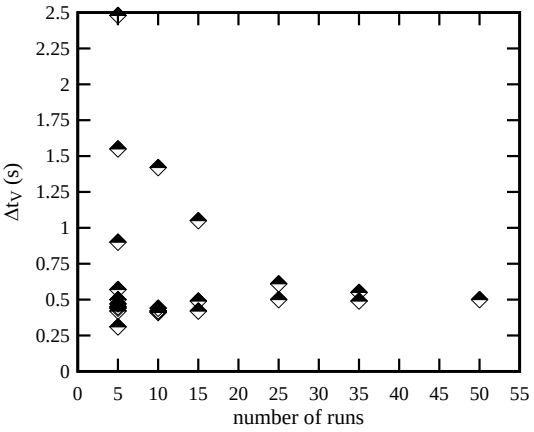

(B) z = 0.043 m

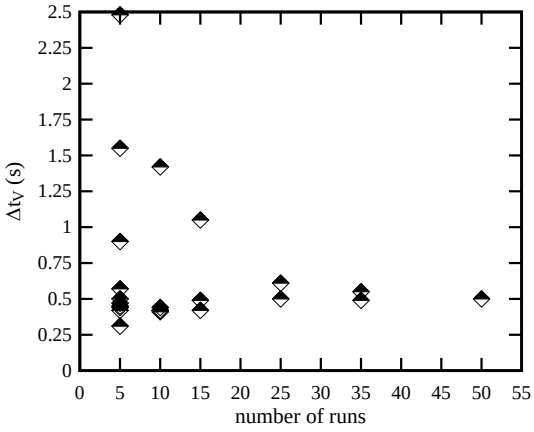

(C) z = 0.038 m

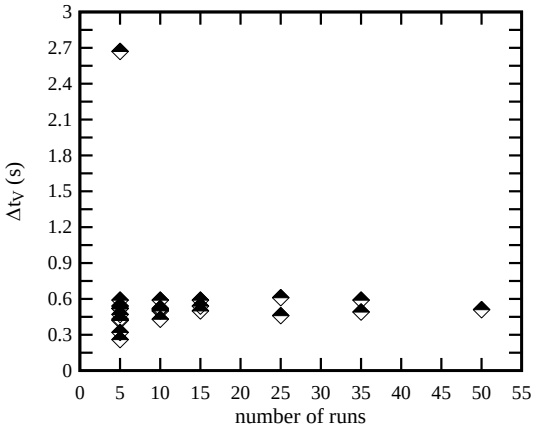

(D) z = 0.033 m

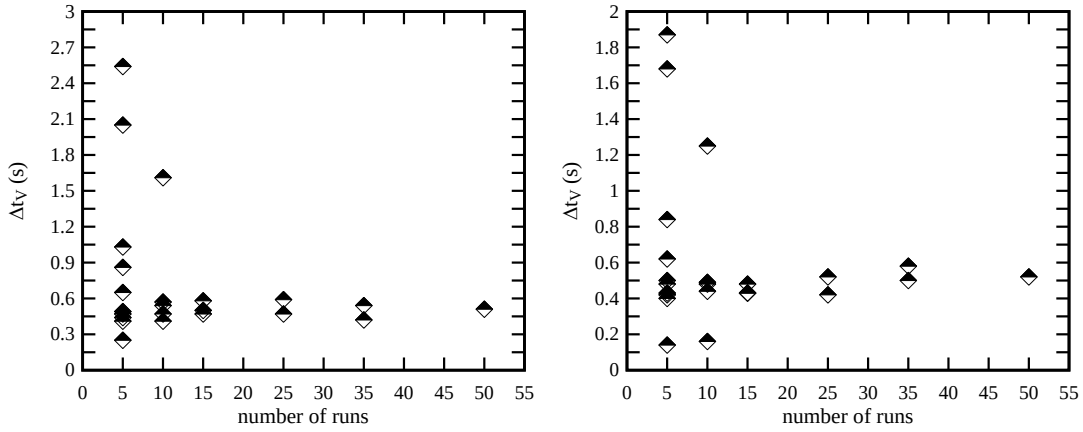

(E) z = 0.028 m (F) z = 0.023 m

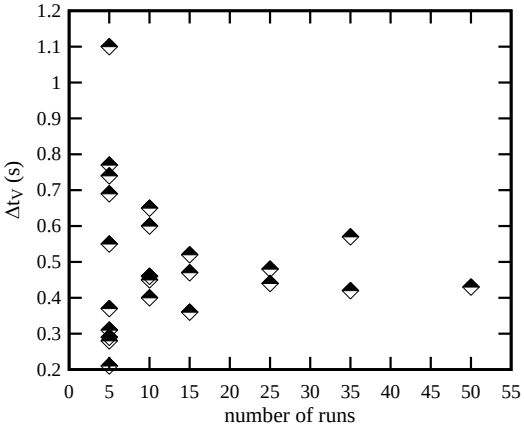

(G) z = 0.018 m

Fig. B-10 - Sensitivity analysis of the time lag of maximum longitudinal velocity fluctuations: comparison between ensemble-averaged results over different number of runs; Profiler sampling with ADV in Setup 2.

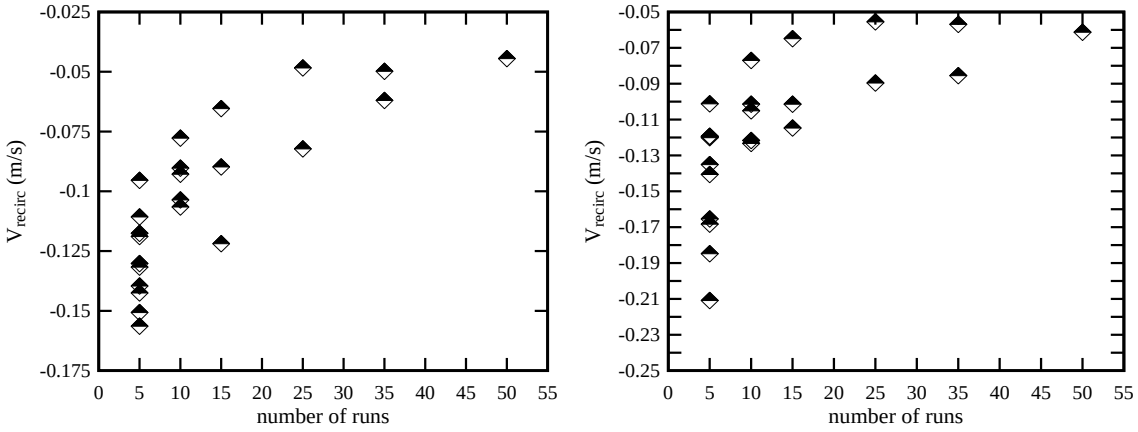

(A) z = 0.048 m (B) z = 0.043 m

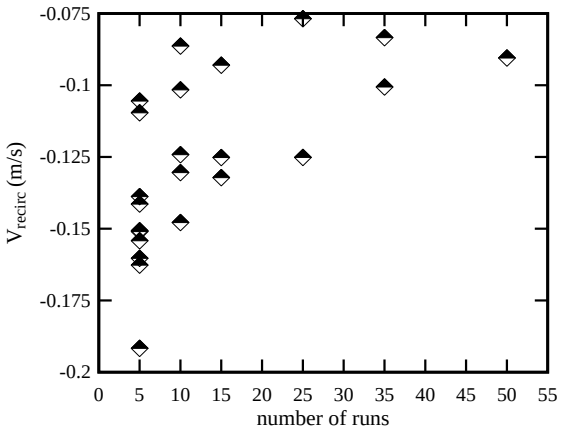

(C) z = 0.038 m

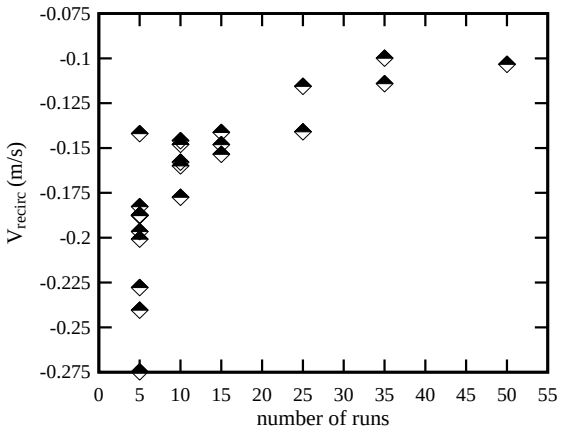

(D) z = 0.033 m

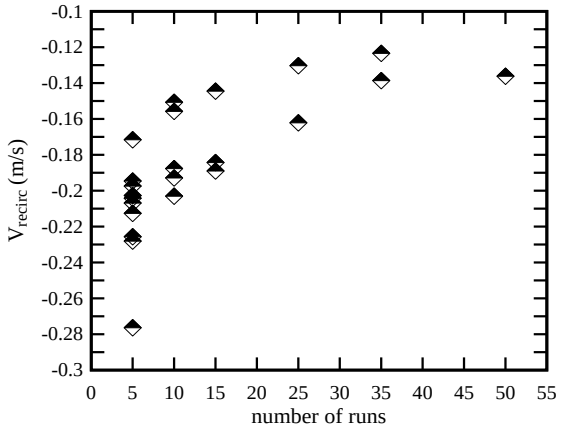

(E) z = 0.028 m

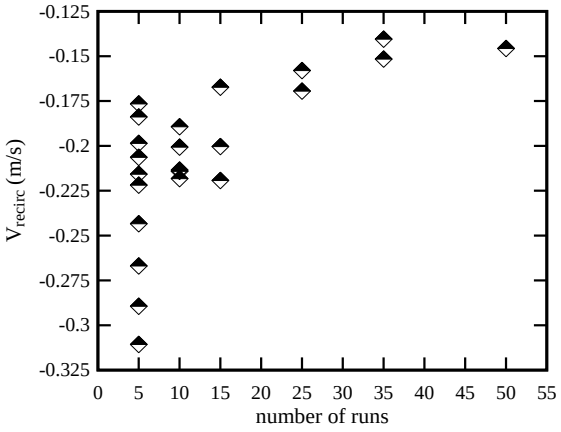

(F) z = 0.023 m

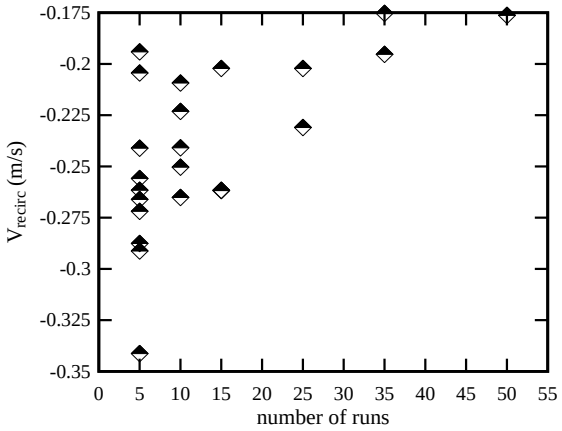

(G) z = 0.018 m

Fig. B-11 - Sensitivity analysis of the longitudinal recirculation velocity: comparison between ensemble-averaged results over different number of runs; Profiler sampling with ADV in Setup 2.

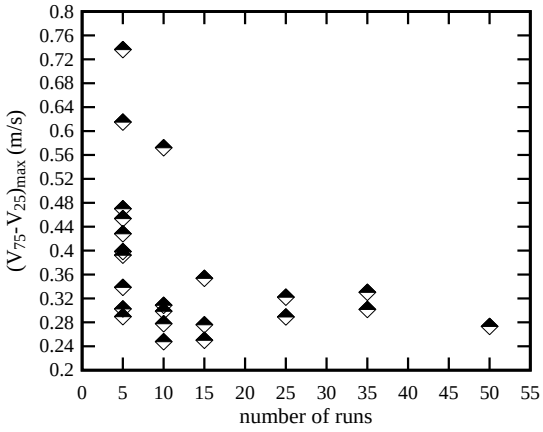

(A) z = 0.048 m

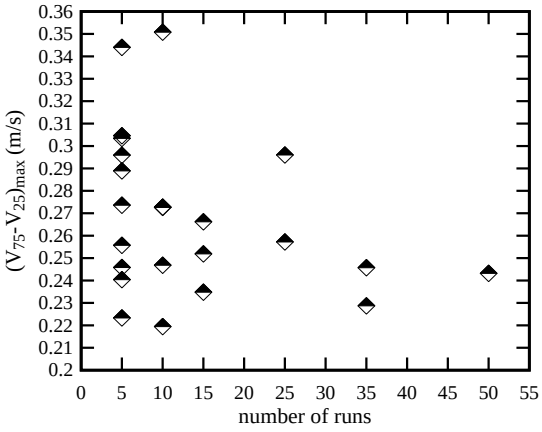

(B) z = 0.043 m

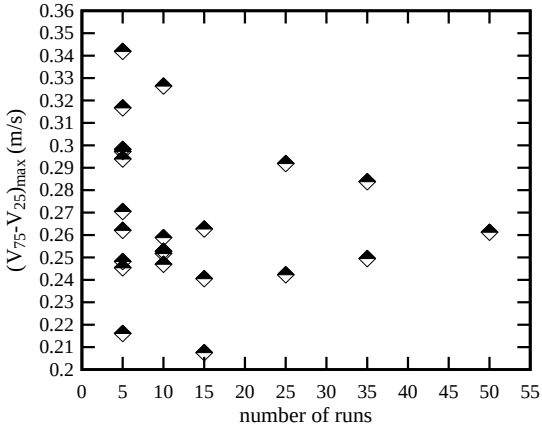

(C) z = 0.038 m

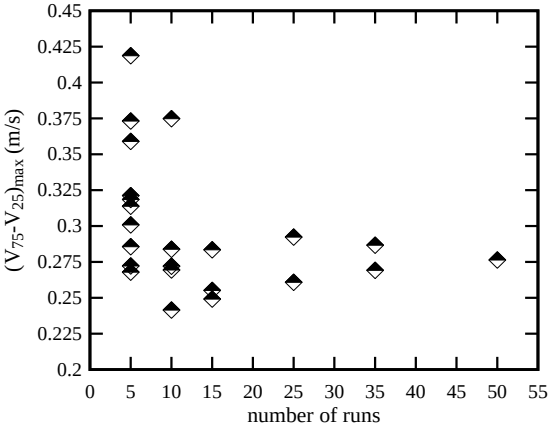

(D) z = 0.033 m

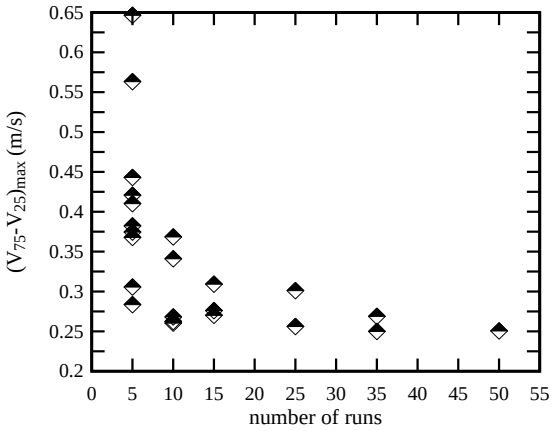

(E) z = 0.028 m

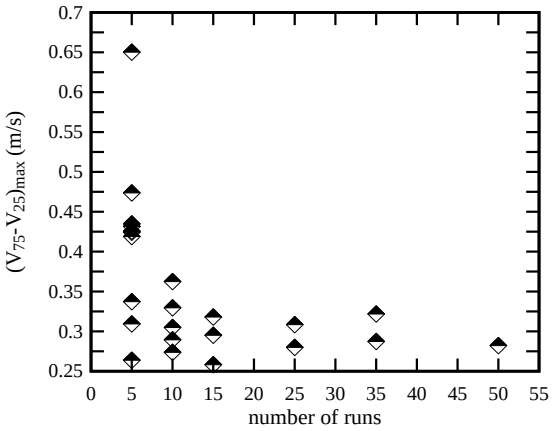

(F) z = 0.023 m

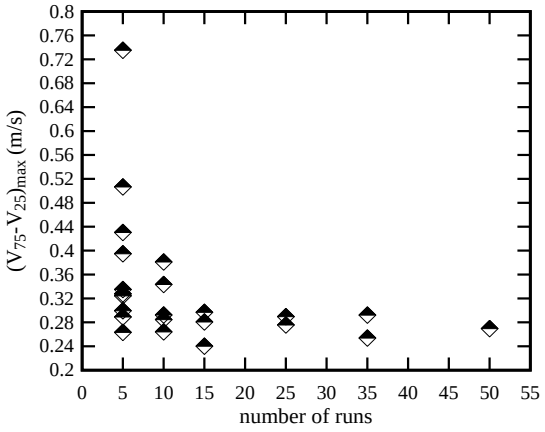

(G) z = 0.018 m

Fig. B-12 - Sensitivity analysis of the maximum longitudinal velocity fluctuations: comparison between ensemble-averaged results over different number of runs; Profiler working alone in Setup 1.

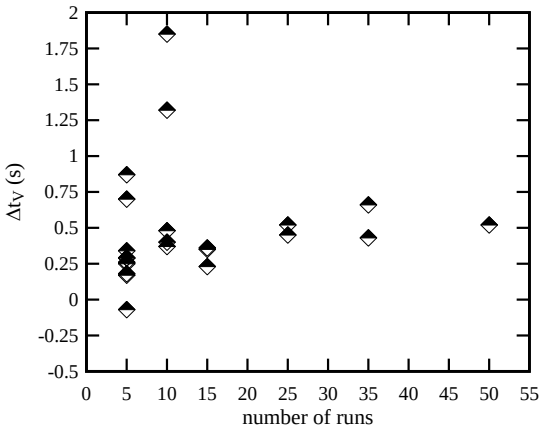

(A) z = 0.048 m

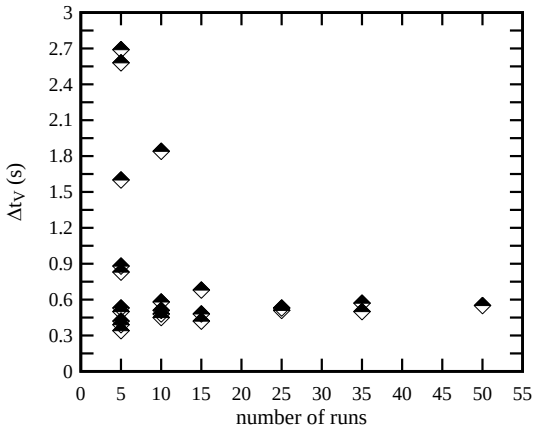

(B) z = 0.043 m

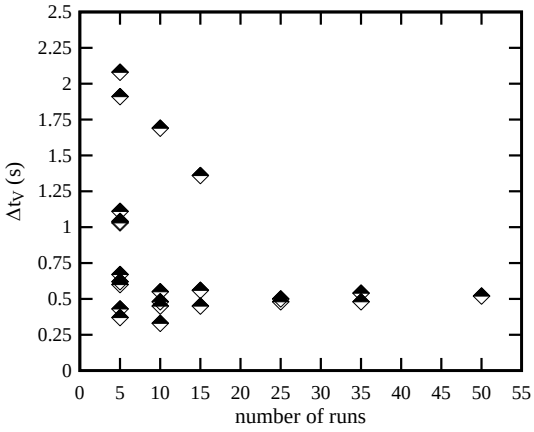

(C) z = 0.038 m

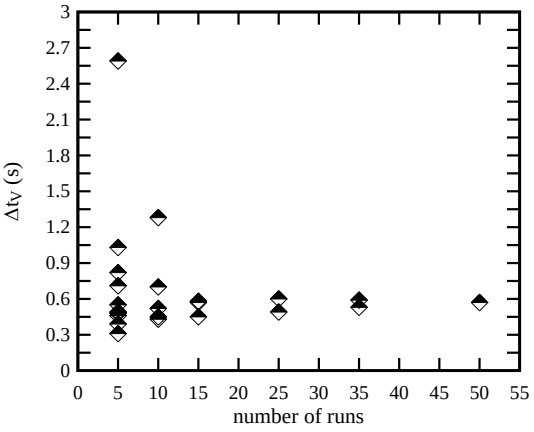

(D) z = 0.033 m

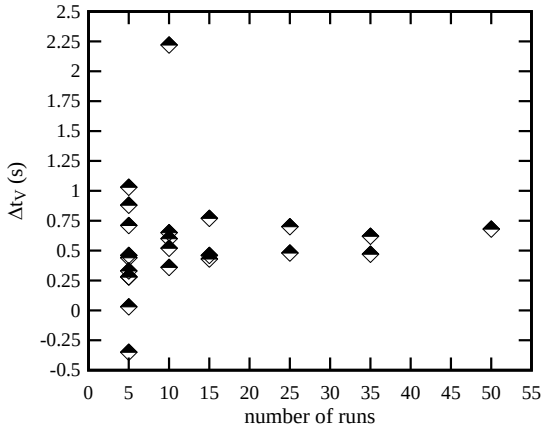

(E) z = 0.028 m

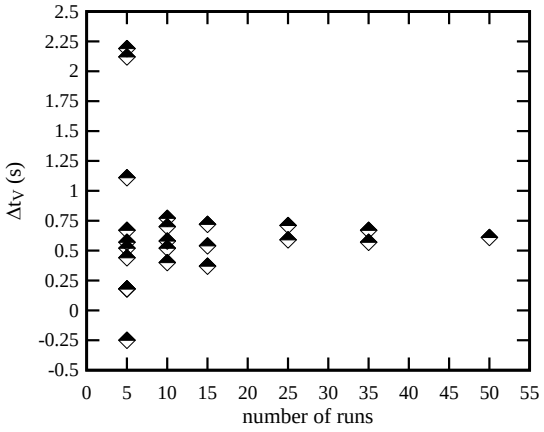

(F) z = 0.023 m

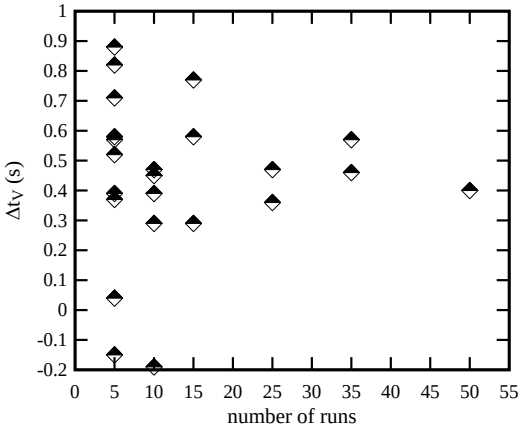

(G) z = 0.018 m

Fig. B-13 - Sensitivity analysis of the time lag of maximum longitudinal velocity fluctuations: comparison between ensemble-averaged results over different number of runs; Profiler working alone in Setup 1.

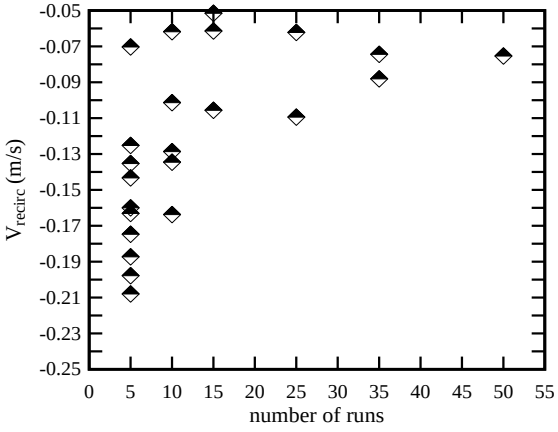

(A) z = 0.048 m

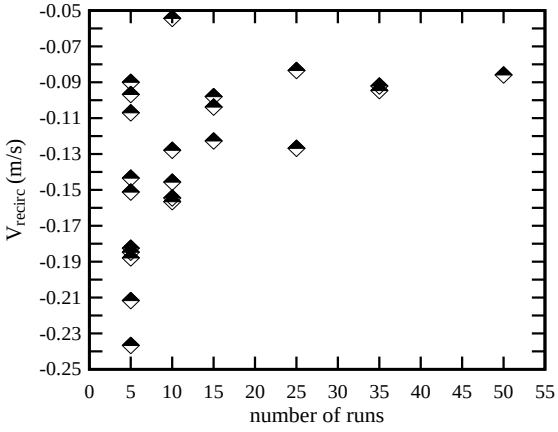

(B) z = 0.043 m

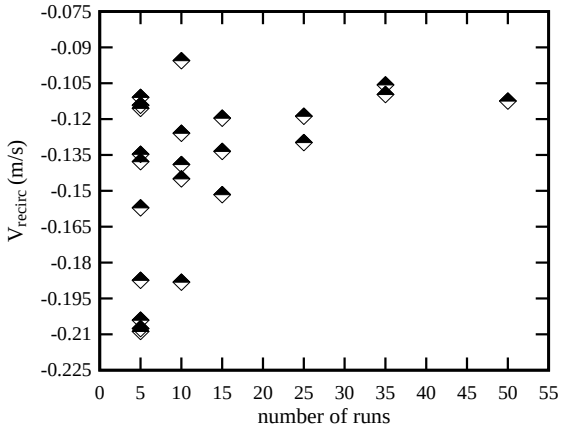

(C) z = 0.038 m

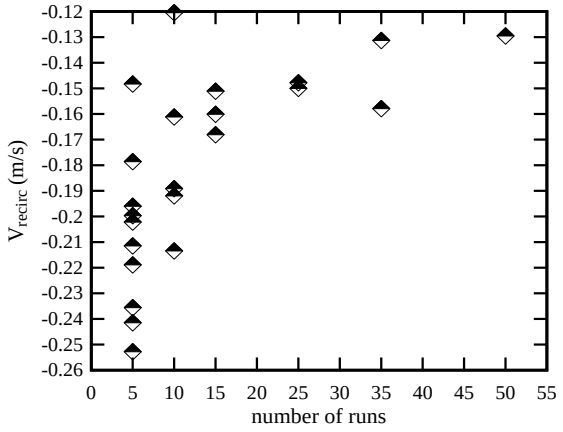

(D) z = 0.033 m

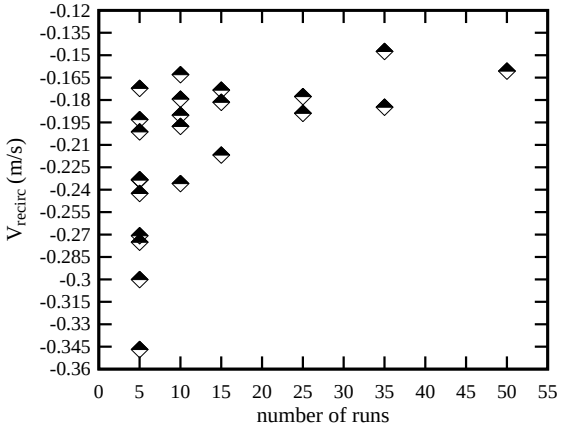

(E) z = 0.028 m

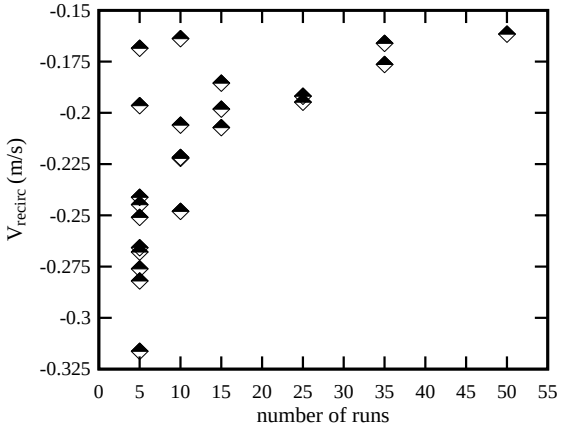

(F) z = 0.023 m

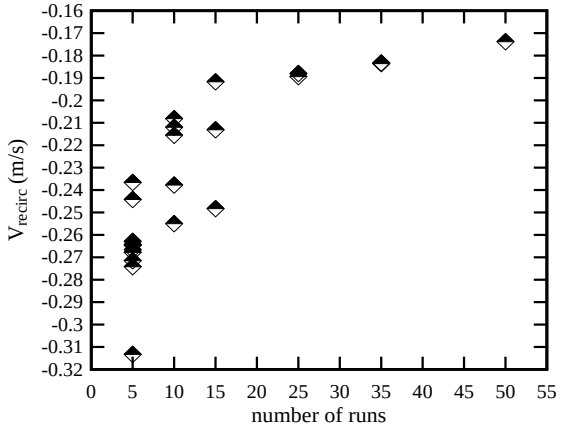

(G) z = 0.018 m

Fig. B-14 - Sensitivity analysis of the longitudinal recirculation velocity: comparison between ensemble-averaged results over different number of runs; Profiler working alone in Setup 1.

APPENDIX C. SPECTRAL ANALYSIS OF STEADY FLOW VELOCITY MEASURED BY VECTRINO II PROFILER

Power spectra of steady flow velocity were obtained by performing Fast Fourier Transforms on the raw velocity fluctuations measured by a Nortek^{TM} Vectrino II Profiler, without any post-processing or filtering. The sampling frequency of the Profiler was 100 Hz and the sampling duration was 60 s. Figure C-1 presents spectra of the longitudinal velocity fluctuations $(v_x')^2$ at different vertical elevations within the same sampling profile. The results showed that for all velocity data analysed, the gradients were overall flatter than the theoretical -5/3 slope, indicating the presence of noise in the collected velocity signals. HURTHER and LEMMIN (2001), using a self-made acoustic Doppler velocity profiler (ADVP), observed similarly flat power spectra for raw velocity fluctuations without any corrections or noise filtering. Hence the noise in the present study was believed to be a white noise, with a flat power spectral density over the investigated frequency band, as discussed by HURTHER and LEMMIN (2001). In Figure C-1, different vertical elevations were associated with spectra of different slope gradients. The slopes about the centre of the sampling profile were closer to the theoretical -5/3 slope. The findings were consistent with observations presented in Appendix A, suggesting that the Profiler had a sweet spot around the centre of a sampling profile.

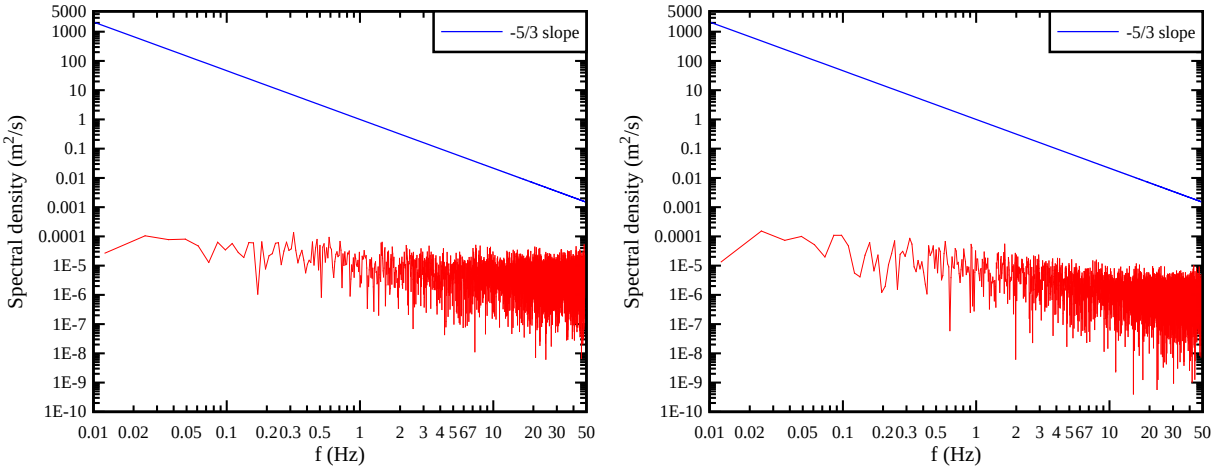

(A) z = 0.035 m

(B) z = 0.031 m

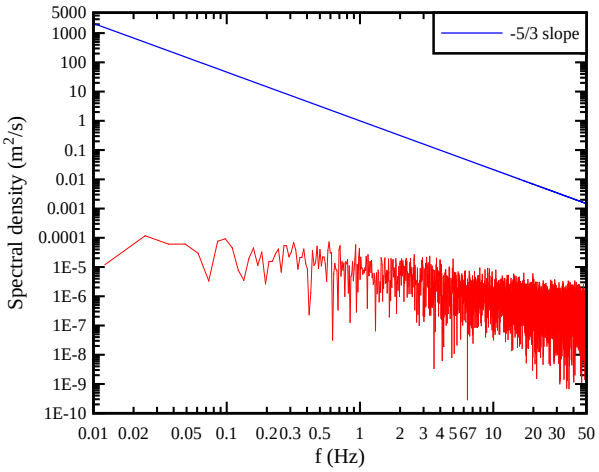

(C) z = 0.026 m

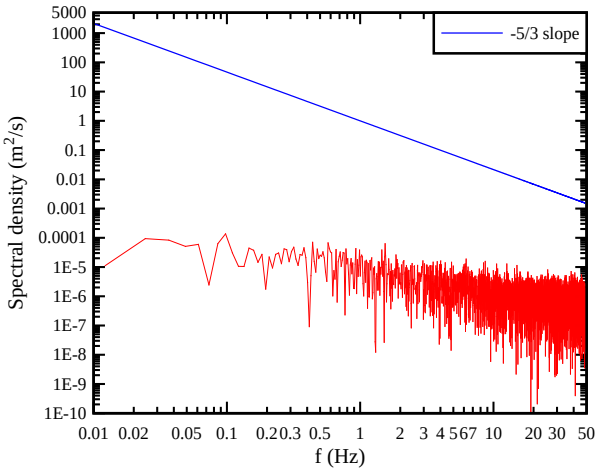

(D) z = 0.021 m

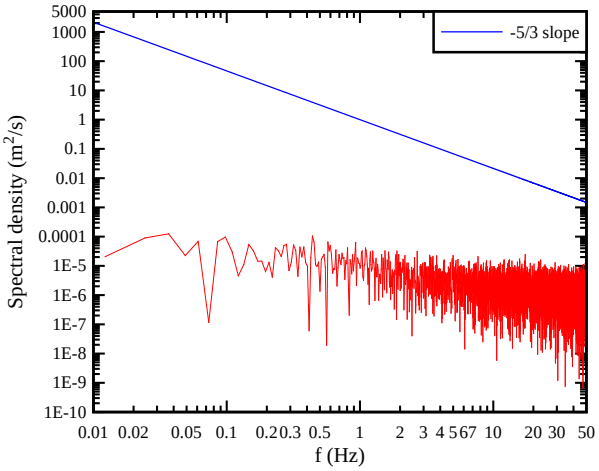

(E) z = 0.016 m

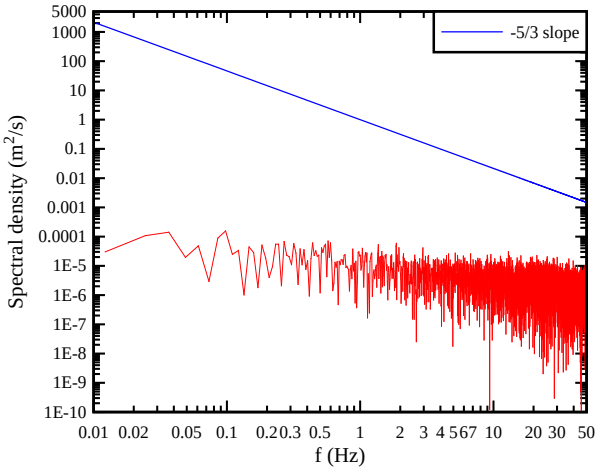

(F) z = 0.011 m

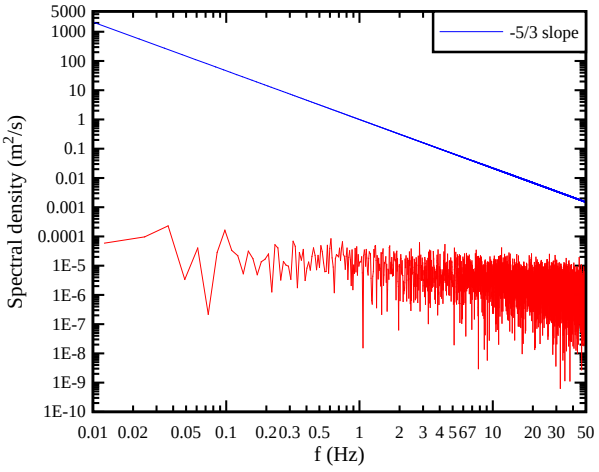

(G) z = 0.006m

Fig. C-1 – Spectra of longitudinal velocity fluctuations $(v_x')^2$ measured by Vectrino II Profiler in steady flows (red line) with a profiling range of z = 0.001 to 0.035 m (35 sampling points): comparison with Kolmogoroff -5/3 slope (blue line) - Flow conditions: Q = 0.099 m^3/s, x = 8.5 m, d_1 = 0.171 m, Fr_o = 0.64.

For locations where the power spectra of velocity fluctuations showed closer agreement with the theoretical slope, spectra obtained from different velocity components were compared. Figure C-2 presents the comparison. By smoothing the spectra of the raw data using a smooth window of 50, the spectra of the vertical velocity fluctuations showed a clearer agreement with the theoretical slope for frequency higher than 20 Hz. The smoothed spectra of the longitudinal velocity fluctuations showed a similar agreement, however for a much lower and narrower frequency range (2 to 10 Hz). The data indicated that the contribution of noise to the velocity signal was anisotropic, due to geometrical configuration of the sensors (HURTHER and LEMMIN 2001). The removal of noise is not included in the scope of this report. Further works are still to be conducted to improve the data quality of the Vectrino II Profiler measurements.

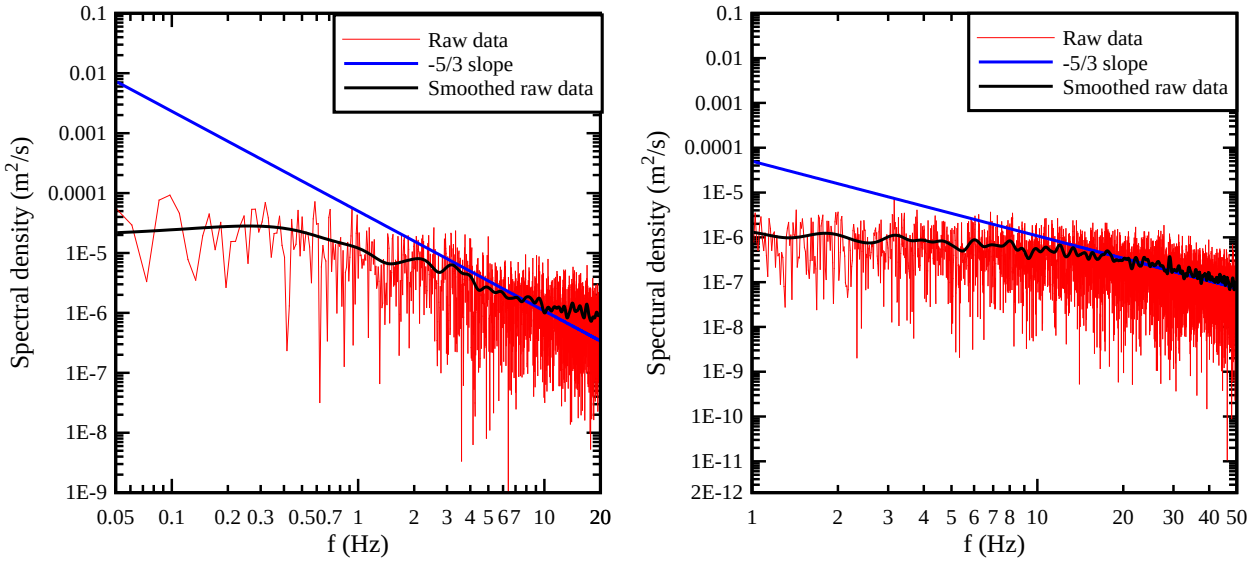

Fig. C-2 – Spectra of longitudinal (left) and vertical (right) velocity fluctuations measured by Vectrino II Profiler in steady flows at z = 0.026 m: comparison with Kolmogoroff -5/3 slope (blue line) - Flow conditions: Q = 0.099 m^3/s, x = 8.5 m, d_1 = 0.171 m, Fr_o = 0.64.

REFERENCES

BECKER, J. (2014). VTMT (Version 1.1) [Computer software]. Federal Waterways Engineering and Research Institute (BAW), Karlsruhe. Retrieved from http://sdrv.ms/12eHgvw/.

BRADSHAW, P. (1971). "An Introduction to Turbulence and its Measurement." *Pergamon Press*, Oxford, UK, The Commonwealth and International Library of Science and technology Engineering and Liberal Studies, Thermodynamics and Fluid Mechanics Division, 218 pages.

CANTWELL, B.J. (1976). "A Flying Hot Wire Study of the Turbulent Near Wake of a circular Cylinder at a Reynolds Number of 140,000." *Ph.D. thesis*, California Institute of Technology, Pasadena, California, USA, 182 pages.

CHANSON, H. (2004). "The Hydraulics of Open Channel Flow: An Introduction." *Butterworth-Heinemann*, 2nd edition, Oxford, UK, 630 pages.

CHANSON, H. (2008). "Acoustic Doppler Velocimetry (ADV) in the Field and in Laboratory: Practical Experiences." *Proceedings of the International Meeting on Measurements and Hydraulics of Sewers IMMHS'08*, Summer School GEMCEA/LCPC, 19-21 Aug. 2008, Bouguenais, Frédérique LARRARTE and Hubert CHANSON Eds., Hydraulic Model Report No. CH70/08, Div. of Civil Engineering, The University of Queensland, Brisbane, Australia, Dec., pp. 49-66.

CHANSON, H. (2009). "Applied Hydrodynamics: An Introduction to Ideal and Real Fluid Flows." *CRC Press*, Taylor & Francis Group, Leiden, The Netherlands, 478 pages.

CHANSON, H. (2010). "Unsteady Turbulence in Tidal Bores: Effects of Bed Roughness." *Journal of Waterway, Port, Coastal, and Ocean Engineering*, ASCE, Vol. 136, No. 5, pp. 247-256 (DOI: 10.1061/(ASCE)WW.1943-5460.0000048).

CHANSON, H. (2011). "Tidal Bores, Aegir, Eagre, Mascaret, Pororoca: Theory and Observations." *World Scientific*, Singapore, 220 pages (ISBN 9789814335416).

CHANSON, H. (2014). "Applied Hydrodynamics: An Introduction." CRC Press, Taylor & Francis Group, Leiden, The Netherlands, 448 pages & 21 video movies (ISBN 978-1-138-00093-3).

CHANSON, H., and DOCHERTY, N.J. (2012). "Turbulent Velocity Measurements in Open Channel Bores." *European Journal of Mechanics B/Fluids*, Vol. 32, pp. 52-58 (DOI 10.1016/j.euromechflu.2011.10.001).

CHANSON, H. and LUBIN, P. (2013). "Mixing and Sediment Processes induced by Tsunamis propagating Upriver" in "Tsunamis: Economic Impact, Disaster Management and Future Challenges." *Nova Science Publishers*, Hauppauge NY, USA, T. CAI Editor, Chapter 3, pp. 65-102 (ISBN 978-1-62808-682-9).

CHANSON, H., and TAN, K.K. (2010). "Turbulent Mixing of Particles under Tidal Bores: an Experimental Analysis." *Journal of Hydraulic Research*, IAHR, Vol. 48, No. 5, pp. 641-649 (DOI: 10.1080/00221686.2010.512779).

CHANSON, H., and TAN, K.K. (2011). "Turbulent Dispersion of Fish Eggs under Tidal Bores." *Fluid Dynamics & Materials Processing*, Tech Science Press, Vol. 7, No. 4, pp. 403-418 (DOI: 10.3970/fdmp.2011.007.403).

CHANSON, H., and TOI, Y.H. (2015). "Physical Modelling of Breaking Tidal Bores: Comparison with Prototype Data." *Journal of Hydraulic Research*, IAHR, Vol. 53, No. 2, pp. 264-273 (DOI: 10.1080/00221686.2014.989458).

CHANSON, H., TREVETHAN, M., and KOCH, C. (2007). "Turbulence Measurements with Acoustic Doppler Velocimeters. Discussion." *Journal of Hydraulic Engineering*, ASCE, Vol. 133, No. 11, pp. 1283-1286 (DOI: 10.1061/(ASCE)0733-9429(2005)131:12(1062)).

CHEN, J., LIU, C., ZHANG, C., and WALKER, H.J. (1990). "Geomorphological Development and Sedimentation in Qiantang Estuary and Hangzhou Bay." *Jl of Coastal Res.*, Vol. 6, No. 3, pp. 559-572.

CRAIG, R. G. A., LOADMAN, C., CLEMENT, B., RUESELLO, P. J., and SIEGEL, E. (2011). "Characterization and Testing of a new Bistatic Profiling Acoustic Doppler Velocimeter: The Vectrino-II." *Proc. IEEE/OES/CWTM 10th Working Conference on Current, Waves and Turbulence Measurement (CWTM)*, Monterey, Canada, 20-23 March, pp. 246-252 (DOI: 10.1109/CWTM.2011.5759559).

DOCHERTY, N.J., and CHANSON, H. (2010). "Characterisation of Unsteady Turbulence in Breaking Tidal Bores including the Effects of Bed Roughness." *Hydraulic Model Report No. CH76/10*, School of Civil Engineering, The University of Queensland, Brisbane, Australia, 112 pages.

FAVRE, A. J., GAVIGLIO, J. J., and DUMAS, R. (1957). "Space-time Double Correlations and Spectra in a Turbulent Boundary Layer." *Journal of Fluid Mechanics*, Cambridge University Press, Vol. 2, No. 4, pp. 313-342 (DOI: 10.1017/S0022112057000166).

FINELLI, C.M., HART, D.D., and FONSECA, D.M. (1999). "Evaluating the Spatial Resolution of an Acoustic Doppler Velocimeter and the Consequences for Measuring Near-Bed Flows." *Limnology & Oceanography*, Vol. 44, No. 7, pp. 1793-1801.

GORING, D.G., and NIKORA, V.I. (2002). "Despiking Acoustic Doppler Velocimeter Data." *Jl of Hyd. Engrg.*, ASCE, Vol. 128, No. 1, pp. 117-126. Discussion: Vol. 129, No. 6, pp. 484-489.

GRAF, W.H. (1971). "Hydraulics of Sediment Transport." *McGraw-Hill*, New York, USA.

HINZE, J.O. (1975). "Turbulence." *McGraw-Hill Publ.*, 2nd Edition, New York, USA.

HENDERSON, F.M. (1966). "Open Channel Flow." *MacMillan Company*, New York, USA.

HORNUNG, H.G., WILLERT, C., and TURNER, S. (1995). "The Flow Field Downstream of a Hydraulic Jump." *Journal of Fluid Mechanics*, Vol. 287, pp. 299-316.

HURTHER, D., and LEMMIN, U. (2001). "A Correction Method for Turbulence Measurements with a 3D Acoustic Doppler Velocity Profiler." *Journal of Atmospheric and Oceanic Technology*, AMS, Vol. 18, pp. 446-458.

JACOBS, W., LE HIR, P., VAN KESTEREN, W., and CANN, P. (2011). Erosion threshold of sand–mud mixtures. *Continental Shelf Research*, Vo. 31, Supplement, pp. S14-S25 (DOI: 10.1016/j.csr.2010.05.012).

KHEZRI, N. (2014). "Modelling Turbulent Mixing and Sediment Process Beneath Tidal Bores: Physical and Numerical Investigations." *Ph.D. thesis*, School of Civil Engineering, The University of Queensland, Brisbane, Australia, 267 pages.

KHEZRI, N., and CHANSON, H. (2012a). "Undular and Breaking Tidal Bores on Fixed and Movable Gravel Beds." *Journal of Hydraulic Research*, IAHR, Vol. 50, No. 4, pp. 353-363.

KHEZRI, N., and CHANSON, H. (2012b). "Inception of Bed Load Motion beneath a Bore." *Geomorphology*, Vol. 153-154, pp. 39-47 & 2 video movies (DOI: 10.1016/j.geomorph.2012.02.006).

KHEZRI, N., and CHANSON, H. (2015). "Turbulent Velocity, Sediment Motion and Particle Trajectories under Breaking Tidal Bores: Simultaneous Physical Measurements." *Environmental Fluid Mechanics*, Vol. 15, No. 3, pp. 633-651 (DOI: 10.1007/s10652-014-9358-z) & (DOI: 10.1007/s10652-014-9360).

KIM, J., and MOIN, P. (1986). "The structure of the vorticity field in turbulent channel flow." *Journal of Fluid Mechanics*, Vol. 162, pp. 339-363.

KOCH, C., and CHANSON, H. (2005). "An Experimental Study of Tidal Bores and Positive Surges: Hydrodynamics and Turbulence of the Bore Front." *Report No. CH56/05*, Dept. of Civil Engineering, The University of Queensland, Brisbane, Australia, July, 170 pages (ISBN 1864998245).

KOCH, C., and CHANSON, H. (2008). "Turbulent Mixing beneath an Undular Bore Front." *Journal of Coastal Research*, Vol. 24, No. 4, pp. 999-1007 (DOI: 10.2112/06-0688.1).

KOCH, C., and CHANSON, H. (2009). "Turbulence Measurements in Positive Surges and Bores." *Journal of Hydraulic Research*, IAHR, Vol. 47, No. 1, pp. 29-40 (DOI: 10.3826/jhr.2009.2954).

LENG, X., and CHANSON, H. (2015a). "Turbulent Advances of a Breaking Bore: Preliminary Physical Experiments." *Experimental Thermal and Fluid Science*, Vol. 62, pp. 70-77 (DOI: 10.1016/j.expthermflusci.2014.12.002).

LENG, X., and CHANSON, H. (2015b). "Breaking Bore: Physical Observations of Roller Characteristics." *Mechanics Research Communications*, Vol. 65, pp. 24-29 (DOI: 10.1016/j.mechrescom.2015.02.008) (ISSN 0093-6413).

LENG, X., and CHANSON, H. (2015c). "Unsteady Turbulence during the Upstream Propagation of Undular and Breaking Tidal Bores: an Experimental Investigation." *Hydraulic Model Report No. CH98/15*, School of Civil Engineering, The University of Queensland, Brisbane, Australia, 235 pages & 4 video movies (ISBN 978 1 74272 135 4).

LENG, X., and CHANSON, H. (2015d). "Unsteady Turbulence in Expansion Waves in Rivers and Estuaries: an Experimental Study." *Environmental Fluid Mechanics*, Vol. 15, No. 5, pp. 905-922 (DOI: 10.1007/s10652-014-9385-9).

LIGGETT, J.A. (1994). "Fluid Mechanics." *McGraw-Hill*, New York, USA.

LIGHTHILL, J. (1978). "Waves in Fluids." *Cambridge University Press*, Cambridge, UK, 504 pages.

MACVICAR, B., DILLING, S., LACEY, J., and HIPEL, K. (2014). "A Quality Analysis of the Vectrino II Instrument using a New Open-source MATLAB Toolbox and 2D ARMA Models to Detect and Replace Spikes." *Proc. 7th International Conference on Fluvial Hydraulics (River Flow)*, Lausanne, Switzerland, 3-5 Sept., pp. 1951-1959.

MARTIN, V., FISHER, T.S.R., MILLAR, R.G., and QUICK, M.C. (2002). "ADV Data Analysis for Turbulent Flows: Low Correlation Problem." *Proc. Conf. on Hydraulic Measurements and Experimental Methods*, ASCE-EWRI & IAHR, Estes Park, USA, 10 pages (CD-ROM).

Microsonic (2015). *Mic+ Ultrasonic sensors*. Retrieved June, 2015, from http://www.microsonic.de/.

NEZU, I., and NAKAGAWA, H. (1993). "Turbulence in Open-Channel Flows." *IAHR Monograph*, IAHR Fluid Mechanics Section, Balkema Publ., Rotterdam, The Netherlands, 281 pages.

NIKORA, V. (2004). Personnel Communication on the suitability of ADV despiking techniques in rapidly-varied unsteady flows.

Nortek (2012). *Vectrino Profiler: User Guide*, Nortek Scientific Acoustic Development Group Inc., User Manual.

PERRY, A.E., and WATMUFF, J.H. (1981). "The phase-averaged large-scale structures in three-dimensional turbulent wakes." *Journal of Fluid Mechanics*, Vol. 103, pp. 33-61.

PERRY, A.E., LIM, T.T., and CHONG, M.S. (1980). "The instantaneous velocity fields of coherent structures in coflowing jets and wakes." *Journal of Fluid Mechanics*, Vol. 101, Part 2, pp. 243-256.

PIQUET, J. (1999). "Turbulent Flows. Models and Physics." *Springer*, Berlin, Germany.

POPE, S.B. (2000). "Turbulent Flows." *Cambridge University Press*, 771 pages.

RAYLEIGH, Lord (1908). "Note on Tidal Bores." *Proc. Royal Soc. of London, Series A containing Papers of a Mathematical and Physical Character*, Vol. 81, No. 541, pp. 448-449.

REUNGOAT, D., CHANSON, H., and KEEVIL, C.E. (2015). "Field Measurements of Unsteady Turbulence in a Tidal Bore: the Garonne River in October 2013." *Journal of Hydraulic Research*, IAHR, Vol. 53, No. 3, pp. 291-301 (DOI: 10.1080/00221686.2015.1021717).

SANCHEZ, M., and LEVACHER, D. (2008). "Erosion d'une vase de l'estuaire de la Loire sous l'action du courant." ('Erosion of a mud from the Loire estuary by a flow.') *Bull Eng Geol Environ*, Vol 67, pp. 597-605 (DOI: 10.1007/s10064-008-0159-9) (in French).

SCHLICHTING, H. (1979). "Boundary-layer Theory." *McGraw-Hill*, New York, USA, 817 pages.

SIMON, B. (2014). "Effects of Tidal Bores on Turbulent Mixing: a Numerical and Physical Study in Positive Surges." *Ph.D. thesis*, School of Civil Engineering, The University of Queensland, Brisbane, Australia, 259 pages & 7 movies.

SIMON, B., and CHANSON, H. (2013). "Turbulence Measurements in Tidal Bore-like Positive Surges over a Rough Bed." *Hydraulic Model Report No. CH90/12*, School of Civil Engineering, The University of Queensland, Brisbane, Australia, 176 pages.

SLEATH, J.F.A. (1987). "Turbulent oscillatory flow over rough beds." *Journal of Fluid Mechanics*, (1987), Vol. 182, pp. 369-409.

SPIEGEL, M.R. (1972). "Theory and Problems of Statistics." *McGraw-Hill Inc.*, New York, USA.

TANAKA, H., NGUYEN, X.T., UMEDA, M., HIRAO, R., PRADJOKO, E., MANO, A., and UDO, K. (2012). "Coastal and Estuarine Morphology Changes Induced by the 2011 Great East Japan Earthquake Tsunami." *Coastal Engineering Journal*, Vol. 54, No. 1, paper 1250010, 25 pages (DOI: 10.1142/S0578563412500106).

TESSIER, B., and TERWINDT, J.H.J. (1994). "An Example of Soft-Sediment Deformations in an intertidal Environment - The Effect of a Tidal Bore". *Comptes-Rendus de l'Académie des Sciences*, Série II, Vol. 319, No. 2, Part 2, pp. 217-233 (in French).

THOMAS, R.E., and McLELLAND, S.J. (2015). "The impact of macroalgae on mean and turbulent flow fields." *Journal of Hydrodynamics*, Vol. 27, No. 3, pp. 427-435 (DOI: 10.1016/S1001-6058(15)60500-5).

TRESKE, A. (1994). "Undular Bores (Favre-Waves) in Open Channels - Experimental Studies." *Jl of Hyd. Res.*, IAHR, Vol. 32, No. 3, pp. 355-370. Discussion : Vol. 33, No. 3, pp. 274-278.

WOLANSKI, E., WILLIAMS, D., SPAGNOL, S., and CHANSON, H. (2004). "Undular Tidal Bore Dynamics in the Daly Estuary, Northern Australia." *Estuarine, Coastal and Shelf Science*, Vol. 60, No. 4, pp. 629-636 (DOI: 10.1016/j.ecss.2004.03.001).

ZEDEL, L., and HAY, A. (2011). "Turbulence Measurements in a Jet: Comparing the Vectrino and Vectrino II." *Proc. IEEE/OES/CWTM 10th Working Conference on Current, Waves and Turbulence Measurements (CWTM)*, Monterey, Canada, 20-23 March, pp. 173-178 (DOI: 10.1109/CWTM.2011.5759547).

Bibliography

CHANSON, H. (2008). "Turbulence in Positive Surges and Tidal Bores. Effects of Bed Roughness and Adverse Bed Slopes." *Hydraulic Model Report No. CH68/08*, Div. of Civil Engineering, The University of Queensland, Brisbane, Australia, 121 pages & 5 movie files.

CHANSON, H. (2011). "Turbulent Shear Stresses in Hydraulic Jumps and Decelerating Surges: An Experimental Study." *Earth Surface Processes and Landforms*, Vol. 36, No. 2, pp. 180-189 & 2 videos (DOI: 10.1002/esp.2031).

CHANSON, H. (2011). "Undular Tidal Bores: Effect of Channel Constriction and Bridge Piers." *Environmental Fluid Mechanics*, Vol. 11, No. 4, pp. 385-404 & 4 videos (DOI: 10.1007/s10652-010-9189-5).

DOCHERTY, N.J., and CHANSON, H. (2012). "Physical Modelling of Unsteady Turbulence in Breaking Tidal Bores." *Journal of Hydraulic Engineering*, ASCE, Vol. 138, No. 5, pp. 412-419 (DOI: 10.1061/(ASCE)HY.1943-7900.0000542).

FAVRE, H. (1935). "Etude Théorique et Expérimentale des Ondes de Translation dans les Canaux Découverts." ('Theoretical and Experimental Study of Travelling Surges in Open Channels.') *Dunod*, Paris, France (in French).

FRIEDRICH, H., SPILLER, S.M., and RÜTHER, N. (2014). "Near-bed flow over a fixed gravel bed." *Proceedings River Flow 2014*, A. SCHLEISS et al. Editors, Taylor & Francis Group, London, pp. 279-285.

KEEVIL, C.E., CHANSON, H., and REUNGOAT, D. (2015)." Fluid Flow and Sediment Entrainment in the Garonne River Bore and Tidal Bore Collision." *Earth Surface Processes and Landforms*, Vol. 40, No. 12, pp. 1574-1586 (DOI: 10.1002/esp.3735).

LENG, X., and CHANSON, H. (2016). "Coupling between Free-surface Fluctuations, Velocity Fluctuations and Turbulent Reynolds Stresses during the Upstream Propagation of Positive

Surges, Bores and Compression Waves." *Environmental Fluid Mechanics*, Vol. 16, 25 pages (DOI: 10.1007/s10652-015-9438-8). (In print)

LUBIN, P., GLOCKNER, S., and CHANSON, H. (2010). "Numerical Simulation of a Weak Breaking Tidal Bore." *Mechanics Research Communications*, Vol. 37, No. 1, pp. 119-121 (DOI: 10.1016/j.mechrescom.2009.09.008).

McLELLAND, S.J., and NICHOLAS, A.P. (2000). "A New Method for Evaluating Errors in High-Frequency ADV Measurements." *Hydrological Processes*, Vol. 14, pp. 351-366.

NAKAGAWA, H., and NEZU, I. (1977). "Prediction of the Contributions to the Reynolds Stress from Bursting Events in Open-Channel Flows." *Journal of Fluid Mechanics*, Vol. 80, pp. 99-128 (DOI:10.1017/S0022112077001554).

NAKAGAWA, H., and NEZU, I. (1981). "Structure of Space-Time Correlations of Bursting Phenomena in an Open-Channel Flow." *Journal of Fluid Mechanics*, Vol. 104, pp. 1-43 (DOI:10.1017/S0022112081002796).

NEZU, I. (2005). "Open-Channel Flow Turbulence and Its Research Prospect in the 21st Century." *Journal of Hydraulic Engineering*, Vol. 131, No. 4, pp. 229-246 (DOI: 10.1061/(ASCE)0733-9429(2005)131:4(229)).

PIQUET, J. (1999). "Turbulent Flows. Models and Physics." *Springer*, Berlin, Germany, 761 pages.

REUNGOAT, D., CHANSON, H., and CAPLAIN, B. (2014). "Sediment Processes and Flow Reversal in the Undular Tidal Bore of the Garonne River (France)." *Environmental Fluid Mechanics*, Vol. 14, No. 3, pp. 591–616 (DOI: 10.1007/s10652-013-9319-y).

VOULGARIS, G., and TROWBRIDGE, J.H. (1998). "Evaluation of the Acoustic Doppler Velocimeter (ADV) for Turbulence Measurements." *Jl Atmosph. and Oceanic Tech.*, Vol. 15, pp. 272-289.

Open Access Repositories

OAIster	{http://www.oaister.org/}
UQeSpace	{http://espace.library.uq.edu.au/}

Bibliographic reference of the Report CH101/15

The Hydraulic Model research report series CH is a refereed publication published by the School of Civil Engineering at the University of Queensland, Brisbane, Australia.

The bibliographic reference of the present report is:

LENG, X., and CHANSON, H. (2016). "Unsteady Turbulent Velocity Profiling in Open Channel Flows and Tidal Bores using a Vectrino Profiler." *Hydraulic Model Report No. CH101/15*, School of Civil Engineering, The University of Queensland, Brisbane, Australia, 118 pages (978-1-74272-145-3).

The Report CH101/15 is available, in the present form, as a PDF file on the Internet at UQeSpace:

http://espace.library.uq.edu.au/

It is listed at:

http://espace.library.uq.edu.au/list/author_id/193/

HYDRAULIC MODEL RESEARCH REPORT CH

The Hydraulic Model Report CH series is published by the School of Civil Engineering at the University of Queensland. Orders of any reprint(s) of the Hydraulic Model Reports should be addressed to the School Secretary.

School Secretary, School of Civil Engineering, The University of Queensland
Brisbane 4072, Australia - Tel.: (61 7) 3365 3619 - Fax: (61 7) 3365 4599
Url: http://http://www.civil.uq.edu.au// Email: enquiries@civil.uq.edu.au

Report CH	**Unit price**	Quantity	**Total price**
LENG, X., and CHANSON, H. (2016). "Unsteady Turbulent Velocity Profiling in Open Channel Flows and Tidal Bores using a Vectrino Profiler." *Hydraulic Model Report No. CH101/15*, School of Civil Engineering, The University of Queensland, Brisbane, Australia, 118 pages (ISBN 978-1-74272-145-3).	AUD$60.00		
WANG, H., and CHANSON, H. (2016). "Velocity Field in Hydraulic Jumps at Large Reynolds Numbers: Development of an Array of Two Dual-Tip Phase-detection Probes." *Hydraulic Model Report No. CH100/15*, School of Civil Engineering, The University of Queensland, Brisbane, Australia, 78 pages (ISBN 978 1 74272 143 9).	AUD$60.00		
SUARA. K., BROWN, R., and CHANSON, H. (2015). "Turbulence and Mixing in the Environment: Multi-Device Study in a Sub-tropical Estuary." *Hydraulic Model Report No. CH99/15*, School of Civil Engineering, The University of Queensland, Brisbane, Australia, 167 pages (ISBN 978 1 74272 138 5).	AUD$60.00		
LENG, X., and CHANSON, H. (2015). "Unsteady Turbulence during the Upstream Propagation of Undular and Breaking Tidal Bores: an Experimental Investigation." *Hydraulic Model Report No. CH98/15*, School of Civil Engineering, The University of Queensland, Brisbane, Australia, 235 pages & 4 video movies (ISBN 978 1 74272 135 4).	AUD$60.00		
ZHANG, G., and CHANSON, H. (2015). "Hydraulics of the Developing Flow Region of Stepped Cascades: an Experimental Investigation." *Hydraulic Model Report No. CH97/15*, School of Civil Engineering, The University of Queensland, Brisbane, Australia, 76 pages (ISBN 978 1 74272 134 7).	AUD$60.00		
LENG, X., and CHANSON, H. (2014). "Turbulent Advances of Breaking Bores: Experimental Observations." *Hydraulic Model Report No. CH96/14*, School of Civil Engineering, The University of Queensland, Brisbane, Australia, 40 pages (ISBN 978 1 74272 130 9).	AUD$40.00		
WANG, H, MURZYN, F., and D., CHANSON, H. (2014). "Pressure, Turbulence and Two-Phase Flow Measurements in Hydraulic Jumps." *Hydraulic Model Report No. CH95/14*, School of Civil Engineering, The University of Queensland, Brisbane, Australia, 154 pages (ISBN 9781742720616978174272l064).	AUD$60.00		
REUNGOAT, D., CHANSON, H., and KEEVIL, C. (2014). "Turbulence, Sedimentary Processes and Tidal Bore Collision in the Arcins Channel, Garonne River (October 2013)." *Hydraulic Model Report No. CH94/14* School of Civil Engineering, The University of Queensland, Brisbane, Australia, 145 pages (ISBN 9781742721033).	AUD$60.00		

LENG, X., and CHANSON, H. (2014). "Propagation of Negative Surges in Rivers and Estuaries: Unsteady Turbulent Mixing including the Effects of Bed Roughness." *Hydraulic Model Report No. CH93/13*, School of Civil Engineering, The University of Queensland, Brisbane, Australia, 108 pages (ISBN 9781742720944).	AUD$60.00		
WUTHRICH, D., and CHANSON, H. (2014). "Aeration and Energy Dissipation over Stepped Gabion Spillways: a Physical Study." *Hydraulic Model Report No. CH92/13*, School of Civil Engineering, The University of Queensland, Brisbane, Australia, 171 pages and 5 video movies (ISBN 9781742720944).	AUD$60.00		
WANG, H., and CHANSON, H. (2013). "Free-Surface Deformation and Two-Phase Flow Measurements in Hydraulic Jumps". *Hydraulic Model Report No. CH91/13*, School of Civil Engineering, The University of Queensland, Brisbane, Australia, 108 pages (ISBN 9781742720746).	AUD$60.00		
SIMON, B., and CHANSON, H. (2013). "Turbulence Measurements in Tidal Bore-like Positive Surges over a Rough Bed". *Hydraulic Model Report No. CH90/12*, School of Civil Engineering, The University of Queensland, Brisbane, Australia, 176 pages (ISBN 9781742720685).	AUD$60.00		
REUNGOAT, D., CHANSON, H., and CAPLAIN, B. (2012). "Field Measurements in the Tidal Bore of the Garonne River at Arcins (June 2012)." Hydraulic Model Report No. CH89/12, School of Civil Engineering, The University of Queensland, Brisbane, Australia, 121 pages (ISBN 9781742720616).	AUD$60.00		
CHANSON, H., and WANG, H. (2012). "Unsteady Discharge Calibration of a Large V-Notch Weir." *Hydraulic Model Report No. CH88/12*, School of Civil Engineering, The University of Queensland, Brisbane, Australia, 50 pages & 4 movies (ISBN 9781742720579).	AUD$60.00		
FELDER, S., FROMM, C., and CHANSON, H. (2012). "Air Entrainment and Energy Dissipation on a 8.9° Slope Stepped Spillway with Flat and Pooled Steps." *Hydraulic Model Report No. CH86/12*, School of Civil Engineering, The University of Queensland, Brisbane, Australia, 82 pages (ISBN 9781742720531).	AUD$60.00		
FELDER, S., and CHANSON, H. (2012). "Air-Water Flow Measurements in Instationary Free-Surface Flows: a Triple Decomposition Technique." *Hydraulic Model Report No. CH85/12*, School of Civil Engineering, The University of Queensland, Brisbane, Australia, 161 pages (ISBN 9781742720494).	AUD$60.00		
REICHSTETTER, M., and CHANSON, H. (2011). "Physical and Numerical Modelling of Negative Surges in Open Channels." *Hydraulic Model Report No. CH84/11*, School of Civil Engineering, The University of Queensland, Brisbane, Australia, 82 pages (ISBN 9781742720388).	AUD$60.00		
BROWN, R., CHANSON, H., McINTOSH, D., and MADHANI, J. (2011). "Turbulent Velocity and Suspended Sediment Concentration Measurements in an Urban Environment of the Brisbane River Flood Plain at Gardens Point on 12-13 January 2011." *Hydraulic Model Report No. CH83/11*, School of Civil Engineering, The University of Queensland, Brisbane, Australia, 120 pages (ISBN 9781742720272).	AUD$60.00		
CHANSON, H. "The 2010-2011 Floods in Queensland (Australia): Photographic Observations, Comments and Personal Experience." *Hydraulic Model Report No. CH82/11*, School of Civil Engineering, The University of Queensland, Brisbane, Australia, 127 pages (ISBN 9781742720234).	AUD$60.00		
MOUAZE, D., CHANSON, H., and SIMON, B. (2010). "Field Measurements in the Tidal Bore of the Sélune River in the Bay of Mont Saint Michel (September 2010)." *Hydraulic Model Report No. CH81/10*, School of Civil Engineering, The University of Queensland, Brisbane, Australia, 72 pages (ISBN 9781742720210).	AUD$60.00		

JANSSEN, R., and CHANSON, H. (2010). "Hydraulic Structures: Useful Water Harvesting Systems or Relics." *Proceedings of the Third International Junior Researcher and Engineer Workshop on Hydraulic Structures (IJREWHS'10)*, 2-3 May 2010, Edinburgh, Scotland, R. JANSSEN and H. CHANSON (Eds), Hydraulic Model Report CH80/10, School of Civil Engineering, The University of Queensland, Brisbane, Australia, 211 pages (ISBN 9781742720159).	AUD$60.00		
CHANSON, H., LUBIN, P., SIMON, B., and REUNGOAT, D. (2010). "Turbulence and Sediment Processes in the Tidal Bore of the Garonne River: First Observations." *Hydraulic Model Report No. CH79/10*, School of Civil Engineering, The University of Queensland, Brisbane, Australia, 97 pages (ISBN 9781742720104).	AUD$60.00		
CHACHEREAU, Y., and CHANSON, H., (2010). "Free-Surface Turbulent Fluctuations and Air-Water Flow Measurements in Hydraulics Jumps with Small Inflow Froude Numbers." *Hydraulic Model Report No. CH78/10*, School of Civil Engineering, The University of Queensland, Brisbane, Australia, 133 pages (ISBN 9781742720036).	AUD$60.00		
CHANSON, H., BROWN, R., and TREVETHAN, M. (2010). " Turbulence Measurements in a Small Subtropical Estuary under King Tide Conditions." *Hydraulic Model Report No. CH77/10*, School of Civil Engineering, The University of Queensland, Brisbane, Australia, 82 pages (ISBN 9781864999969).	AUD$60.00		
DOCHERTY, N.J., and CHANSON, H. (2010). "Characterisation of Unsteady Turbulence in Breaking Tidal Bores including the Effects of Bed Roughness." *Hydraulic Model Report No. CH76/10*, School of Civil Engineering, The University of Queensland, Brisbane, Australia, 112 pages (ISBN 9781864999884).	AUD$60.00		
CHANSON, H. (2009). "Advective Diffusion of Air Bubbles in Hydraulic Jumps with Large Froude Numbers: an Experimental Study." *Hydraulic Model Report No. CH75/09*, School of Civil Engineering, The University of Queensland, Brisbane, Australia, 89 pages & 3 videos (ISBN 9781864999730).	AUD$60.00		
CHANSON, H. (2009). "An Experimental Study of Tidal Bore Propagation: the Impact of Bridge Piers and Channel Constriction." *Hydraulic Model Report No. CH74/09*, School of Civil Engineering, The University of Queensland, Brisbane, Australia, 110 pages and 5 movies (ISBN 9781864999600).	AUD$60.00		
CHANSON, H. (2008). "Jean-Baptiste Charles Joseph BÉLANGER (1790-1874), the Backwater Equation and the Bélanger Equation." *Hydraulic Model Report No. CH69/08*, Div. of Civil Engineering, The University of Queensland, Brisbane, Australia, 40 pages (ISBN 9781864999211).	AUD$60.00		
GOURLAY, M.R., and HACKER, J. (2008). "Reef-Top Currents in Vicinity of Heron Island Boat Harbour, Great Barrier Reef, Australia: 2. Specific Influences of Tides Meteorological Events and Waves." *Hydraulic Model Report No. CH73/08*, Div. of Civil Engineering, The University of Queensland, Brisbane, Australia, 331 pages (ISBN 9781864999365).	AUD$60.00		
GOURLAY, M.R., and HACKER, J. (2008). "Reef Top Currents in Vicinity of Heron Island Boat Harbour Great Barrier Reef, Australia: 1. Overall influence of Tides, Winds, and Waves." *Hydraulic Model Report CH72/08*, Div. of Civil Engineering, The University of Queensland, Brisbane, Australia, 201 pages (ISBN 9781864999358).	AUD$60.00		
LARRARTE, F., and CHANSON, H. (2008). "Experiences and Challenges in Sewers: Measurements and Hydrodynamics." *Proceedings of the International Meeting on Measurements and Hydraulics of Sewers*, Summer School GEMCEA/LCPC, 19-21 Aug. 2008, Bouguenais, Hydraulic Model Report No. CH70/08, Div. of Civil Engineering, The University of Queensland, Brisbane, Australia (ISBN 9781864999280).	AUD$60.00		

CHANSON, H. (2008). "Photographic Observations of Tidal Bores (Mascarets) in France." *Hydraulic Model Report No. CH71/08*, Div. of Civil Engineering, The University of Queensland, Brisbane, Australia, 104 pages, 1 movie and 2 audio files (ISBN 9781864999303).	AUD$60.00		
CHANSON, H. (2008). "Turbulence in Positive Surges and Tidal Bores. Effects of Bed Roughness and Adverse Bed Slopes." *Hydraulic Model Report No. CH68/08*, Div. of Civil Engineering, The University of Queensland, Brisbane, Australia, 121 pages & 5 movie files (ISBN 9781864999198)	AUD$70.00		
FURUYAMA, S., and CHANSON, H. (2008). "A Numerical Study of Open Channel Flow Hydrodynamics and Turbulence of the Tidal Bore and Dam-Break Flows." *Report No. CH66/08*, Div. of Civil Engineering, The University of Queensland, Brisbane, Australia, May, 88 pages (ISBN 9781864999068).	AUD$60.00		
GUARD, P., MACPHERSON, K., and MOHOUPT, J. (2008). "A Field Investigation into the Groundwater Dynamics of Raine Island." *Report No. CH67/08*, Div. of Civil Engineering, The University of Queensland, Brisbane, Australia, February, 21 pages (ISBN 9781864999075).	AUD$40.00		
FELDER, S., and CHANSON, H. (2008). "Turbulence and Turbulent Length and Time Scales in Skimming Flows on a Stepped Spillway. Dynamic Similarity, Physical Modelling and Scale Effects." *Report No. CH64/07*, Div. of Civil Engineering, The University of Queensland, Brisbane, Australia, March, 217 pages (ISBN 9781864998870).	AUD$60.00		
TREVETHAN, M., CHANSON, H., and BROWN, R.J. (2007). "Turbulence and Turbulent Flux Events in a Small Subtropical Estuary." Report No. CH65/07, Div. of Civil Engineering, The University of Queensland, Brisbane, Australia, November, 67 pages (ISBN 9781864998993)	AUD$60.00		
MURZYN, F., and CHANSON, H. (2007). "Free Surface, Bubbly flow and Turbulence Measurements in Hydraulic Jumps." *Report CH63/07*, Div. of Civil Engineering, The University of Queensland, Brisbane, Australia, August, 116 pages (ISBN 9781864998917).	AUD$60.00		
KUCUKALI, S., and CHANSON, H. (2007). "Turbulence in Hydraulic Jumps: Experimental Measurements." *Report No. CH62/07*, Div. of Civil Engineering, The University of Queensland, Brisbane, Australia, July, 96 pages (ISBN 9781864998825).	AUD$60.00		
CHANSON, H., TAKEUCHI, M, and TREVETHAN, M. (2006). "Using Turbidity and Acoustic Backscatter Intensity as Surrogate Measures of Suspended Sediment Concentration. Application to a Sub-Tropical Estuary (Eprapah Creek)." *Report No. CH60/06*, Div. of Civil Engineering, The University of Queensland, Brisbane, Australia, July, 142 pages (ISBN 1864998628).	AUD$60.00		
CAROSI, G., and CHANSON, H. (2006). "Air-Water Time and Length Scales in Skimming Flows on a Stepped Spillway. Application to the Spray Characterisation." *Report No. CH59/06*, Div. of Civil Engineering, The University of Queensland, Brisbane, Australia, July (ISBN 1864998601).	AUD$60.00		
TREVETHAN, M., CHANSON, H., and BROWN, R. (2006). "Two Series of Detailed Turbulence Measurements in a Small Sub-Tropical Estuarine System." *Report No. CH58/06*, Div. of Civil Engineering, The University of Queensland, Brisbane, Australia, Mar. (ISBN 1864998520).	AUD$60.00		
KOCH, C., and CHANSON, H. (2005). "An Experimental Study of Tidal Bores and Positive Surges: Hydrodynamics and Turbulence of the Bore Front." *Report No. CH56/05*, Dept. of Civil Engineering, The University of Queensland, Brisbane, Australia, July (ISBN 1864998245).	AUD$60.00		
CHANSON, H. (2005). "Applications of the Saint-Venant Equations and Method of Characteristics to the Dam Break Wave Problem." *Report No. CH55/05*, Dept. of Civil Engineering, The University of Queensland, Brisbane, Australia, May (ISBN 1864997966).	AUD$60.00		

CHANSON, H., COUSSOT, P., JARNY, S., and TOQUER, L. (2004). "A Study of Dam Break Wave of Thixotropic Fluid: Bentonite Surges down an Inclined plane." *Report No. CH54/04*, Dept. of Civil Engineering, The University of Queensland, Brisbane, Australia, June, 90 pages (ISBN 1864997710).	AUD$60.00		
CHANSON, H. (2003). "A Hydraulic, Environmental and Ecological Assessment of a Sub-tropical Stream in Eastern Australia: Eprapah Creek, Victoria Point QLD on 4 April 2003." *Report No. CH52/03*, Dept. of Civil Engineering, The University of Queensland, Brisbane, Australia, June, 189 pages (ISBN 1864997044).	AUD$90.00		
CHANSON, H. (2003). "Sudden Flood Release down a Stepped Cascade. Unsteady Air-Water Flow Measurements. Applications to Wave Run-up, Flash Flood and Dam Break Wave." *Report CH51/03*, Dept of Civil Eng., Univ. of Queensland, Brisbane, Australia, 142 pages (ISBN 1864996552).	AUD$60.00		
CHANSON, H,. (2002). "An Experimental Study of Roman Dropshaft Operation : Hydraulics, Two-Phase Flow, Acoustics." *Report CH50/02*, Dept of Civil Eng., Univ. of Queensland, Brisbane, Australia, 99 pages (ISBN 1864996544).	AUD$60.00		
CHANSON, H., and BRATTBERG, T. (1997). "Experimental Investigations of Air Bubble Entrainment in Developing Shear Layers." *Report CH48/97*, Dept. of Civil Engineering, University of Queensland, Australia, Oct., 309 pages (ISBN 0 86776 748 0).	AUD$90.00		
CHANSON, H. (1996). "Some Hydraulic Aspects during Overflow above Inflatable Flexible Membrane Dam." *Report CH47/96*, Dept. of Civil Engineering, University of Queensland, Australia, May, 60 pages (ISBN 0 86776 644 1).	AUD$60.00		
CHANSON, H. (1995). "Flow Characteristics of Undular Hydraulic Jumps. Comparison with Near-Critical Flows." *Report CH45/95*, Dept. of Civil Engineering, University of Queensland, Australia, June, 202 pages (ISBN 0 86776 612 3).	AUD$60.00		
CHANSON, H. (1995). "Air Bubble Entrainment in Free-surface Turbulent Flows. Experimental Investigations." *Report CH46/95*, Dept. of Civil Engineering, University of Queensland, Australia, June, 368 pages (ISBN 0 86776 611 5).	AUD$80.00		
CHANSON, H. (1994). "Hydraulic Design of Stepped Channels and Spillways." *Report CH43/94*, Dept. of Civil Engineering, University of Queensland, Australia, Feb., 169 pages (ISBN 0 86776 560 7).	AUD$60.00		
POSTAGE & HANDLING (per report)	AUD$10.00		
GRAND TOTAL			

OTHER HYDRAULIC RESEARCH REPORTS

Reports/Theses	Unit price	Quantity	Total price
WANG, H. (2014). "Turbulence and Air Entrainment in Hydraulic Jumps." *Ph.D. thesis*, School of Civil Engineering, The University of Queensland, Brisbane, Australia, 341 pages (DOI: 10.14264/uql.2014.542).	AUD$100.00		
KHEZRI, N. (2014). "Modelling Turbulent Mixing and Sediment Process Beneath Tidal Bores: Physical and Numerical Investigations." *Ph.D. thesis*, School of Civil Engineering, The University of Queensland, Brisbane, Australia, 267 pages.	AUD$100.00		

SIMON, B. (2014). "Effects of Tidal Bores on Turbulent Mixing: a Numerical and Physical Study in Positive Surges." *Ph.D. thesis*, School of Civil Engineering, The University of Queensland, Brisbane, Australia, 259 pages (DOI: 10.14264/uql.2014.19).	AUD$100.00		
FELDER, S. (2013). "Air-Water Flow Properties on Stepped Spillways for Embankment Dams: Aeration, Energy Dissipation and Turbulence on Uniform, Non-Uniform and Pooled Stepped Chutes." *Ph.D. thesis*, School of Civil Engineering, The University of Queensland, Brisbane, Australia.	AUD$100.00		
REICHSTETTER, M. (2011). "Hydraulic Modelling of Unsteady Open Channel Flow: Physical and Analytical Validation of Numerical Models of Positive and Negative Surges." *MPhil thesis*, School of Civil Engineering, The University of Queensland, Brisbane, Australia, 112 pages.	AUD$80.00		
TREVETHAN, M. (2008). "A Fundamental Study of Turbulence and Turbulent Mixing in a Small Subtropical Estuary." Ph.D. thesis, Div. of Civil Engineering, The University of Queensland, 342 pages.	AUD$100.00		
GONZALEZ, C.A. (2005). "An Experimental Study of Free-Surface Aeration on Embankment Stepped Chutes." *Ph.D. thesis*, Dept of Civil Engineering, The University of Queensland, Brisbane, Australia, 240 pages.	AUD$80.00		
TOOMBES, L. (2002). "Experimental Study of Air-Water Flow Properties on Low-Gradient Stepped Cascades." *Ph.D. thesis*, Dept of Civil Engineering, The University of Queensland, Brisbane, Australia.	AUD$100.00		
CHANSON, H. (1988). "A Study of Air Entrainment and Aeration Devices on a Spillway Model." *Ph.D. thesis*, University of Canterbury, New Zealand.	AUD$60.00		
POSTAGE & HANDLING (per report)	AUD$10.00		
GRAND TOTAL			

CIVIL ENGINEERING RESEARCH REPORT CE

The Civil Engineering Research Report CE series is published by the School of Civil Engineering at the University of Queensland. Orders of any of the Civil Engineering Research Report CE should be addressed to the School Secretary.

School Secretary, School of Civil Engineering, The University of Queensland
Brisbane 4072, Australia
Tel.: (61 7) 3365 3619 Fax: (61 7) 3365 4599
Url: http://http://www.civil.uq.edu.au// Email: enquiries@civil.uq.edu.au

Recent Research Report CE	Unit price	Quantity	Total price

CALLAGHAN, D.P., NIELSEN, P., and CARTWRIGHT, N. (2006). "Data and Analysis Report: Manihiki and Rakahanga, Northern Cook Islands - For February and October/November 2004 Research Trips." *Research Report CE161*, Division of Civil Engineering, The University of Queensland (ISBN No. 1864998318).	AUD$10.00		
GONZALEZ, C.A., TAKAHASHI, M., and CHANSON, H. (2005). "Effects of Step Roughness in Skimming Flows: an Experimental Study." *Research Report No. CE160*, Dept. of Civil Engineering, The University of Queensland, Brisbane, Australia, July (ISBN 1864998105).	AUD$10.00		
CHANSON, H., and TOOMBES, L. (2001). "Experimental Investigations of Air Entrainment in Transition and Skimming Flows down a Stepped Chute. Application to Embankment Overflow Stepped Spillways." *Research Report No. CE158*, Dept. of Civil Engineering, The University of Queensland, Brisbane, Australia, July, 74 pages (ISBN 1 864995297).	AUD$10.00		
HANDLING (per order)	AUD$10.00		
GRAND TOTAL			

Note: Prices include postages and processing.

PAYMENT INFORMATION

1- VISA Card

Name on the card :	
Visa card number :	
Expiry date :	
Amount :	AUD$ .....

2- Cheque/remittance payable to: THE UNIVERSITY OF QUEENSLAND and crossed "Not Negotiable".

N.B.: For overseas buyers, cheque payable in Australian Dollars drawn on an office in Australia of a bank operating in Australia, payable to: THE UNIVERSITY OF QUEENSLAND and crossed "Not Negotiable".

Orders of any Research Report should be addressed to the School Secretary.

School Secretary, School of Civil Engineering, The University of Queensland
Brisbane 4072, Australia - Tel.: (61 7) 3365 3619 - Fax: (61 7) 3365 4599
Url: http://http://www.civil.uq.edu.au// Email: enquiries@civil.uq.edu.au